Octacyanometalphthalocyanine-metal Complex Crystals in Thin Films

柳，久雄

(Degree)
博士（理学）

(Date of Degree)
1988-03-31

(Date of Publication)
2014-04-02

(Resource Type)
doctoral thesis

(Report Number)
甲0732

(URL)
https://hdl.handle.net/20.500.14094/D1000732

博 士 論 文

Octacyanometalphthalocyanine-metal Complex Crystals in Thin Films

(薄膜中のオクタシアノ金属フタロシアニン—
金属錯体結晶に関する研究)

昭和 63 年 1 月

神戸大学大学院自然科学研究科

柳　　久　雄

Contents

Introduction

Phthalocyanine compounds are structural analogues of porphyrins which are important functional compounds in nature. Metalloporphyrins in living organisms such as chlorophyll and hemoglobin act as an initiator of photosynthesis in green plants and an oxygen carrier in blood. Their characteristic properties such as oxidation-reduction, acid-base, electron-optical properties and catalytic activity are closely related to coordination between the macrocyclic ligand with conjugated π-electron system and the central metal ions. Because of the structural similarities to porphyrins, phthalocyanines have been cited as biophysical and chemical model system of porphyrins. Their thermal stability, fastness to light, inertness to acids and alkalis, and insolubility in most solvents have ensured wide application as pigments. Recently, they have been attracting much attention as new functional materials such as semiconductors, photoconductors, sensors and solar energy devices. The interest for these physical properties have led to extensive research to synthesize various phthalocyanine derivatives and polymeric phthalocyanines. The introduction of functional substituents into phthalocyanine rings permits improvements in their solubility, reactivity and all other properties. Polymeric phthalocyanines are prepared by various procedures and several types of polymers have been reported. Cofacial polymers, in which phthalocyanine units are connected together through the central metal linkage, are known as new low-dimensional molecular materials. Their halogen-doped polymers

have high electron conductivity along the direction of the molecular stacking and their structure has been given in detail. The pendant-type of polymeric phthalocyanines are prepared by addition of phthalocyanine units into polymer chains such as polystyrene. Another type of polymeric phthalocyanine is planar polymer in which phthalocyanine units are linked each other by their peripheral benzene rings. This polymer is synthesized from bifunctional monomers such as 1,2,4,5-tetracyanobenzene and pyromellitic acid derivatives with metal or metal salts in bulk. It is expected that these polymers are structure-enforced metal-like materials with high electron conductivity because of their large two-dimensional conjugated π-electron system. However, the products of these reactions are crude and their structure uniformity is low due to various by-products. For practical applications, it is necessary to form these polymers into thin films in which no impurity is included. According to Wöhrle, thin films of polymeric phthalocyanines of high purity are prepared by vapor-solid reaction of gaseous tetracyanobenzene with metal substrates. It has been considered that the films are composed of polymeric phthalocyanines and monomeric octacyanophthalocyanines as a precursor of the former. However, the structure of polymeric phthalocyanine has not been elucidated because of their insolubility in most solvents. Furthermore, the structure, morphology, crystallinity and growth mechanism of the film have not been investigated in detail.

The aim of the present work is characterization and structural elucidation of thin films of monomeric and polymeric

phthalocyanines produced by vapor-solid reaction of tetracyanobenzene with metals. Chapter 1 is concerned with preparation and characterization of the films. The films were prepared in different reaction conditions with various substrate materials such as alkali halides and metal films. The products were characterized by infrared, UV/Visible spectroscopy. The composition of the films was examined by photoelectron spectroscopy and X-ray microanalysis and the morphology of the films was observed by scanning electron microscopy. The films consisted of metal containing polymerized products and monomeric octacyanometalphthalocyanines. The latter products formed peculiar tentacle-like crystals on the substrates and included extra metal atoms more than would be required for coordination in phthalocyanine rings. It was found that these crystals were composed of octacyanophthalocyanine-metal complexes. In order to elucidate the structure of the complex crystals, the thin films were examined by high resolution electron microscopy. The crystal structure and molecular arrangement of the complex produced on a KCl substrate was determined directly from molecular images with aid of computer image simulation based on the dynamical theory of electron scattering in Chapter 2. It revealed that octacyanophthalocyanine molecules crystallized in a column and the complex crystal was formed by coordination of their peripheral nitrile groups with intercalated metal atoms. In Chapter 3, metal derivatives of octacyanopthalocyanine-metal complex crystals formed on various metal substrates were identified as isomorphous crystals of that formed on KCl by high

resolution structure images. The column structure of the complex crystals, in which octacyanometalphthalocyanine molecules stacked in parallel with their molecular planes perpendicular to the column axis, was different from a well-known herringbone structure of metalphthalocyanines. It seemed that this peculiar molecular stacking was attributed to formation of charge transfer complexes between octacyanometalphthalocyanines and intercalated metals. These structure features lead to interest for their low-dimensional properties and a practical architecture of new molecular materials. For constructing molecular assemblies with restricted dimension, well-defined crystal growth is required and molecular arrangements must be crystallographically controlled in thin films. In Chapter 4, crystal growth of thin films of octacyanometalphthalocyanine-metal complexes was examined by electron microscopy and their growth mechanism was discussed. It revealed that growth of the complex crystals was affected by diffusion of metal atoms from the substrates to the crystals and could be controlled selectively by the reaction condition and kinds of the substrate material. The final Chapter 5 contains epitaxial growth of the complex crystals formed on substrates, and several types of orientations were observed. The origin of their epitaxy was interpreted in terms of anisotropic interaction between octacyanometalphthalocyanine molecules and the substrate surfaces.

It is expected that octacyanometalphthalocyanine-metal complexes possess interesting physical properties because of

their peculiar crystal and electronic structure. The structural investigation and elucidation of crystal growth in thin films will lead to practical architecture of these new organic materials, and then phthalocyanines will be cited essentially as functional materials as well as porphyrins in nature.

Chapter 1 Characterization of Monomeric and Polymeric Octacyanometalphthalocyanines in Thin Films

Abstract

Thin films were prepared by reaction of 1,2,4,5-tetracyanobenzene with substrates of a KCl single crystal, and Cu, Ni, Co, Fe, Zn films at various temperatures. The films were characterized by infrared, UV/Visible and photoelectron spectroscopy and analytical electron microscopy. The films produced on the metal films below 400 °C were composed of tentacle-like crystals growing from the surfaces and an amorphous layer condensed over the metal substrate. The tentacle-like crystals were soluble in concentrated sulfuric acid and were identified as respective octacyanometalphthalocyanine-metal complexes. The amorphous layers contained polymerization products with polynitrile structure which were insoluble in concentrated sulfuric acid. The films produced on the metal films at 450 °C were composed of a thick layer and had a very limited solubility in concentrated sulfuric acid. They were ascribed to polymetalphthalocyanines (poly-MPc) and cross-linked polymers with structure elements such as polynitrile and triazine.

1. Introduction

For constructing low-dimensional and metal-like organic materials, recently many efforts have been made to synthesize new

classes of molecular and polymeric compounds such as TTF-TCNQ[1,2] and polyacetylene[3,4]. Phthalocyanines (1:MPc)[5-11] and their polymeric derivatives[12-16] also have attracted a good deal of attention as organic semiconductors because of their interesting electronic and optical properties. In a previous work[17], phthalocyanine polymer was synthesized from 1,2,4,5-tetracyanobenzene(2:TCNB) vapor on substrates such as a KCl crystal and a Cu plate according to the method by D.Wöhrle[18,19]. Thin films of octacyanometalphthalocyanines (3:$MPc(CN)_8$, M=K_2,Cu) were produced on these substrates as a precursor of phthalocyanine polymer by the reaction at temperatures between 250 and 400°C. The films were composed of tentacle-like crystals intertwisted each other on the substrate. The film included extra metals more than would be required for coordination in phthalocyanine rings and the metals were distributed uniformly in the film. High resolution electron micrscopic observation of the thin crystal produced on KCl[20] has elucidated that $K_2Pc(CN)_8$ molecules coordinate to intercalated potassium atoms to form a charge transfer complex of $K_2Pc(CN)_8$-K. The reaction of TCNB with KCl or Cu above 450°C produced amorphous and continuous films of polymeric metalphthalocyanine (4:poly-MPc, M=K_2,Cu). The ratio of polymeric phthalocyanine to monomeric one increased with elevating reaction temperature. The structure of polymeric phthalocyanines has been considered that phthalocyanine units link each other by the peripheral benzene ring to form either a ribbon or a sheet of parquet pattern. D.Wöhrle has reported[19]

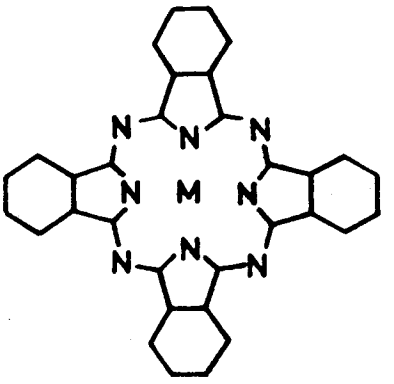

1 : MPc

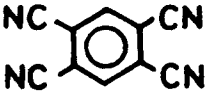

3,4

2 : TCNB

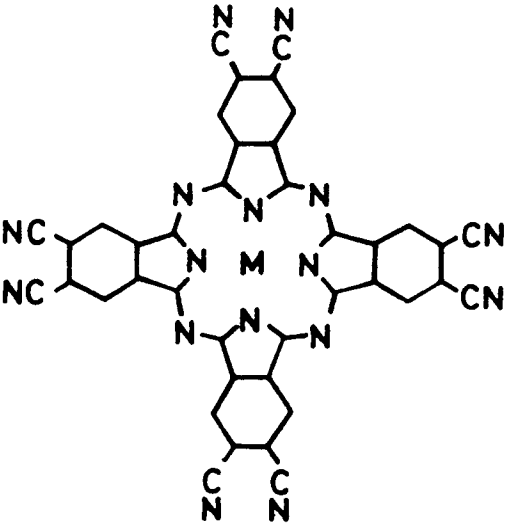

3: $MPc(CN)_8$

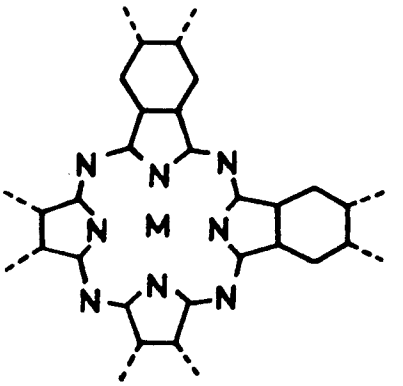

4 : poly-MPc

that the structure of polymer is affected by condition of the reaction. He has pointed out that polymeric phthalocyanines with uniform structure are obtained only in a limited reaction condition and that the molecular weights cannot be examined owing to the poor solubility of polymers. Thus, further informations are required for determination of their detailed structure.

In this chapter, thin films were prepared by the reaction of TCNB vapor with various substrates such as KCl, Cu, Ni, Co, Fe and Zn. The products were characterized by infrared and UV/Visible spectroscopy and morphology of the films was observed by scanning electron microscopy. The composition of the films produced on the substrates was examined by photoelectron spectroscopy and X-ray microanalysis.

2. Experimental

Synthesis A sample of TCNB was synthesized from pyromellitic dianhydride by the method of Bailey et al.[21]. The crude TCNB was purified by recrystallization from acetic acid. The substrate materials used were a cleavage surface of a KCl single crystal and metallic films. As metallic films, Cu, Ni, Co, Fe and Zn were evaporated on a cleavage surface of KCl which had been preheated at 150 °C and then kept at room temperature in a vacuum of 1×10^{-4} Pa. The refined TCNB and the substrate material were sealed in an evacuated pyrex glass tube at 10Pa after flushing with argon gas. The tube was heated at a temperature between 250 and 450 °C for 10 hr in a hot air oven. After the reaction the tube was opened in air at room temperature.

Infrared and UV/VIS Spectra Infrared spectra were recorded on a Shimazu 20 DXB spectrometer. The produced films were milled and pressed together with the substrates and examined by the KCl tablet method. The films were dissolved in concentrated sulfuric acid and UV/VIS spectra of the solutions were recorded by a Shimazu UV-240 spectrometer.

Photoelectron Spectroscopy X-ray photoelectron spectra (XPS) were taken on a KRATOS EXAM800, using MgK_{α} radiation ($h\nu$ = 1254eV). A produced film on a substrate was directly attached to a sample holder. All measurements were performed at a pressure of $1x10^{-7}$Pa in the analyzing chamber. Surface cleanliness was checked by scanning through the region of binding energy from 0 to 1150 eV. The binding energy was calibrated by a thin gold film vacuum-deposited on the sample, taking the $Au(4f_{7/2})$ peak as reference at 83.8eV. The C(1s) spectra were deconvoluted with Gaussian curves after subtraction of the background. The spectra of the films were compared with those of metal-free octacyanophthalocyanine ($H_2Pc(CN)_8$) synthesized by Wöhrle et al.[18] and copper phthalocyanine (CuPc) evaporated on a cleavage surface of KCl. The sample of powdered $H_2Pc(CN)_8$ was examined on a indium plate.

Scanning electron microscopy and X-ray microanalysis Morphology of the films produced on substrates was observed by the SEM mode of a JEM-200CX electron microscope. Metal distribution in the films was analyzed by a Kevex-7000 energy dispersive X-ray spectrometer.

3. Results and Discussion

(1) UV/VIS spectra

Films with green or dark blue color were formed on the substrates of Ni, Co, Fe and Zn films by reaction of TCNB at temperatures from 250 to 400°C. The films produced below 300°C were soluble completely in concentrated sulfuric acid. Figure 1 shows UV/VIS absorption spectra of solutions of the films produced at 300°C. The absorption peaks of each spectrum are listed in Table 1. The films produced on Ni, Co, Fe and Zn films showed identical absorption bands with those of octacyanometalphthalocyanines ($MPc(CN)_8$) reported by Wöhrle et

Table 1. UV/VIS absorption data of films produced on substrates at 300°C and various octacyanophthalocyanines in conc. sulfuric acid.

compound	Q band (nm)	Soret band (nm)
film on Ni	746, 694, 664, 632	396, 343, 291, 227, 212
film on Co	745, 692, 662, 629	398, 344, 290, 230, 211
film on Fe	746, 683, 663, 632	400, 342, 288, 226, 212
film on Zn	747, 693, 664, 632	402, 344, 290, 226, 200
$K_2Pc(CN)_8$ [17]	747, 694, 663, 632	400, 343, 311, 292, 213
$CuPc(CN)_8$ [17]	738, 691, 660, 629	389, 314, 290, 238, 204
$H_2Pc(CN)_8$ [18]	742, 691, 660, 638	390, 343, 290, 230, 210

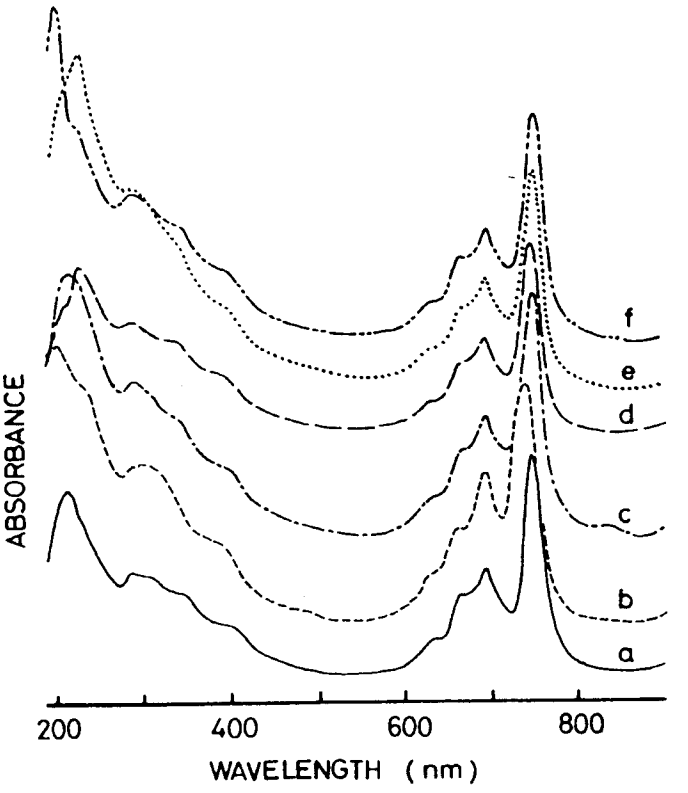

Fig.1 UV/VIS spectra (in conc. sulfuric acid) of films produced on KCl(a), Cu(b), Ni(c), Co(d), Fe(e) and Zn(f) at 300 °C.

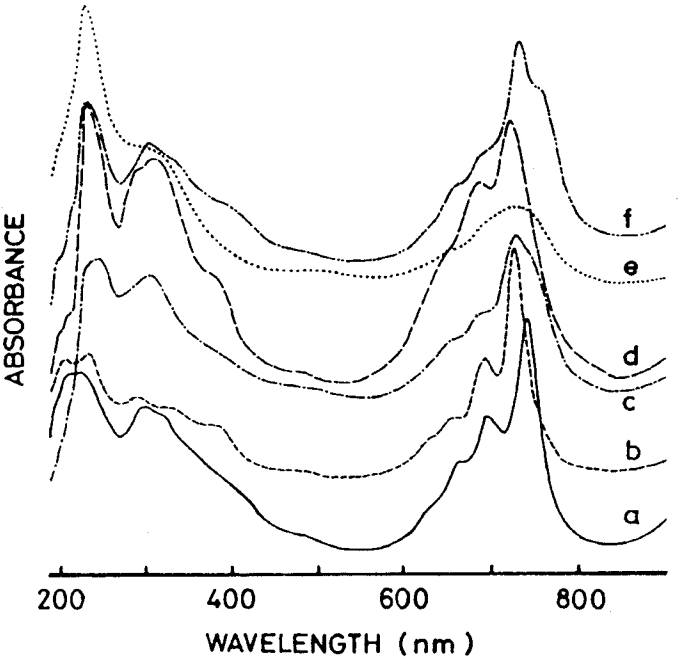

Fig.2 UV/VIS spectra (in conc. sulfuric acid) of films produced on KCl(a), Cu(b), Ni(c), Co(d), Fe(e) and Zn(f) at 450°C.

al.[18]. The intense bands in the 600-750 and 200-400 nm regions are assigned respectively as Q-band and Soret band caused by $\pi-\pi^*$ transitions in phthalocyanine macrocycles. The maximum peaks in Q-band of those products appear at shorter wave length than those of metal phthalocyanines (MPc)[22]. This shift of Q-band peaks is caused by the electron withdrawing effect of peripheral nitrile groups in $MPc(CN)_8$ molecules. Because the electronegative nitrile groups attract a certain amount of electrons from the conjugated π electron system of the Pc macrocycle, the ground state of π electrons becomes a lower energy level giving rise to increase the $\pi-\pi^*$ transition energy. Therefore, Q-band peaks of $MPc(CN)_8$ shift to shorter wave lengths. The films became less soluble in concentrated sulfuric acid with elevating the reaction temperature. The films produced at 350 °C contained a small amount of insoluble portion in concentrated sulfuric acid, and those at 400 °C contained a considerable amount of insoluble one. The soluble portions of the films produced on the substrates at 350 and 400 °C, except the film produced on Zn at 400 °C, showed the same spectra as those produced at 300 °C. The films produced on the substrates at 450 °C were gray and black color with metallic gloss and had a very limited solubility in concentrated sulfuric acid. Figure 2 shows UV/VIS absorption spectra of the soluble portions of the films produced at 450 °C. The film produced on Zn at 400 °C showed the same spectrum as that at 450 °C. The absorption bands became broader and the maximum peaks in Q-band shifted to shorter wave length by 15 to 21 nm than those of the films produced at 300 °C.

The blue shifts of Q-bands have been observed for associated porphyrins[23] and phthalocyanines[24,25], dimeric phthalocyanines[26,27], and cofacially polymerized phthalocyanines[13]. These shifts were discussed in terms of exciton coupling[28] which is based on interaction between the excited states of phthalocyanine molecules. On the other hand, Wörhle et al.[19] have found a red shift of the maximum peak in Q-band for polymerized metal phthalocyanines and they concluded that the red shift was caused by intramolecular π electron delocalization in the phthalocyanine polymer. In the present case, it is considered that the soluble portion of the films produced at 450 °C is associated $MPc(CN)_8$ or oligomeric phthalocyanines with low molecular weight and that the insoluble portion of the films produced above 350 °C is polymerization products of TCNB with high molecular weight.

(2) Infrared spectra

Figure 3 shows IR absorption spectra of the films produced on metal substrates at 350 °C. The absorption bands are listed in Table 2. The spectra of the films produced on Ni, Co, Fe and Zn showed similar absorption bands to those of $K_2Pc(CN)_8$ and $CuPc(CN)_8$[17] though slight changes of wave number. Absorption bands in a range from 1000 to 1600 cm^{-1} are characteristic ones of phthalocyanines, which are assigned to C-C and C-N stretching in a phthalocyanine skeleton. The absorption bands with high intensity at 2220-2240 cm^{-1} are ascribed to C≡N stretching of peripheral nitrile groups of $MPc(CN)_8$ molecules. In the case of

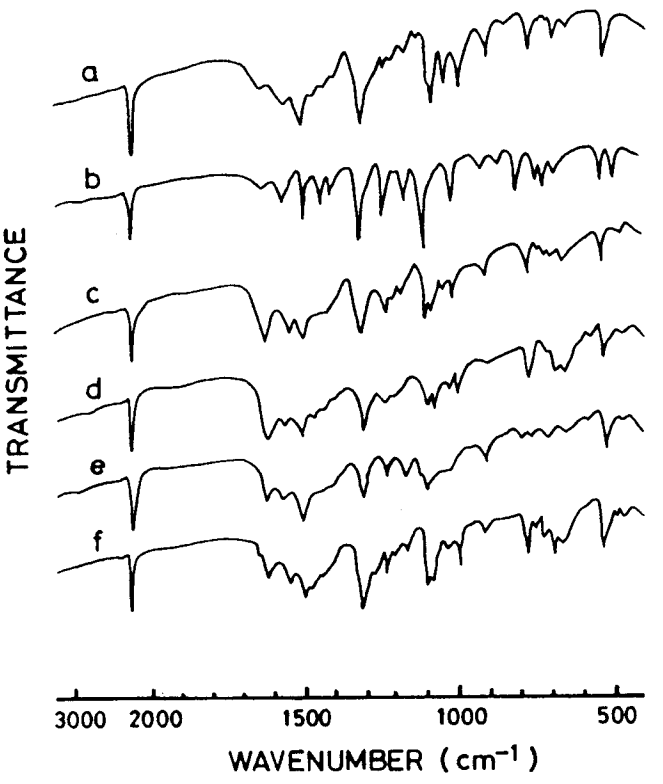

Fig.3 Infrared spectra of films produced on KCl(a), Cu(b), Ni(c), Co(d), Fe(e) and Zn(f) at 350°C.

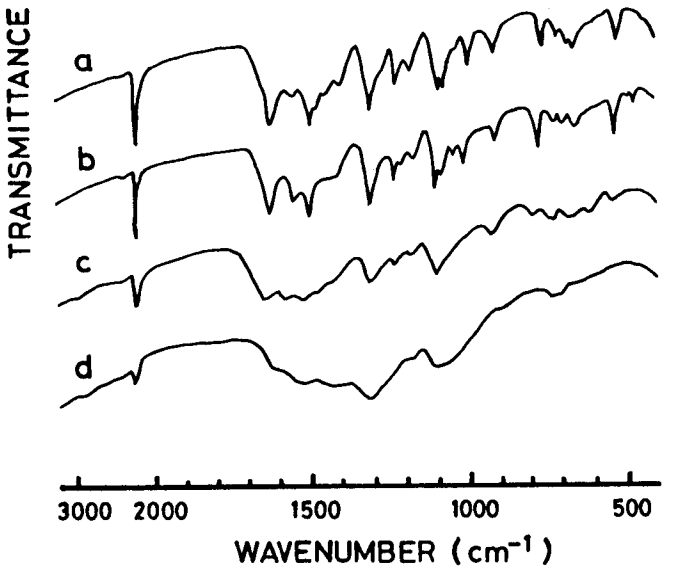

Fig.4 Infrared spectra of films produced on Ni at 300°C(a), 350°C(b), 400°C(c) and 450°C(d).

Table 2. Infrared absorption bands of $K_2Pc(CN)_8$, $CuPc(CN)_8$ and films produced on various metal substrates at 350 °C.

assignment	compound					
	$K_2Pc(CN)_8$ [17]	$CuPc(CN)_8$ [17]	film on Ni	film on Co	film on Fe	film on Zn
	716w	720m	710w	712w	715w	715w
def.(C-H)	787s	800m	765m	765m	765w	766m
					795w	
	924m	870w	915w	910m	910m	915m
			995m	996m	995w	995m
	1022m	1020m	1025w	1025w	1020m	1020w
	1082s		1075m	1080m		1080s
	1105s	1095s	1100s	1100s	1100s	1100s
str.(C-C)	1165w	1165w	1165w	1164w	1168m	1160w
str.(C-N)	1231m	1230s	1220w	1225w	1220m	1225w
str.(C=N)	1318s	1310s	1310s	1310s	1310s	1305s
	1449w	1460m	1410w		1400w	1440w
	1498m	1500w	1500m	1510m	1510s	1500m
	1555w	1550w	1540m		1560m	1550m
	1610w	1615w	1620m	1610s	1620m	1620m
str.(C≡N)	2231s	2230s	2225s	2230s	2220s	2240s
$\frac{I_{2220-2240}}{I_{1095-1105}}$	0.51	0.78	1.01	1.32	1.33	1.04

$MPc(CN)_8$ the band appears at 2220 cm^{-1} independent of metals[19]. In the present case, however, the bands are higher wave number than 2220 cm^{-1} depending on kinds of metal. In a previous work[20], the film produced on KCl formed a complex of $K_2Pc(CN)_8$-K by coordination of the peripheral nitrile groups with intercalated potassium atoms. It is assumed that a certain amount of charge is transferred from the potassium atom to the nitrile groups by this coordinate bond. The band of C≡N may be affected by this charge transfer which depends on electronic configuration of metal atoms. Therefore, the shift suggests that the films produced on the metal substrates form similar complexes between the nitrile groups and the respective metals. The formation of these complexes will be confirmed by direct imaging of the thin films with high resolution electron microscopy as described in Chapters 2 and 3. The ratio of absorption intensity of the nitrile group at 2220-2240cm^{-1} to the characteristic band of MPc at 1095-1105cm^{-1}, listed in Table 2, reveals a quantitative value of the nitrile groups per phthalocyanine unit[29]. Those ratios of the films produced on Ni, Co, Fe and Zn are larger than those of $K_2Pc(CN)_8$ and $CuPc(CN)_8$[17]. It suggests that $MPc(CN)_8$ units are less produced in the reaction with Ni, Co, Fe and Zn in comparison with $K_2Pc(CN)_8$ and $CuPc(CN)_8$ produced in the reaction with KCl and Cu. It is also noted that the films on Ni, Co, Fe and Zn show absorption bands at 1610-1620 cm^{-1}, which are stronger than those of the films on KCl and Cu. Lin et al.[30] have observed this band for polymeric copper phthalocyanine and Wöhrle et al.[19] have reported that this

absorption band is attributed to -C=N-C=N- linkage in polynitrile structure (5) produced by polymerization of nitrile groups. Therefore, it is considered that the films produced on Ni, Co, Fe, Zn contain a certain amount of polynitrile, and their structural uniformity is poor in comparison with those of the films produced on KCl and Cu. Figure 4 shows infrared spectra of the films produced on Ni at various reaction temperatures. The films produced at 300 and 350 °C showed almost same absorption bands. The spectrum of the film produced at 400°C showed some signs of structural change. The absorption of C≡N stretching at 2225 cm^{-1} decreased to a small band and other absorption bands became broader than those of the films produced below 350°C. The spectrum of the film produced at 450 °C showed a very weak absorption at 2225 cm^{-1} and a broad band without fine structure between 1600 and 1000 cm^{-1}. The ratios, I_{2225}/I_{1100}, decrease with elevating of reaction temperature. The films produced on Co ,Fe and Zn showed the same inclination of the spectra with elevating the reaction temperature. It seems that phthalocyanine

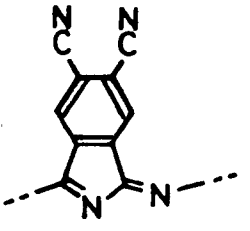

5

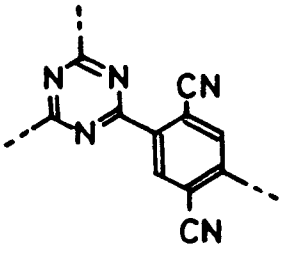

6

units link each other to form poly-MPc and polynitriles polymerize each other by their residual peripheral nitrile groups to form cross-linkage such as triazine structure (6) at high temperature[19]. These polymeric products are considered to correspond to the insoluble portions of the films in concentrated sulfuric acid as mentioned in the previous section.

(3) Photoelectron spectroscopy

Figure 5 shows C(1s) XPS spectra of CuPc, $H_2Pc(CN)_8$, and the films produced on KCl and Cu at 350 °C. The spectra were deconvoluted to bands shown with dashed lines and the data were summarized in Table 3. The spectrum of CuPc consists of two C(1s) peaks with an intensity ratio of 1:3 because the molecule has eight carbon atoms bonding with two nitrogen atoms and 24 carbon atoms in benzene rings[31,32]. The spectrum of $H_2Pc(CN)_8$ shows three C(1s) peaks in relative intensity of about 1:2:6. The lowest energy peak is attributed to the carbons of benzene rings and the intermediate peak to the carbons bonding with two nitrogen atoms. The third peak with FWHM of 2.5 eV is observed at 288.6 eV. As well-known, a satellite peak which is accompanied with the C(1s) peak is observed at about 288 eV for H_2Pc and MPc[32,33]. However, the third peak indicates a considerably strong intensity and a large FWHM for $H_2Pc(CN)_8$ as compared with that of the satellite peak. Chemical shifts in photoelectron spectrum of core electrons are caused by variation of valence electron state. Nitrile groups polarize to draw the valence electrons from the carbon atom to the nitrogen atom, and

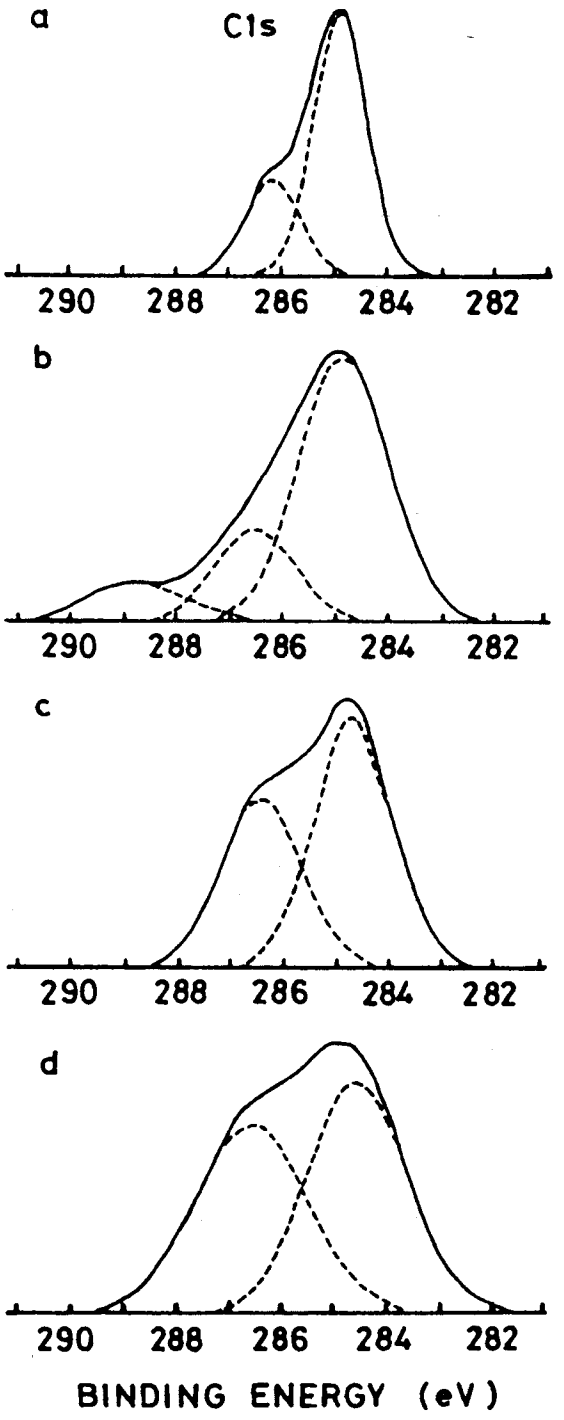

Fig.5 Carbon 1s photoelectron spectra of CuPc(a), $H_2Pc(CN)_8$(b) and films produced on KCl(c) and Cu(d) at 350°C.

Table 3. Carbon 1s photoelectron spectroscopic data of CuPc, $H_2Pc(CN)_8$, and the films produced on KCl and Cu at 350°C.

compound	binding energy (eV)	FWHM* (eV)	integrated** area
CuPc	284.8	1.2	72.5
	286.1	1.2	25.9
$H_2Pc(CN)_8$	284.7	2.0	66.5
	286.4	1.8	20.7
	288.6	2.5	11.6
film on KCl	284.6	1.7	59.7
	286.3	1.8	42.3
film on Cu	284.5	2.2	51.2
	286.5	2.5	46.2

*) Full width at half maximum.
**) The ares evaluated from deconvoluted bands are considered accurate to ±5%.

core electrons in the carbon atom are attracted to the nucleus more tightly than those in an isolated carbon atom. Therefore, the binding energy of C(1s) electron in the nitrile groups is higher than that of normal carbon atoms. Thus, the third peak of $H_2Pc(CN)_8$ may be assigned to the carbon of the peripheral nitrile groups. However, the intensity ratio of the nitrile group is smaller than that estimated from the molecular structure of $H_2Pc(CN)_8$, which would give the intensity ratio of 1:1:3. The finding suggests that the sample of $H_2Pc(CN)_8$ would include a certain amount of polymeric products such as poly-MPc and

triazine structure, because contents of nitrile groups in these compounds are lower than that of $H_2Pc(CN)_8$. The C(1s) spectrum of the film produced on KCl showed two peaks with the intensity ratio of 2:3 but the third peak ascribed to the nitrile groups was not observed in the spectrum and the peak of high energy is twice intensity that of CuPc. The film produced on KCl is composed of a $K_2Pc(CN)_8$-K complex crystal, in which half of nirile groups coordinate to the intercalated potassium atom and other ones overlap in antiparallel between the adjacent $K_2Pc(CN)_8$ molecules owing to counterbalance of the opposite polarity of $-C\overset{\delta+}{\equiv}N^{\delta-}$, as described in Chapter 2. Because the polarization in -C≡N is relaxed by the coordinate bond and antiparallel overlap, the C(1s) spectrum from nitrile groups in the complex crystal would shift to lower energy than that of the nitrile groups in $H_2Pc(CN)_8$. Consequently, the peak of high energy in the film produced on KCl is ascribed to eight carbons in the nitrile groups and eight carbons bonding with nitrogen atoms in a Pc ring, and the peak of low energy to 24 carbons in the benzene rings of a $K_2Pc(CN)_8$ molecule. The C(1s) spectrum of the film produced on Cu showed two peaks similar to that of the film produced on KCl and did not show the third peak ascribed to isolated nitrile groups. It suggests that the film on Cu is composed of a $CuPc(CN)_8$-Cu complex crystal, which is the isomorphous crystal of the $K_2Pc(CN)_8$-K crystal.

Figure 6 shows N(1s) spectra of CuPc, $H_2Pc(CN)_8$, and the films produced on KCl and Cu at 350°C. The N(1s) peak of $H_2Pc(CN)_8$ is broad because a $H_2Pc(CN)_8$ molecule has four kinds of nitrogen

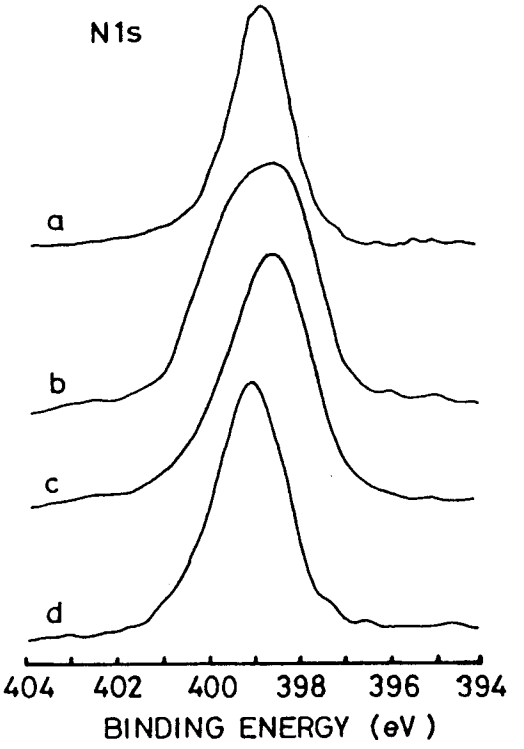

Fig.6 Nitrogen 1s photoelectron spectra of CuPc(a), $H_2Pc(CN)_8$(b) and films produced on KCl(c) and Cu(d) at 350°C.

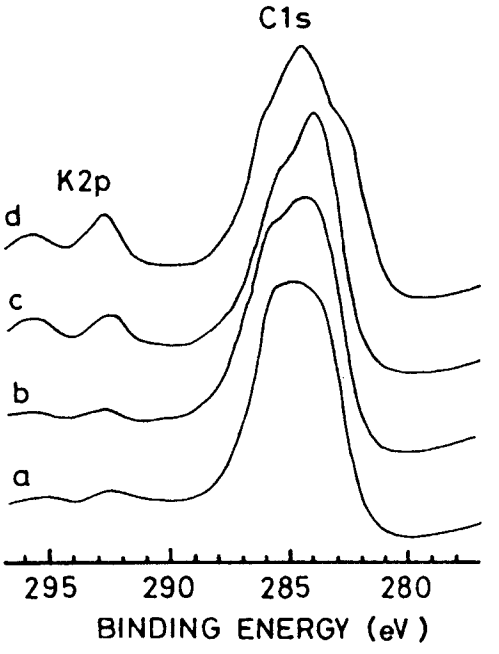

Fig.7 Carbon 1s and potassium 2p photoelectron spectra of films produced on KCl at 300°C(a), 350°C(b), 400°C(c) and 450°C(d).

atoms, that is, two nitrogens bonding with inner protons and two aza nitrogens in the central part, four meso-bridging aza nitrogens, and eight nitrogens of the peripheral nitrile groups. On the other hand, the N(1s) spectrum of CuPc showed a narrow peak, because energy separation between four equivalent central nitrogens and four meso-bridging aza nitrogens is estimated to be small[33]. The N(1s) spectra of the films produced on KCl and Cu also showed relatively narrow peaks. The nitrogen atoms of the peripheral nitrile groups seem to have a binding energy close to those of the other nitrogens in $K_2Pc(CN)_8$ and $CuPc(CN)_8$ molecules owing to formation of the complex crystals. The films produced on Ni, Co, Fe and Zn at 350 °C showed similar N(1s) spectra to those of films produced on KCl and Cu.

Figure 7 shows C(1s) and K(2p) spectra of the films produced on KCl at various temperatures. The film produced at 300°C shows one broad C(1s) peak, which can not be separated to two peaks by deconvolution. It suggests that octacyanophthalocyanine is not formed completely at 300 °C, and the film would contain a certain amount of products with low molecular weights. In the film produced at 400 °C, the peak of high energy of C(1s) spectrum shows a large intensity and K(2p) spectrum emerges clearly. The film produced at 450 °C shows a C(1s) shoulder of low energy at about 283 eV. Such a low energy C(1s) peak is well-known for graphite, which consists of a planar conjugated system of π electrons. It seems that the film produced at 450°C is composed of poly-MPc and cross-linked planar polymers with structure elements such as polynitrile and triazine. The intensity of

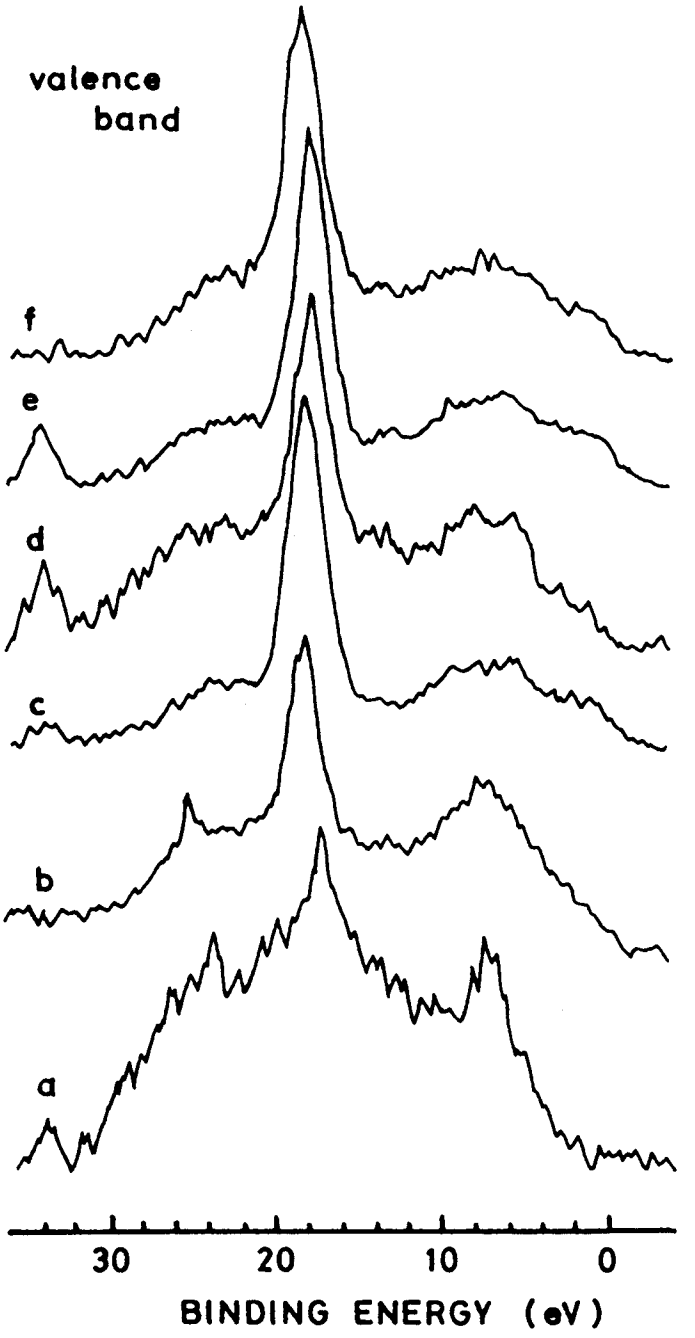

Fig.8 Valence band photoelectron spectra of films produced on KCl(a), Cu(b), Ni(c), Co(d), Fe(e) and Zn(f) at 350°C.

K(2p) peak increased with elevating the reaction temperature. It indicates that more potassium atoms diffuse from the substrate to the surface of the produced film as temperature increases.

Figure 8 shows valence band spectra of the films produced on the various substrates at 350 °C. The spectrum of the film produced on KCl is in good agreement in binding energy from 8 to 30 eV with that of phthalocyanines reported by Höchst et al.[32]. The valence band spectra in this region of phthalocyanines were explained as the spectra of benzene and pyrrole and the spectra were not interfered by the bond between central metals and Pc ligands[32,33]. The spectrum of the film produced on Cu shows similar peaks to those of the film produced on KCl although their relative intensities are different. The spectral features of the films produced on Ni, Co, Fe and Zn deviate from that of the film produced on KCl and the relative intensities in their spectra are different from that of phthalocyanines. It seems that the spectral deviation is ascribed to less yield of $MPc(CN)_8$ in these films as compared with the films produced on KCl and Cu.

(4) Scanning electron microscopy and X-ray microanalysis

Figure 9 shows scanning electron micrographs of sections of the films produced on Cu at various temperatures and distributions of Cu measured by EDS in which the electron beam was scanned from the surface to the bottom of the film along the center line of the figure. The film produced at 250 °C is composed of long and slender crystals of the $CuPc(CN)_8$-Cu complex. At 350 °C, the

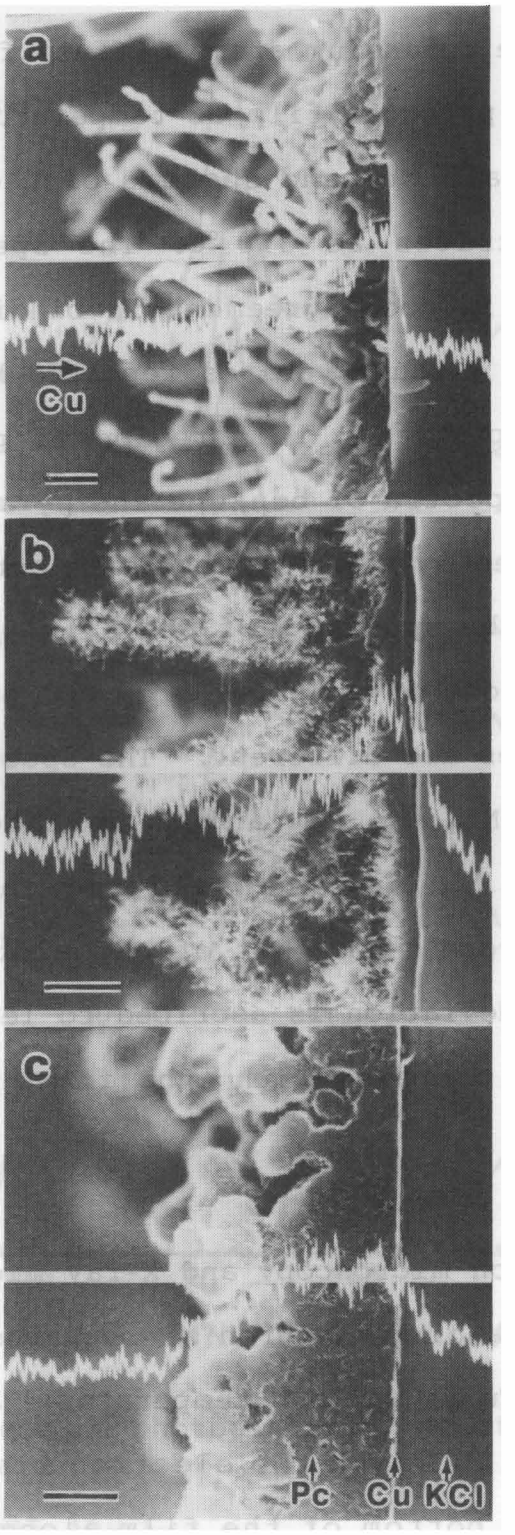

Fig.9 Scanning electron micrographs and X-ray microanalyses of copper of films produced on Cu at 250°C(a),350°C(b) and 450°C(c). Bar=5μm.

crystals grow thin and fine tentacle-like ones branching from each thick crystal. The EDS signals show that Cu atoms are distributed from the bottom to the surface of the film and the tentacle-like crystals contain Cu atoms. At 450°C, the film is composed of an amorphous thick layer with bulb-like crystals on the surface. The thick layer is considered to be highly polymerized products of poly-MPc and cross-linked polymers with structure elements such as polynitrile and triazine which are insoluble in concentrated sulfuric acid.

Figure 10 shows morphology of the films produced on various substrates at 350 °C and distribution of the respective metal atoms. The film on KCl is composed of long tentacle-like crystals of the $K_2Pc(CN)_8$-K complex as observed previously[17]. These crystals grow directly on the surface of the KCl substrate. On the other hand, the films on Ni, Co, Fe and Zn consist of three layers, that is, a thin metal layer evaporated on KCl, a thick amorphous layer, and tentacle-like crystals in the top layer. The EDS signals show that the respective metals are distributed from the substrates to the surfaces of the films. The tentacle-like crystals are considered to be $MPc(CN)_8$-M (M=Ni, Co, Fe and Zn) complexes, because their morphology resembles that of the $K_2Pc(CN)_8$-K complex. It seems that the amorphous layer contains polynitriles which condense among the tentacle-like crystals. Furthermore, this layer may correspond to the insoluble portion in concentrated sulfuric acid, because the film on Cu (Fig.9 (b)) which has only a thin amorphous layer shows a higher solubility than the others.

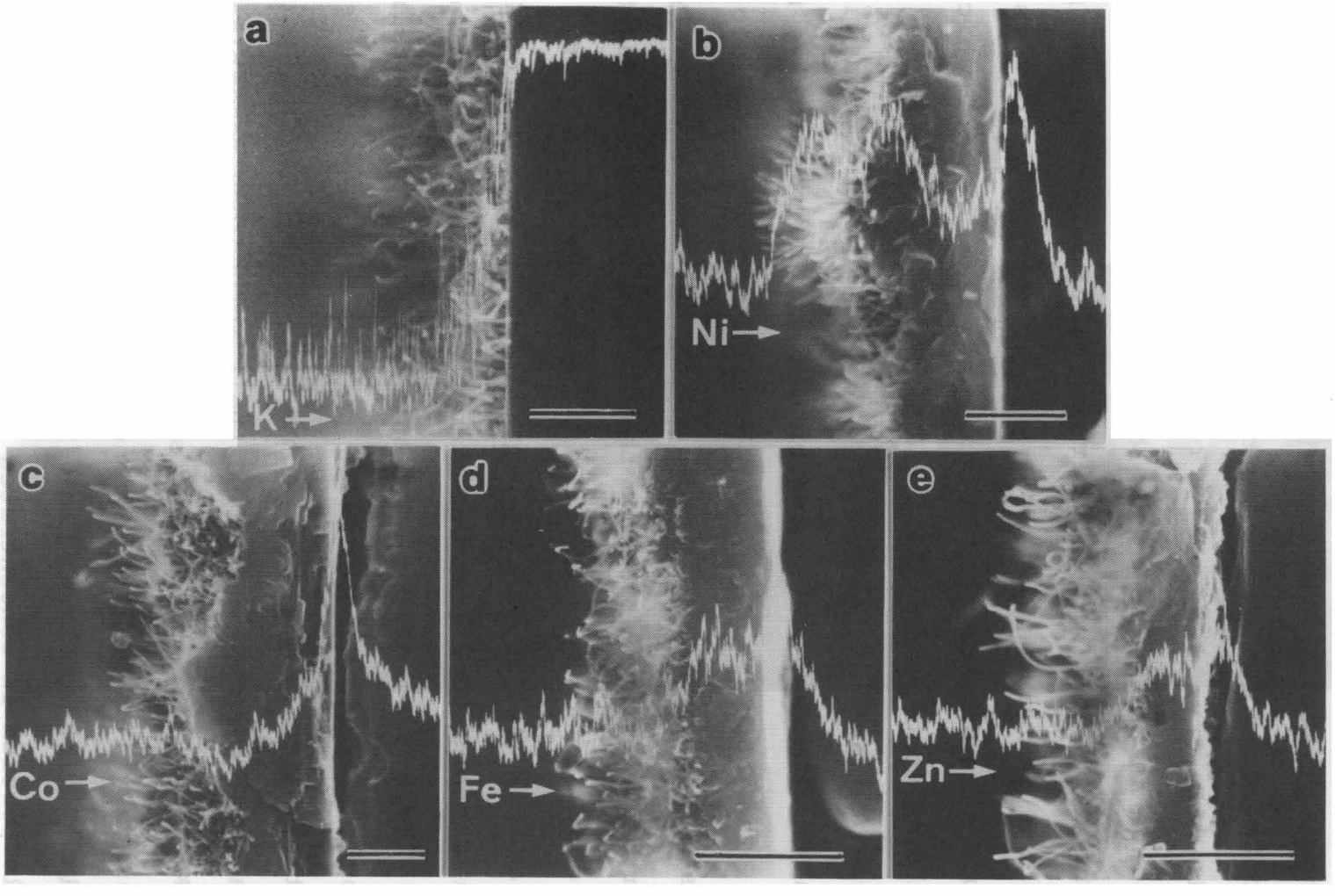

Fig.10 Scanning electron micrographs and X-ray microanalyses of films produced on KCl(a), Ni(b), Co(c), Fe(d) and Zn(e) at 350 °C. Bar=5μm.

Consequently, the films produced on Cu, Ni, Co, Fe and Zn below 400 °C contained $MPc(CN)_8$ (M=Cu, Ni, Co, Fe and Zn) and polymerized products such as polynitrile. The $MPc(CN)_8$ molecules formed tentacle-like crystals of the $MPc(CN)_8$-M complex and were soluble in concentrated sulfuric acid. The $MPc(CN)_8$-M complexes were less produced in these films in comparison with $K_2Pc(CN)_8$-K in the film produced on KCl. The polymerized products formed amorphous layers, which were insoluble in concentrated sulfuric acid. These polymerized products increased in the films with elevating the reaction temperature. The film produced at 450 °C contained highly polymerized products of poly-MPc and cross-linked polymers with structure elements such as polynitrile and triazine. The small amount of soluble portion in concentrated sulfuric acid was identified as associated $MPc(CN)_8$ or oligomeric phthalocyanines.

References

[1] J.Ferraris, D.O.Cowan, V.V.Walatka.Jr. and J.H.Perlstein, J. Am. Chem. Soc. 95 (1973) 948.

[2] L.B.Coleman, M.J.Cohen, D.J.Sandman, F.G.Yamagishi, A.F.Carito and A.J.Heeger, Solid State Commun. 12 (1973) 1125.

[3] H.Shirakawa and S.Ikeda, Polym.J. 2 (1971) 231.

[4] H.Shirakawa, E.J.Louis, A.G.MacDiarmid, C.K.Chiang and A.J.Heegar, J.Chem.Soc. Chem. Commun.(1977) 578.

[5] A.Girandeau, F.R.F.Fan and A.J.Bard. J.Chem.Soc. 103 (1980) 5137.

[6] C.J.Schramm, R.P.Scaringe, D.R.Stojakovic, B.M.Hoffmann, J.A.Ibers and T.J.Marks, J.Am. Chem.Soc. 102 (1980) 6702.

[7] B.N.Diehl, T.Inabe, J.W.Lyding, K.F.Schoch, C.R.Kannewurf and T.J.Marks, J.Am.Chem.Soc. 105 (1983) 1551.

[8] Z.D.Popovic and J.H.Sharp, J.Chem.Phys. 66 (1977) 5076.

[9] E.R.Menzel and R.O.Loufty, Chem.Phys.Lett. 72 (1980) 522.

[10] R.O.Loufty, J.H.Sharp and C.K.Hsiao and R.Ho, J.Appl.Phys. 52 (1981) 5218.

[11] R.O.Loufty and L.F.McIntyre, Can.J.Chem. 61 (1983) 73.

[12] R.S.Nohr, P.M.Kuznesof, K.J.Wynne, M.E.Kenny and P.G.Siebenman, J.Am. Chem. Soc. 103 (1981) 4371.

[13] C.W.Dirk, T.Inabe, K.F.Schoch,Jr. and T.J.Marks, J.Am. Chem. Soc. 105 (1983) 1539.

[14] B.N.Diel, T.Inabe, J.W.Lyding, K.F.Schoch,Jr., C.R.Kannewurf and T.J.Marks, J.Am. Chem. Soc. 105 (1983) 1551.

[15] B.N.Diel, T.Inabe, N.K.Jaggi, J.W.Lyding, O.Schneider, M.Hanack, C.R.Kannewurf, T.J.Marks and L.H.Schwartz, J.Am. Chem. Soc. 106 (1984) 3207.

[16] E.Ciliberto, K.A.Doris, W.J.Pietro, G.M.Reinser, D.E.Ellis, I.Fragala, F.H.Herbstein, M.A.Ranter and T.J.Marks, J.Am. Chem. Soc. 106 (1984) 7748.

[17] M.Ashida, Y.Ueda, H.Yanagi and K.Sayo, J.Polym.Sci., Polym.Chem.Ed. received.

[18] D.Wöhrle and U.Hündorf, Makromol.Chem. 186 (1985) 2177.

[19] D.Wöhrle, U.Marose and P.Knoop, Makromol.Chem. 186 (1985) 2209.

[20] M.Ashida, Y.Ueda, H.Yanagi, Y.Fujiyoshi, N.Uyeda and

J.R.Fryer, Acta Cryst. accepted.

[21] A.S.Bailey, R.B.Henn and J.M.Langdon, Tetrahedron 19 (1963) 161.

[22] D.Wöhrle, G.Meyer and B.Wahl, Makromol.Chem. 181 (1980) 2127.

[23] S.Konishi, M.Hoshino and M.Imamura, J. Phys. Chem. 86 (1982) 4888.

[24] M.Abkowitz and A.R.Monahan, J.Chem.Phys. 58 (1973) 2281.

[25] A.T.Davidson, J. Chem. Phys. 77 (1982) 168.

[26] A.R.Kane, J.F.Sullivan, D.H.Kenny and M.E.Kenny, Inorg.Chem. 9 (1970) 1445.

[27] W.A.Nevin, M.R.Hempstead, W.Lui, C.C.Leznoff and A.B.P.Lever, Inorg.Chem. 26 (1987) 570.

[28] M.Gouterman, D.Holten and E.Lieberman, Chem.Phys. 25 (1977) 139.

[29] R.Bannehr, N.Jager, G.Meyer and D.Wöhrle, Makromol.Chem. 182 (1981) 2683

[30] J.W.P.Lin and L.P.Dudek, J.Polym.Sci.,Polym.Chem.Ed. 23 (1985) 1579.

[31] M.V.Zeller and R.G.Hayes, J.Am.Chem.Soc. 95 (1973) 3855.

[32] H.Höchst, A.Goldmann, S.Hüfner and H.Malter, Phys. Stat. Sol.(b) 76 (1976) 559.

[33] Y.Niwa and T.Tsuchiya, J.Chem.Phys. 60 (1974) 799.

Chapter 2 Direct Structure Determination of Octacyanophthalocyanine-potassium Complex Crystal by HREM Image Simulation

Abstract

The molecular arrangement of octacyanophthalocyanine-potassium complex crystal was directly determined from high resolution electron micrographs by comparison to images simulated with the multislice method. The crystal assumed a tetragonal symmetry P4/mcc with lattice parameters a=b=1.570nm and c=0.674nm. The molecular arrangement in the crystal was explained as follows: Octacyanophthalocyanine molecules are piled up in parallel holding their molecular planes perpendicular to the c-axis, and the phthalocyanine rings staggered around the c-axis alternately by $\pm 27.4^{\circ}$ to the a-axis. Each peripheral nitrile group of eight octacyanophthalocyanine molecules coordinates to a potassium atom which is located at the middle of the interlayer. The remaining nitrile groups overlap each other between the adjacent molecules so that they counterbalance their opposite polarity. The observed molecular image was reproduced very closely by the simulated image calculated at 70nm underfocus for the crystal 4nm in thickness.

1. Introduction

Since the molecular image of chlorinated copper phthalocyanine was observed by Uyeda et al.[1], high resolution electron

microscopy (HREM) has been applied to radiation-sensitive organic compounds[2,3]. HREM images should be interpreted by comparison with the computer-simulated images. For some radiation-sensitive organic compounds, a series of molecular images is not taken by the through-focus method, but only one image is taken in the minimum exposure technique[4]. It is necessary to pay attention especially to the interpretation of HREM images from those compounds, because their electron micrographs are not always obtained under the optimum condition. The calculation of dynamical electron scattering was formulated in the multislice method by Cowley and Moodie[5], and this method has been extensively applied in a series of n-Beam Lattice Images[6-11]. The practical computing technique for the multislice calculation has been improved by Ishizuka and Uyeda using a fast Fourier transform(FFT) algorithm[12]. Nowadays, a number of computer programs have been supplied for calculating image simulation with accuracy. In order to simulate HREM images precisely, there are many parameters to be considered for calculation. According to Ishizuka and Uyeda[12], a large number of beams must be included in the multislice iteration, and slice thickness should be properly small. Furthermore, Uyeda et al.[13] indicated that the image contrast was affected significantly by the value of defocus and crystal thickness and that specimens should be as thin as possible when the molecule examined had a complicated structure.

One of the ultimate objectives in HREM study is to determine the structure of an unknown reaction product by the direct observation of the atomic arrangement. In a previous work[14], a

thin crystalline film was formed on a cleavage surface of a KCl substrate by reaction with tetracyanobenzene (TCNB) in a sealed tube. It was determined from elemental analysis and electron spectra that the product was octacyanopotassium-phthalocyanine($K_2Pc(CN)_8$) and was demetallized to metal-free octacyanophthalocyanine($H_2Pc(CN)_8$) shown in Fig.1 when it was dipped in water. The HREM study of the film[15] elucidated that eight $H_2Pc(CN)_8$ molecules coordinated to a potassium atom giving rise to a potassium complex crystallized on the KCl (001) plane. The molecular arrangement of the $H_2Pc(CN)_8$-K complex was determined directly from the molecular image, that was an attempt to determine the crystal structure of an unknown reaction product by means of HREM image. This chapter is concerned with the precise determination of the molecular arrangement in the crystal by comparing the HREM image with the simulated images based on the multislice method.

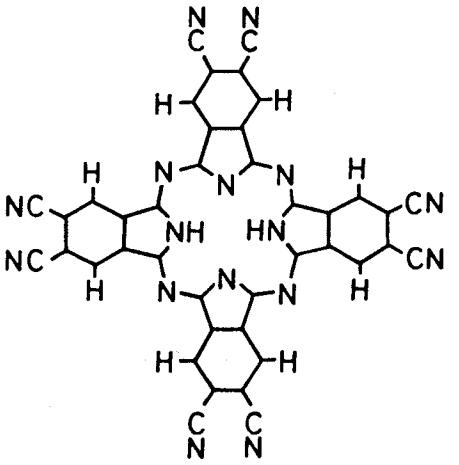

Fig.1 Molecular structure of $H_2Pc(CN)_8$.

2. Molecular and crystal structure

Figure 2 (a) shows a high resolution molecular image of the extremely thin layer of the $H_2Pc(CN)_8$-K crystal. The image was noise-reduced by a translational multiple exposure technique. This real image was found to be in the vicinity of Scherzer focus by the broad scattering band of the carbon film superposed in the optical Fourier transform[15]. The crystal has been determined to assume a tetragonal symmetry (P4/mcc) with lattice parameters a=b=1.570nm and c=0.674nm from its electron diffraction pattern[15]. The intensity distribution in the image was measured optically along the lines X-X' and Y-Y' as shown in Fig.2 (b). Four black rings with a diameter of 0.56nm are situated at each corner of the square in the image, which correspond to tetraazaporphyrin rings in $H_2Pc(CN)_8$ molecules stacked in parallel to the substrate surface. A potassium atom is intercalated at the center of the square lattice, which corresponds to a high intensity peak in the center of the Y-Y' line in Fig.2 (b). Figure 3 shows the schematic explanation of this molecular image projected along the c-axis. The structure of the phthalocyanine skeleton was assumed to be that of metal-free phthalocyanine reported by Robertson[16], and the peripheral nitrile groups bonded to the benzene ring were assumed to make an angle of 120° with the carbon-carbon bond in the benzene ring corresponding to the molecular structure of the tetracyanobenzene crystal[17]. The corner shown with the letter R indicates the overlapping tetraazaporphyrin rings which rotate alternately around the c-axis. Each molecule in the first layer indicated by

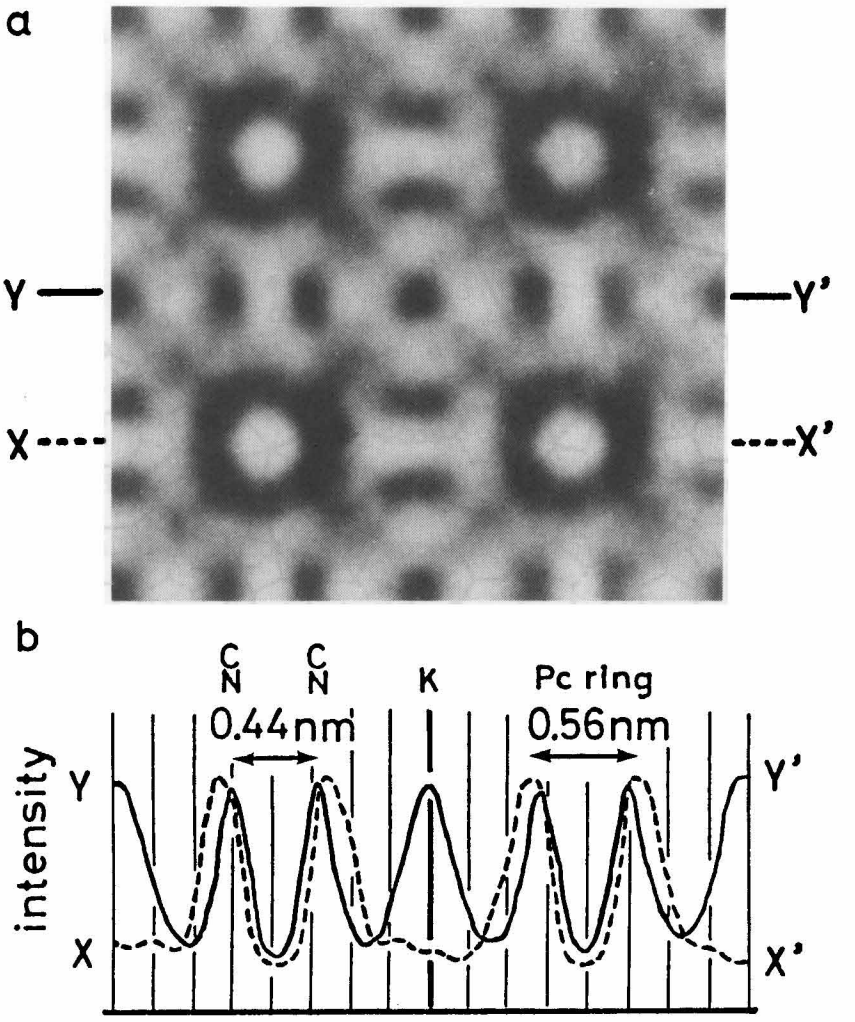

Fig.2 High resolution molecular image projected along the c-axis (a) and intensity distribution along the lines X-X' and Y-Y' (b).

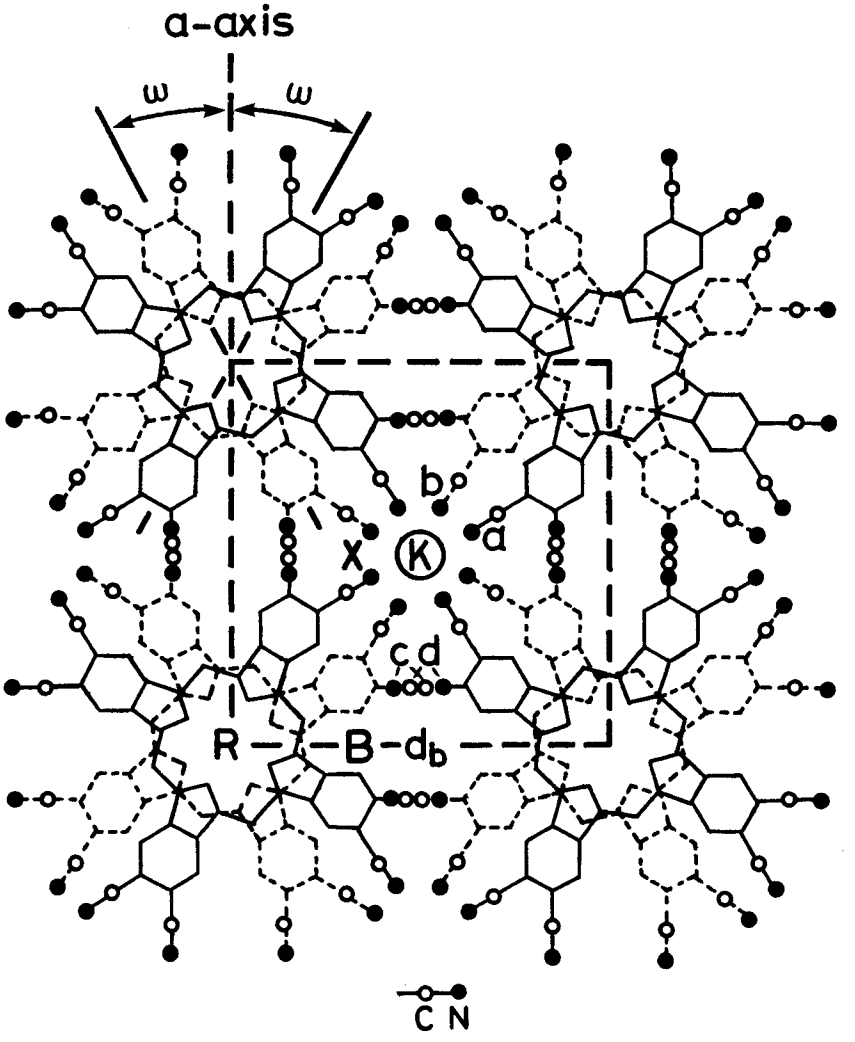

Fig.3 Predicted molecular arrangement in the crystal projected along the c-axis.

a solid line staggers clockwise by the angle ω, and that in the second layer indicated by a dashed line staggers counter-clockwise by the same angle. Therefore, the overlapping molecules rotate by 2ω about each other. The interplanar distance between the layers has been previously determined to be 0.337nm from the high resolution image in which the planar molecules are piled up in parallel along the c-axis[15]. The three-dimensional structure constructed in this way is shown schematically in Fig.4. The $H_2Pc(CN)_8$-K complex crystal is composed of two column structures; one column is the sequence of the staggered $H_2Pc(CN)_8$ molecules and the other is intercalated potassium atoms. Consequently, one potassium atom is interposed at the center of the distorted cube formed by peripheral nitrile groups from eight molecules in the successive layers. Their superposed nitrile groups, coordinated to the potassium atom, form a crossing potential distribution in the area shown with the letter X in Fig.3. These nitrile groups(a and b) are arranged most closely to the potassium atom at angle of ω about 29.3°. When ω is near 30°, however, the other nitrile groups(c and d) overlap in parallel between the molecules in the adjacent columns so that they counterbalance the opposite polarity of the $-C^{\delta+}\equiv N^{\delta-}$ group, as shown in the part of Fig.3 labeled B. These superposed nitrile groups produce the high contrast image of the parallel bars, the distance of which, d_b, is estimated to be 0.44nm from the intensity curve along Y-Y' in Fig.2(b). From these consideration it is assumed that the $H_2Pc(CN)_8$ molecules would be alternately rotated at roughly 30° to the a-axis.

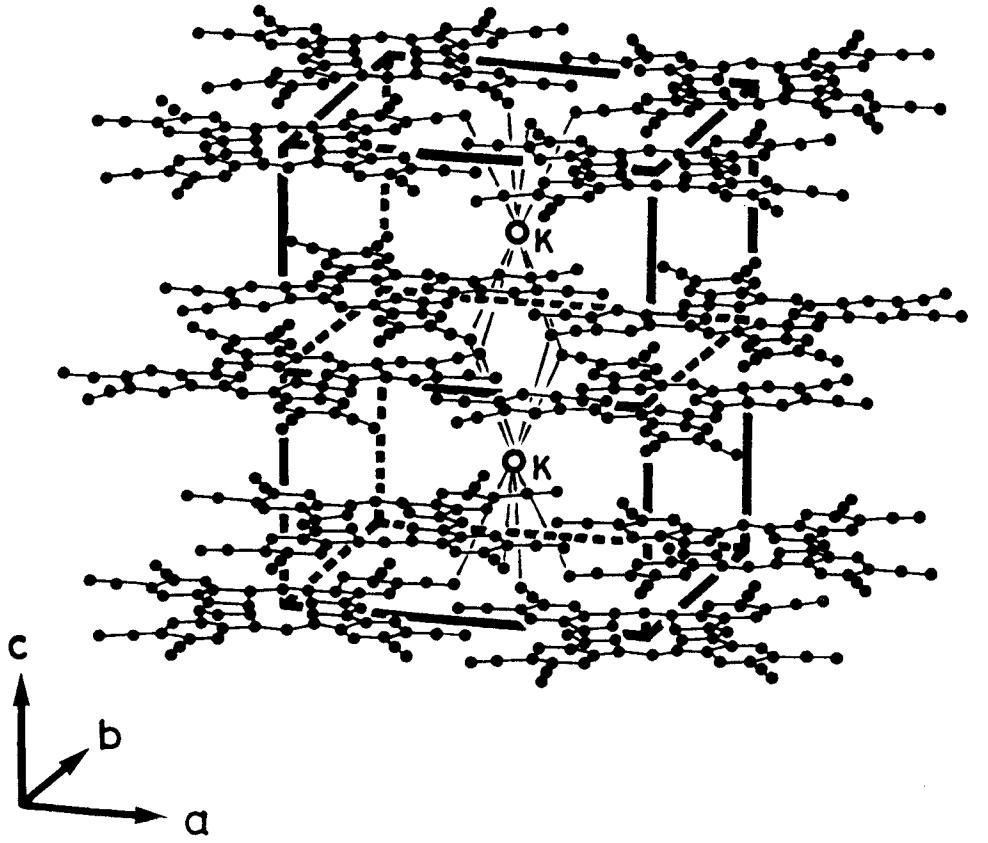

Fig.4 Schematic diagram of the crystal structure of the $H_2Pc(CN)_8$-K complex.

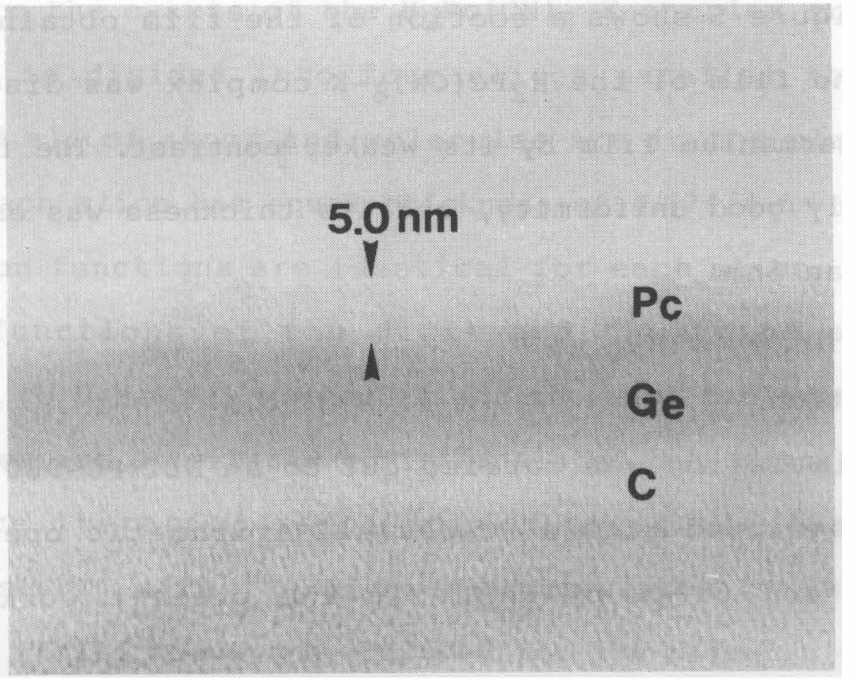

Fig.5 Electron micrograph of the film section by mesh-holding method.

The crystal thickness was obtained directly from the observation of the film section using the mesh-folding method as follows: a specimen film on a KCl substrate was covered with vacuum-evaporated germanium and carbon films, and the film was carefully broken on a microgrid so as to expose the edge of the film. Figure 5 shows a section of the film obtained by this method. The film of the $H_2Pc(CN)_8$-K complex was discriminated from the germanium film by its weaker contrast. The film showed sufficiently good uniformity, and its thickness was estimated to be less than 5nm.

3. Computation

Image simulation was carried out on an NEC PC-9801VM microcomputer equipped with a PC-9801-22 arithmetic operation coprocessor and 640kB of RAM. In the present work, a image

Table 1. Electron microscopic parameters for image simulation

Electron microscope:	JEOL JEM-200CX
Accelerating voltage:	200 kV
Spherical aberration coefficient C_s :	2.0 mm
Defocus spread Δ:	10 nm
Beam divergence α :	0.5 mrad
Scherzer focus (underfocus Δf):	85 nm

simulation system has been developed in the C language under the MS-DOS operating system. The necessary data for the calculation are listed in Table 1. The structure factors are calculated up to 5000 reflections using the atomic scattering amplitudes reported by Smith and Burge[18]. When the incident beam is parallel to the c-axis of the $H_2Pc(CN)_8$-K complex crystal, the unit cell is divided into four slices parallel to the (001) plane, and all of atoms and molecules are in the planes of the slices. Each slice has equal thickness of 0.674/4 nm so that the propagation functions are identical for each slice. The phase grating functions of the first and the third slices are attributed to $H_2Pc(CN)_8$ molecules and those of the second and the forth slices are attributed to intercalated potassium atoms. The multislice iteration is performed using the fast Fourier transforms(FFT) with the algorithm developed by Ishizuka and Uyeda[12]. 64x64 beams are included for the calculation. Figure 6 shows the contrast transfer functions(CTF) calculated over the defocus range around Scherzer focus. The effect of partial coherence was taken into account according to Hanszen[19] and Frank[20]. The angular width α of the illuminating source and the chromatic defocus spread Δ were assumed as reasonable values for the used microscope as shown in Table 1. Representative reciprocal points of the hk0 reflections for the $H_2Pc(CN)_8$-K complex crystal are plotted along the spatial frequency(nm^{-1}) axes. The CTF shows that the Sherzer limit shifts to higher frequency at larger values of underfocus. The CTF curves at 85nm and 95nm underfocus rise to low amplitudes in a concave

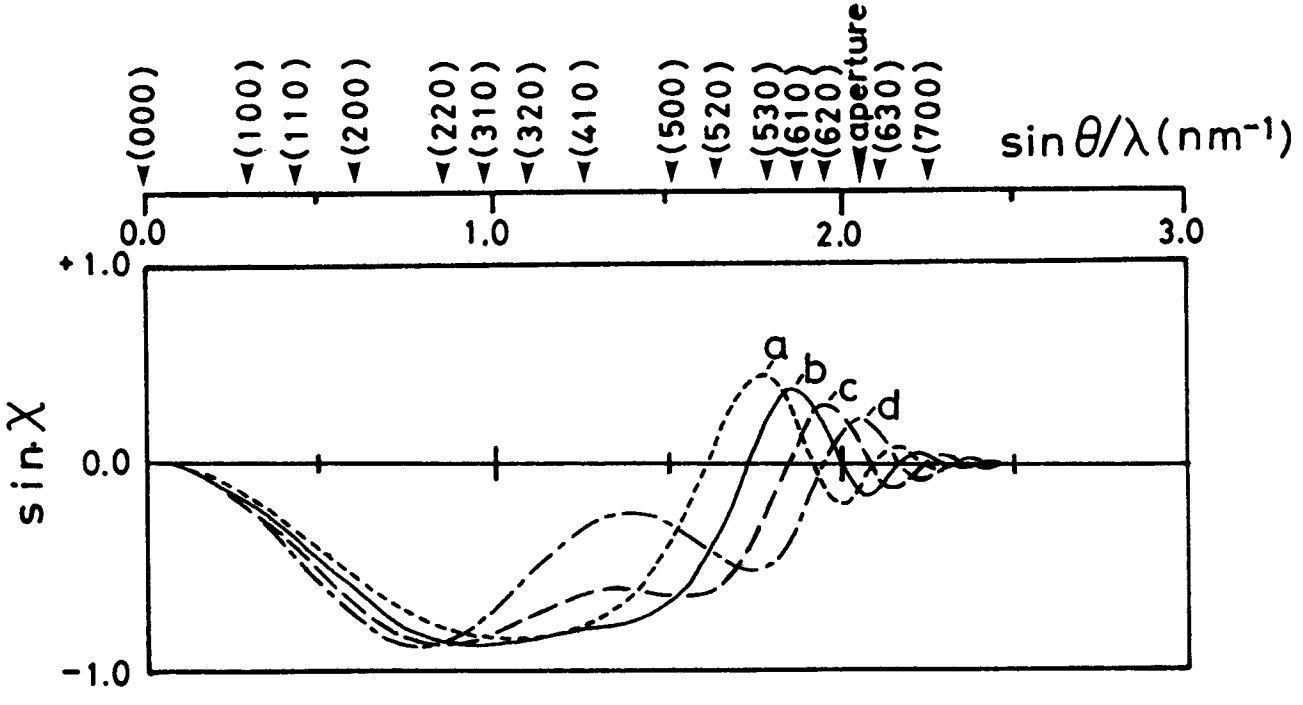

Fig.6 Contrast transfer functions (CTF) at underfocus of 65nm (a), 75nm (b), 85nm (c) and 95nm (d). The representative reflections of the $H_2Pc(CN)_8$-K complex crystal and the practical cut-off by objective aperture are plotted in frequencies ($\sin\theta / \lambda$).

fashion around 1.3nm^{-1}, while those at 65nm and 75nm underfocus have relatively flat plateaus below -0.8 in $\sin\chi$. The objective aperture used for this HREM observation cuts off the waves beyond a frequency of 2.05nm^{-1}. Consequently, 137 scattered waves pass through the objective aperture and contribute to the image formation.

4. Results and discussion

Numerous image simulations were calculated by taking account of various parameters as follows: the staggering angle ω was varied around 30°by steps of 1°, underfocus was varied from 65nm to 95nm by steps of 5nm, and crystal thickness was varied near 5nm by steps of 0.674nm. Figures 7 and 8 show that the simulations calculated at 70nm and 75nm underfocus give reasonable images by comparison with the real image of Fig.2 (a). These images reveal that the contrast distribution is very sensitive to the change of both staggering angle and crystal thickness. The crossed rod at the center of each image becomes clearer in contrast with increasing staggering angle, and those at the angles of 29° and 30°show a higher density than that of the real image. In the case of 75nm underfocus, the center of the crossed rod indicates inverse contrast in the range of angle above 28° and thickness above 4.7nm. Furthermore, the parallel bars linking the Pc rings become shorter with increasing staggering angle and those at the angles of 29° and 30° are not consistent with that of the real image. Therefore, the comparison of the simulated images with the real one suggests qualitatively that

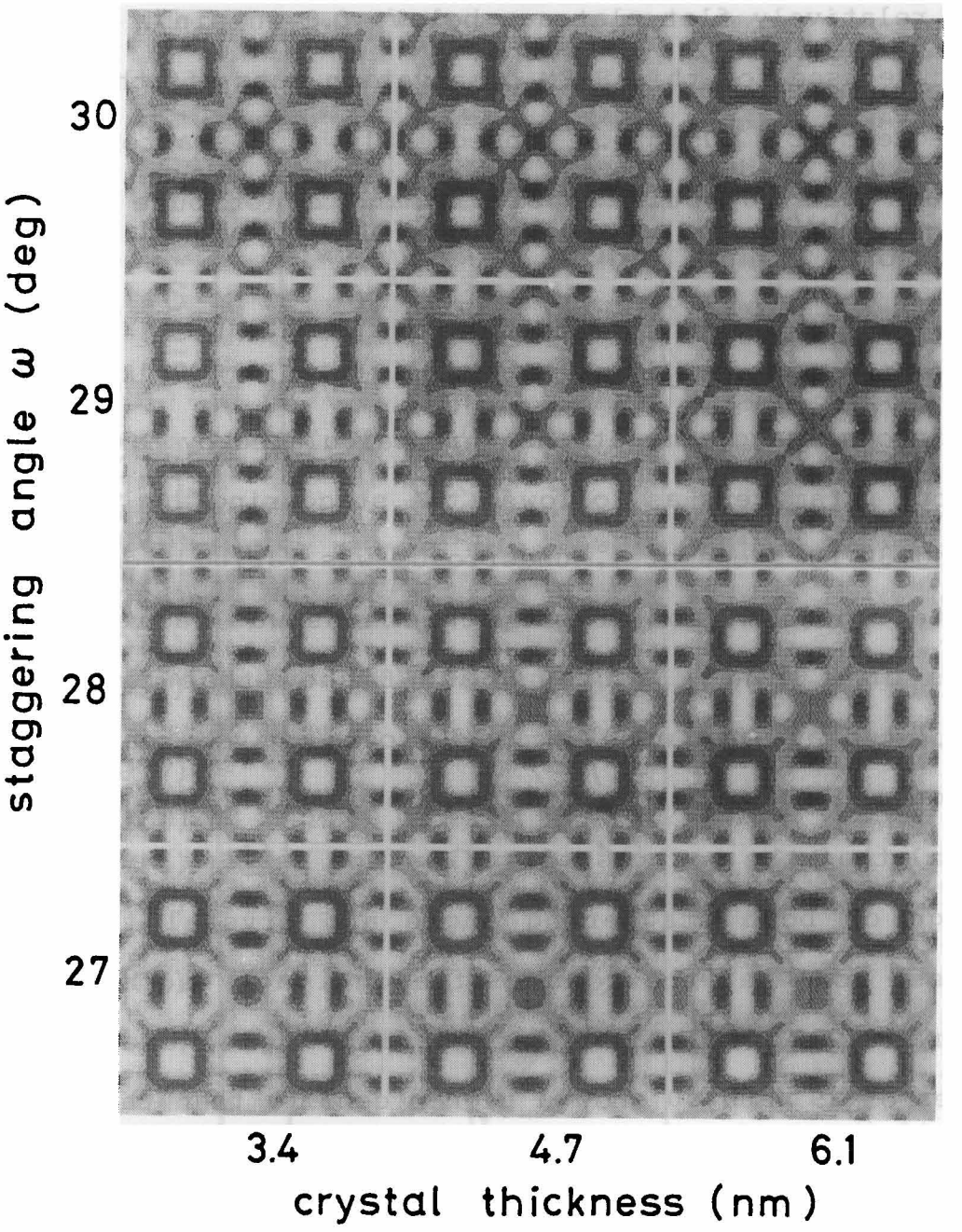

Fig.7 Simulated images in the projection along the c-axis at 70nm underfocus.

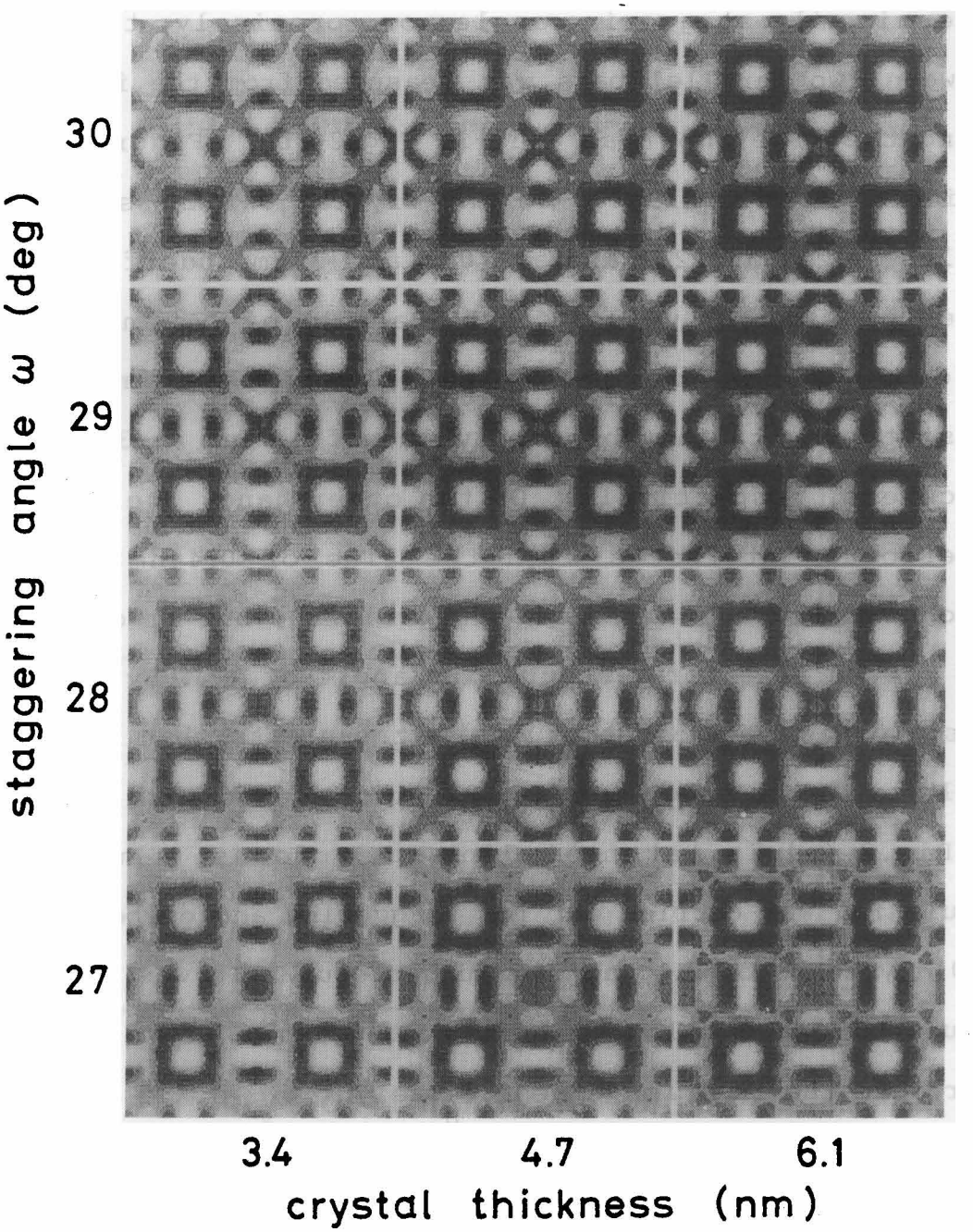

Fig.8 Simulated images in the projection along the c-axis at 75nm underfocus.

the staggering angle is between 27° and 28°. In order to determine the staggering angle more precisely, the distance d_b between two parallel bars was measured from the intensity peaks along the line shown as Y-Y' in Fig.2 (b). Figure 9 shows the variation of d_b relative to the crystal thickness at staggering angles of 27° and 28° and at 70nm and 75nm underfocus. At 70nm underfocus the d_b values for the angles of 27° and 28° decrease gradually with increasing the crystal thickness, and are consistent with the observed value of 0.44nm at 3.3nm and 6.4nm thickness, respectively. On the other hand, the curve at 75nm underfocus intersects with the line of 0.44nm at about 3nm thickness for a staggering angle of 28°, but it does not cross the dotted line for a staggering angle of 27°. By considering a crystal thickness of about 5nm, it suggests that the staggering angle is in the range between 27° and 28° and that the real image in Fig.2 (a) is taken at 70nm underfocus. A more detailed simulation was carried out for staggering angles between 27.0°and 28.0° by steps of 0.1° at 70nm underfocus. It was found that the simulated image calculated at a staggering angle of 27.4° could reproduce the real image most closely.

Figure 10 shows the focal series at a staggering angle of 27.4°. The images are considerably sensitive to a change of defocus around Sherzer focus. The simulated images at 65nm underfocus show the contrast distribution of the crossed rod and the central dot similar to that of the real image. However, the d_b value is estimated to be considerably larger than 0.44nm in every crystal thickness. At 75nm underfocus, the central dot

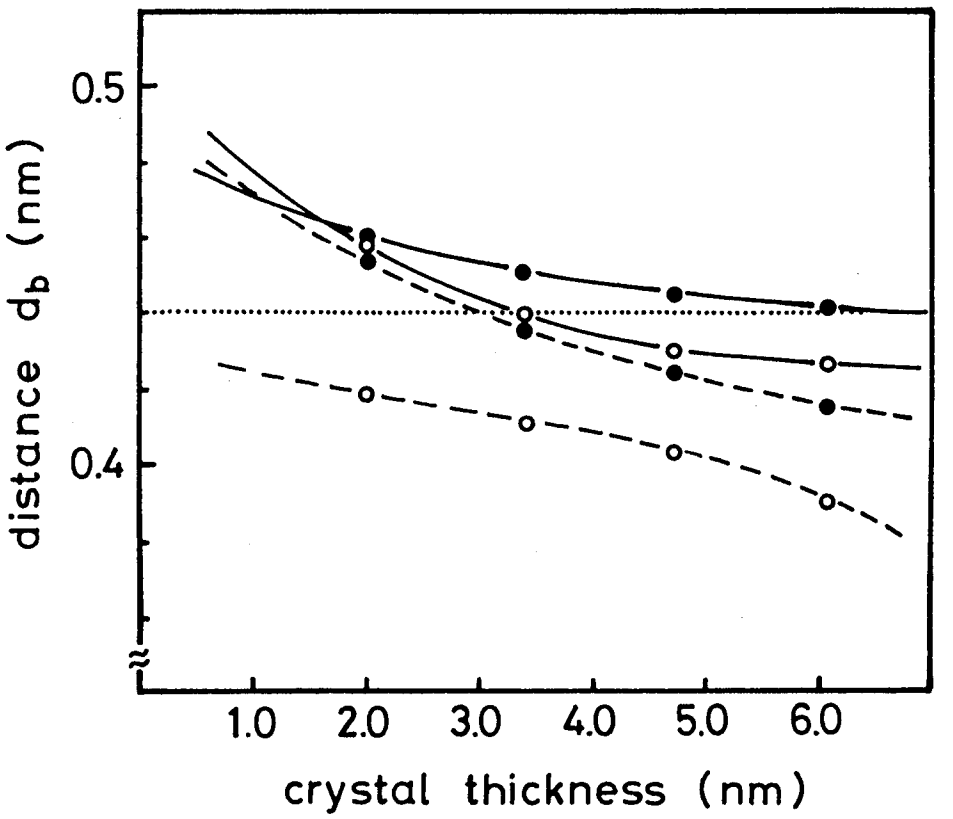

Fig.9 Variation of distance d_b between the parallel bars with crystal thickness. Staggering angles are 27°(o) and 28°(●), underfocuses are 70nm (——) and 75nm (----), and observed d_b (·····).

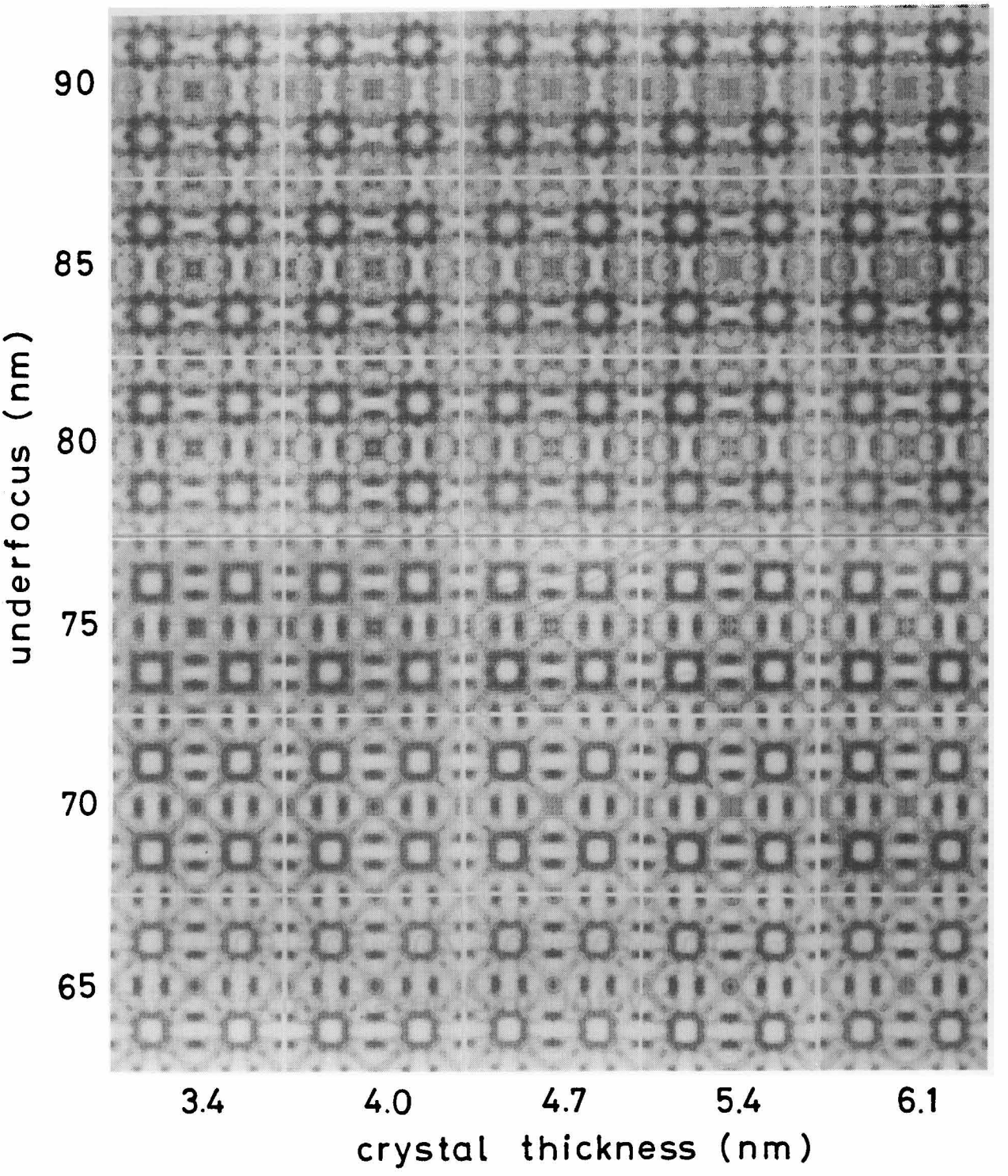

Fig.10 Effect of defocus and crystal thickness on simulated images at the staggering angle of 27.4°.

shows a bright spot in the center of the crystal for thickness above 4.0nm. At a defocus of 85nm, fine structure which is not observed in the real image appears in the ring and parallel bar regions, and the d_b value becomes less than 0.4nm for every crystal. As the underfocus increases to 90nm, the simulated images do not show the crossed rod and deviate from the real one. In the case of 70nm underfocus at which a close match to the real image is obtained, the structural features such as the crossed rod, the central dot and the parallel bars are recognized clearly. These clear images facilitated the direct determination of the molecular arrangement as mentioned above. As shown in Fig.6, however, the Sherzer limit was about $1.65nm^{-1}$ at 70nm underfocus, which was a lower frequency than that at 85nm underfocus. Since the objective aperture cuts off the scattering waves beyond a frequency of $2.05nm^{-1}$, many undesirable scattering waves from $1.65nm^{-1}$ to $2.05nm^{-1}$ may contribute to the image by passing through the aperture in the case of 70nm underfocus. Therefore, the resolution of the image observed at 70nm underfocus is lower than that observed at 85nm underfocus, so that the simulated images at 70nm under focus may not be able to reproduce the fine structures obtained at 85nm.

The effect of the crystal thickness on the image is not so remarkable as that of the defocus. The calculated amplitude of the diffracted wave increases monotonously with increasing thickness. The phase difference between the diffracted wave and the transmitted one is kept approximately at $\pi/2$. Therefore, it seems that dynamical interference by the second-order scattering

waves, which was discussed by O'Keefe et al.[21], is not a serious problem. Consequently, the contrast distribution in the simulated images varies gradually with increasing crystal thickness. In the case of the multislice calculation the atoms out of the slice plane are approximately transferred onto the top or bottom plane of the slice. The phase grating and propagation functions are calculated using this approximate slice. On the other hand, it is noted that all the atoms exist in the plane of the slices in the present case. Therefore, the phase grating and propagation functions are calculated without approximation, and the multislice calculation can reproduce electron scattering in the crystal precisely. P.G.Self et al.[22] have pointed out that the amplitude and phase of the diffracted wave are obtained precisely only when a great number of beams are included in the calculation. In the present calculation 64x64 beams are included, and the quantity is judged to be adequate because the intensity of the scattering waves outside the limit of reciprocal space is negligibly small. Consequently, the multislice calculation in the present work could provide sufficient information for the direct determination of an unknown structure.

The best match of the simulated image with the HREM image was obtained at a crystal thickness of 4nm as shown in Fig.11. The crossed rod and the central dot in the simulated image show remarkable correspondence with those in the real image. The width and length of the parallel bars in the simulated image agree well also with those of the real image. When the staggering angle is 27.4°, the nitrile groups, c and d shown in Fig.3, do not overlap

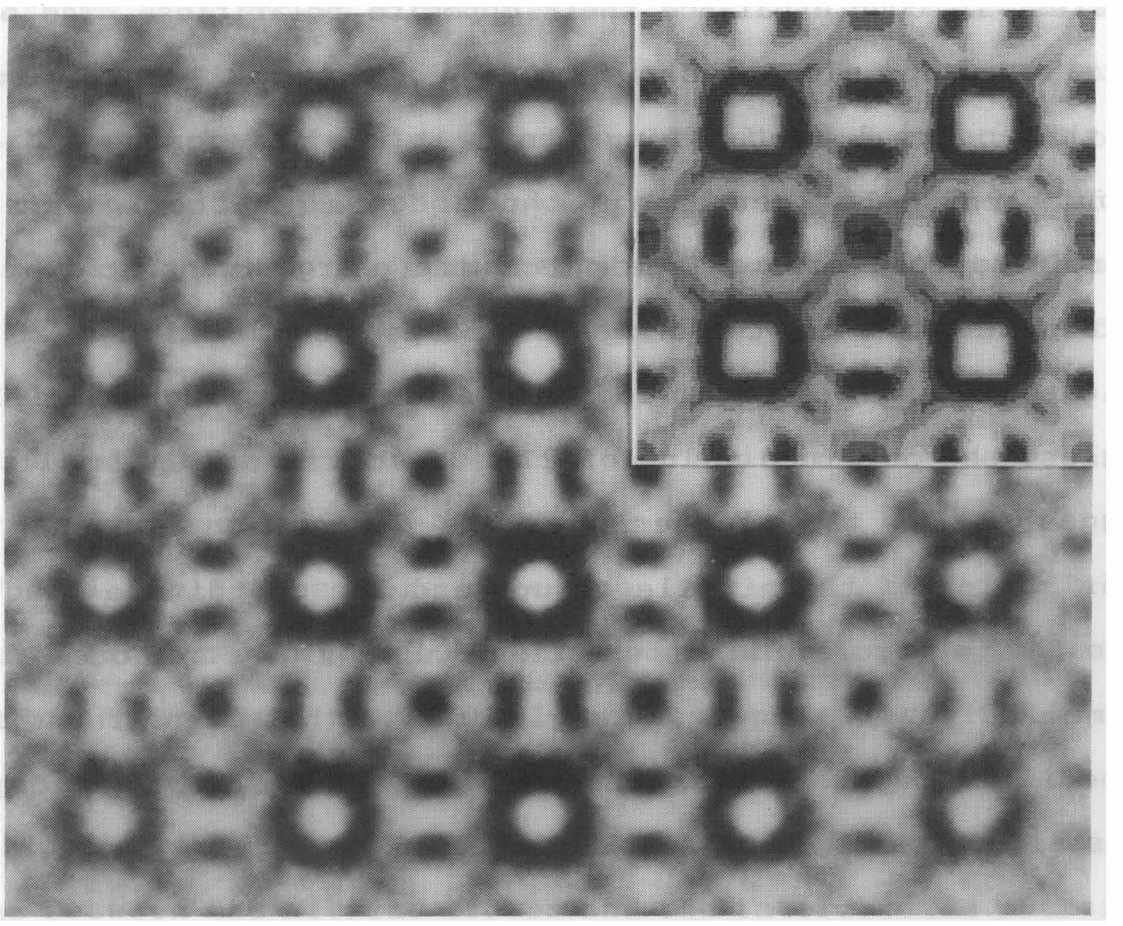

Fig.11 Reproduction of high resolution structure image obtained at the crystal thickness of 4 nm and the corresponding simulated image calculated at 70 nm underfocus.

in line but rotate slightly so that these molecules keep away from the central potassium atom. When the staggering angle is about 34°, the distance between the carbon atom in the nirile group c and the nitrogen atom in the nitrile group d becomes the shortest to counterbalance their opposite polarities. The other nitrile groups, a and b shown in Fig.3, coordinate most closely to the central potassium atom at the staggering angle of about 29.3°. It seems from those considerations that the coordinate bond becomes strong and the charge transfer from the potassium atom to the nitrile groups becomes large at the staggering angle between 29° and 34°. By comparison with these angles, the obtained value of 27.4° is considerably small. It suggests that the staggering angle depends on not only the overlapping of the nitrile groups and the coordinate bond but also the intermolecular interaction due to π electron orbitals of Pc molecules. A staggering angle of 27.4° has been found from experiment on the epitaxial growth of the $K_2Pc(CN)_8$-K complex crystal, which is described in Chapter 5.

5. Conclusions

The molecular arrangement of the $H_2Pc(CN)_8$-K complex crystal was determined precisely by comparing the HREM image with the simulated image based on the multislice method. The contrast distribution of the HREM image varied with defocus value and crystal thickness. The film thickness obtained from the section was about 5nm. Numerous simulations were carried out to determine the molecular staggering angle precisely. The contrast

distribution varies gradually with change of the staggering angle from 27° to 30°. In the simulated image calculated at a staggering angle of 29° and 30°, the crossed rod attributed to the peripheral nitrile groups coordinating to the intercalated potassium atom showed higher density than that of the real image. At staggering angles of 27° and 28°, the central dot attributed to the potassium atom and the parallel bars attributed to the nitrile groups linking Pc rings agreed well with those of the real image. Thus, the staggering angle was estimated to be in the range between 27° and 28°. The intensity distribution of the HREM image and the simulated images was compared along the line which passed through the central dot and crossed the parallel bars perpendicularly. As the result, it is concluded that $H_2Pc(CN)_8$ molecules were piled up in parallel holding their molecular planes perpendicular to the c-axis and the molecules staggered alternately by $\pm 27.4°$ to the a-axis around the c-axis. It seems that the staggering angle depends on not only the overlapping arrangement of the nitrile groups and the coordinate bond between the nitrile groups and the intercalated potassium atom, but also the intermolecular interaction due to π electron orbitals of Pc molecules. The best match of the simulated image with the HREM image was obtained at 70nm underfocus for the crystal 4nm in thickness. In the present work, an adequate small slice thickness was selected to produce the precise projected potential, and an adequate number of beams were included in the multislice calculation. The image simulation provided sufficient analytical imformation for the direct determination of the

$H_2Pc(CN)_8$-K complex crystal by comparison with the HREM image.

References

[1] N.Uyeda, T.Kobayashi, E.Suito, Y.Harada and M.Watanabe, J.Appl.Phys. 43 (1972) 5181.

[2] P.N.T.Unwin and R.Henderson, J.Mol.Biol. 94 (1975) 425.

[3] J.R.Fryer and D.J.Smith, Proc.R.Soc.London Ser.A 381 (1982) 225.

[4] Y.Fujiyoshi, T.Kobayashi, K.Ishizuka, N.Uyeda, Y.Ishida and Y.Harada, Ultramicroscopy 5 (1980) 459.

[5] J.M.Cowley and A.F.Moodie, Acta Cryst. 10 (1957) 609.

[6] J.G.Allpress, E.A.Hewat, A.F.Moodie and J.V.Sanders, Acta Cryst. A28 (1972) 528.

[7] D.F.Lynch and M.A.O'Keefe, Acta Cryst. A28 (1972) 536.

[8] G.R.Anstis, D.F.Lynch , A.F.Moodie and M.A.O'Keefe, Acta Cryst. A29 (1973) 138.

[9] M.A.O'Keefe, Acta Cryst. A29 (1973) 389.

[10] D.F.Lynch, A.F.Moodie and M.A.O'Keefe, Acta Cryst. A31 (1975) 300.

[11] M.A.O'Keefe and J.V.Sanders, Acta Cryst. A31 (1975) 307.

[12] K.Ishizuka and N.Uyeda, Acta Cryst. A33 (1977) 740.

[13] N.Uyeda, T.Kobayashi, K.Ishizuka and Y.Fujiyoshi, Chemica Scripta. 14 (1978-79) 47.

[14] M.Ashida, Y.Ueda, H.Yanagi and K.Sayo, J.Polym.Sci., Polym.Chem.Ed. received.

[15] M.Ashida, Y.Ueda, H.Yanagi, Y.Fujiyoshi, N.Uyeda and J.R.Fryer, Acta Cryst. accepted.

[16] J.M.Robertson, J.Chem.Soc. (1936) 1195.

[17] C.K.Prout and I.J.Tickle, J.Chem.Soc. Perkin II (1973) 520.

[18] G.H.Smith and R.E.Burge, Acta Cryst. 15 (1962) 182.

[19] K.J.Hanszen and L.Trepte, Optik 32 (1971) 519.

[20] J.Frank, Optik 38 (1973) 519.

[21] M.A.O'Keefe, J.R.Fryer and D.J.Smith, Acta Cryst. A39 (1983) 838.

[22] P.G.Self, M.A.O'Keefe, P.R.Buseck and A.E.C.Spargo, Ultramicroscopy 11 (1983) 35.

Chapter 3 High Resolution Molecular Images of Octacyanometalphthalocyanine-metal Complexes in Thin Films

Abstract

Octacyanometalphthalocyanine-metal complexes ($MPc(CN)_8$-M, M=Cu,Ni,Co,Fe, and $K_2Pc(CN)_8$-K) were synthesized by vapor-solid reaction of tetracyanobenzene(TCNB) with evaporated matal films and a KCl crystal. Their crystal structures were directly analyzed from high resolution molecular images with aid of image simulation. The $MPc(CN)_8$-M complex crystals formed column structures which were isomorphous crystals of the $K_2Pc(CN)_8$-K crystal. The $MPc(CN)_8$ molecules were stacked in parallel with an interplanar distance of 0.34nm taking molecular planes perpendicular to the column axis. The Pc rings staggered alternately around the c-axis to form the complex between peripheral nitrile groups and intercalated metal atoms. The crystals belonged to space group of tetragonal P4/mcc and the cell parameter a became shorter in order of Cu>Ni>Co>Fe>K. Various structure images were obtained from thin films of the $MPc(CN)_8$-M crystals in which the column axes inclined against the substrates by different angles. These images were interpreted as projection images along different [h0l] zone axes of the crystal by comparison with simulated images.

1. Introduction

High resolution electron microscopy(HREM) is very useful for an observation of local structures in thin films. Vacuum-deposited phthalocyanine (Pc) films on cleaved surfaces of muscovite or alkali halides exhibit well-defined epitaxial orientations[1-3]. Their crystal structure and molecular arrangement have been studied by direct obsevation of molecular images with HREM[4,5] and the computer image simulation[6]. Kobayashi et al.[7] have observed a local change of molecular orientation in a NiPc film induced by iodine doping. NiPc molecules crystallized in a well-known herringbone column structure, in which planar molecules were piled up in parallel with a distance of 0.345nm and tilted by 74° to the column axis. By treatment with iodine the column structure was changed to make the angle perpendicular to the column axis and to decrease the intermolecular distance to 0.325nm. The crystal structure analysis of the stoichiometric complex $NiPcI_{1.0}$ has revealed that the eclipsed stacking molecules in the NiPc crystal rotate alternately around the column axis making a staggering angle of 39.5° by iodine doping[8].

A similar molecular stacking has been observed in the $K_2Pc(CN)_8$-K complex crystal which was synthesized from TCNB vapor on a KCl substrate[9]. As described in Chapter 2, HREM observation of the complex crystal and the multislice image simulation have elucidated that $K_2Pc(CN)_8$ molecules are stacked in parallel with an interplanar distance of 0.337nm and staggered alternately with an angle of $\pm 27.4°$ to the a-axis. It is noteworthy that this crystal involves considerably strong

interaction between columns caused by antiparallel overlapping of the nirile groups between molecules in adjacent columns and by charge transfer from an intercalated potassium atom to other nitrile groups. Therefore, it is expected that the details of the complex structure depend on an electronic configuration of the intercalated metal atom.

In this chapter, thin films of various metal derivatives of $K_2Pc(CN)_8$ were synthesized by vapor-solid reaction of TCNB with evaporated films of first transition metals (Cu, Ni, Co, Fe) as shown in Scheme 1. Various HREM images observed in the films were interpreted by comparison with computer simulated images. The structure of these crystals was discussed especially in regard to an intermolecular interaction and formation of a charge transfer complex.

2. Experimental

A sample of TCNB was synthesized by the method of Bailey et al.[10]. Substrate materials used were a cleavage surface of a KCl single crystal and metallic films. As metallic films, Cu, Ni, Co and Fe were evaporated on a cleavage surface of KCl

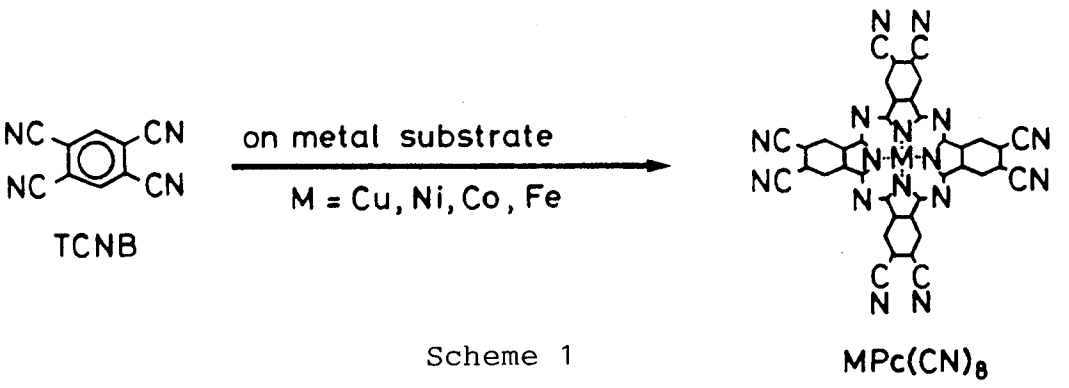

Scheme 1

maintained at a temperature between 350 and 450 °C in a vacuum of $1x10^{-4}$Pa. The purified TCNB and the substrate material were sealed in an evacuated pyrex glass tube at 10Pa after flushing with argon gas. The tube was heated at a temperature from 300 to 350 °C for 10 hr in a hot air oven. Synthesized films were separated from KCl substrates in water, and the residual metal films were dissolved away in dilute acid solutions. The specimen film was mounted on a microgrid coated with an evaporated gold film. HREM observation was carried out by a JEM-200CX electron microscope equipped with a high resolution objective pole piece (C_s=2.0mm) at 200 kV accelerating. High resolution electron micrographs were obtained with aid of a minimum exposure device and their enlarged images were noise-reduced by translational multiple exposure technique. Accurate spacings were calibrated using the (111) lattice image of gold. Optical transforms were obtained from electron micrographs using a He-Ne gas laser. Image simulation was performed by the multislice program developed on an NEC PC-9801VM micro-computer equipped with a PC-9801-22 arithmetic operation co-processor and 640kB of RAM as described in Chapter 2. For construction of a crystal model, the molecular structure of a phthalocyanine skeleton was assumed to be that of CuPc reported by Brown[11]. It was also assumed that a peripheral nitrile group made 120° to C-C bonds of a benzene ring by reference to the molecular structure of the TCNB crystal[12]. Scattering amplitude was calculated using crystal potentials projected along various zone axes and including 4096 beams. Contrast transfer functions (CTF) were

calculated with attenuation by chromatic defocus spread of 10nm, and beam divergence α of 0.5mrad, and cut off frequency of an objective aperture was chosen to be 2.05 nm^{-1} ($\sin\theta / \lambda$).

3. Results and Discussion

(1) High resolution structure images of the $MPc(CN)_8$-M complex crystals

The reaction of TCNB with metal(Cu,Ni,Co,Fe) substrates produced blue or green films. In Chapter 1, they were identified as respective octacyanometalphthalocyanine-metal complex crystals, which were composed of similar tentacle-like crystals to the $K_2Pc(CN)_8$-K complex[13]. Figure 1 shows a representative electron micrograph obtained from a very thin film on a Cu substrate. Crystallites in areas marked with A,B,C and D show different lattice fringes respectively. A lattice image in the area A is composed of a square network of 1.63nm spacing, which resembles an image of the $K_2Pc(CN)_8$-K crystal projected along the c-axis[9]. A crystallite in the area B grows in long parallel columns with a distance of 1.63nm and has various lattice fringes along the column axis. A lattice image in the area C also shows a column structure with a distance of 1.63nm, but lattice fringes are not observed clearly along the column axis. A crystallite in the area D shows a similar lattice image to that observed in the area C but a distance between the columns, 1.15 nm, is shorter than that of other crystallites. The square lattice images were observed in films obtained from other metal substrates. Their enlarged and noise-reduced high resolution electron micrographs

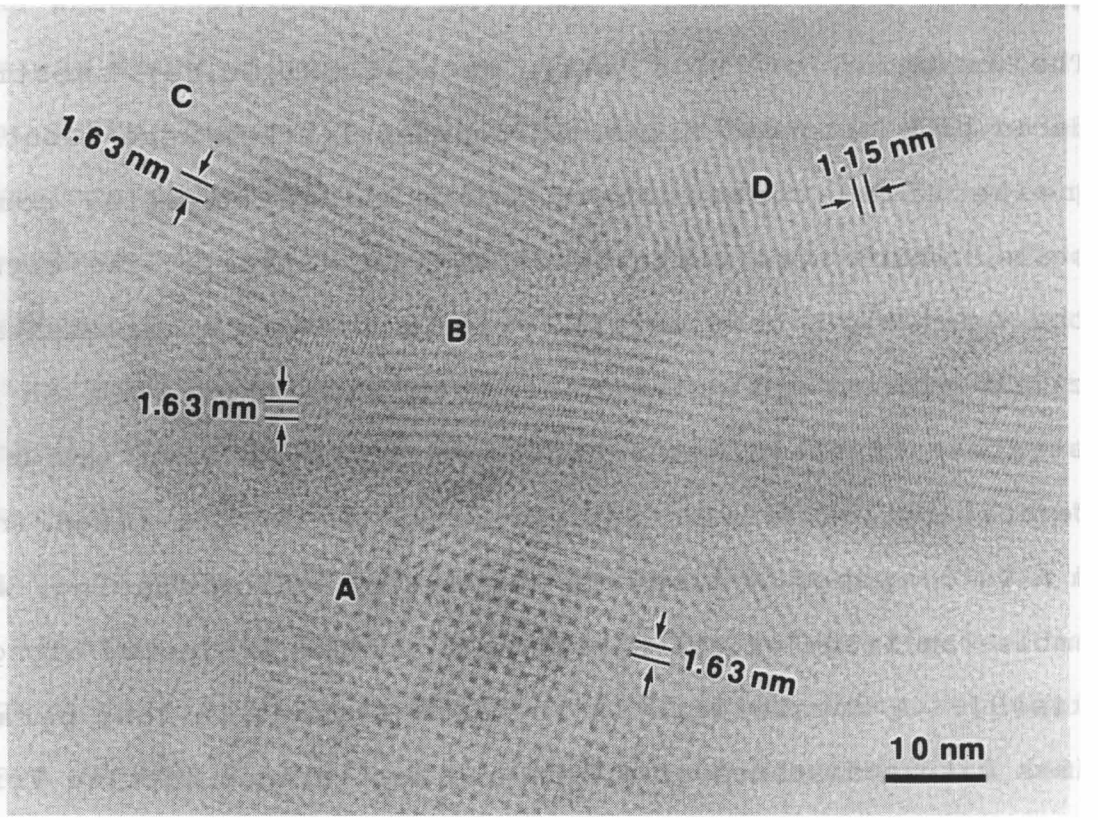

Fig.1 Electron micrograph of a thin film synthesized from TCNB on an evaporated Cu film showing various aspects of lattice fringes marked with A, B, C and D.

are shown in Fig.2 together with a reproduction of the $K_2Pc(CN)_8$-K crystal. Their lattice spacings are 1.63, 1.61, 1.59, 1.58 and 1.57nm for substrates of Cu, Ni, Co, Fe and K, respectively. The analogy among those images suggests that octacyanometalphthalocyanine-metal complex ($MPc(CN)_8$-M) crystals are isomorphous crystals of the $K_2Pc(CN)_8$-K crystal. By comparison with a molecular arrangement of the $K_2Pc(CN)_8$-K crystal, high contrast parts on the corners of the square are attributed to $MPc(CN)_8$ molecules stacked in parallel on a substrate and a black dot at the center of the square is attributed to an intercalated metal atom. $K_2Pc(CN)_8$ molecules only give ring-like images on the corners of the square, as shown in Fig.2 (e). Because $K_2Pc(CN)_8$ molecules are easily demetallized to the metal-free derivative ($H_2Pc(CN)_8$) in water, the Pc ring image shows a circle whose inside is blank[9]. On the other hand, $MPc(CN)_8$ molecules show high intensity inside of the dot images, because MPc molecules are not demetallized even in a dilute acid solution.

As mentioned above, planar Pc molecules are perpendicular to the column axis in the $MPc(CN)_8$-M complex crystals, owing to interaction between peripheral nitrile groups of $MPc(CN)_8$ and intercalated metal atoms. The interaction between the metals and Pc molecules is probably strong in order of Cu<Ni<Co<Fe<K, because lattice constants a of the complex crystals decrease in the reverse order. This order of the interaction is explained in terms of strength of coordinate bonds between the peripheral nitrile groups and the metal atoms. The coordinate bonds relate

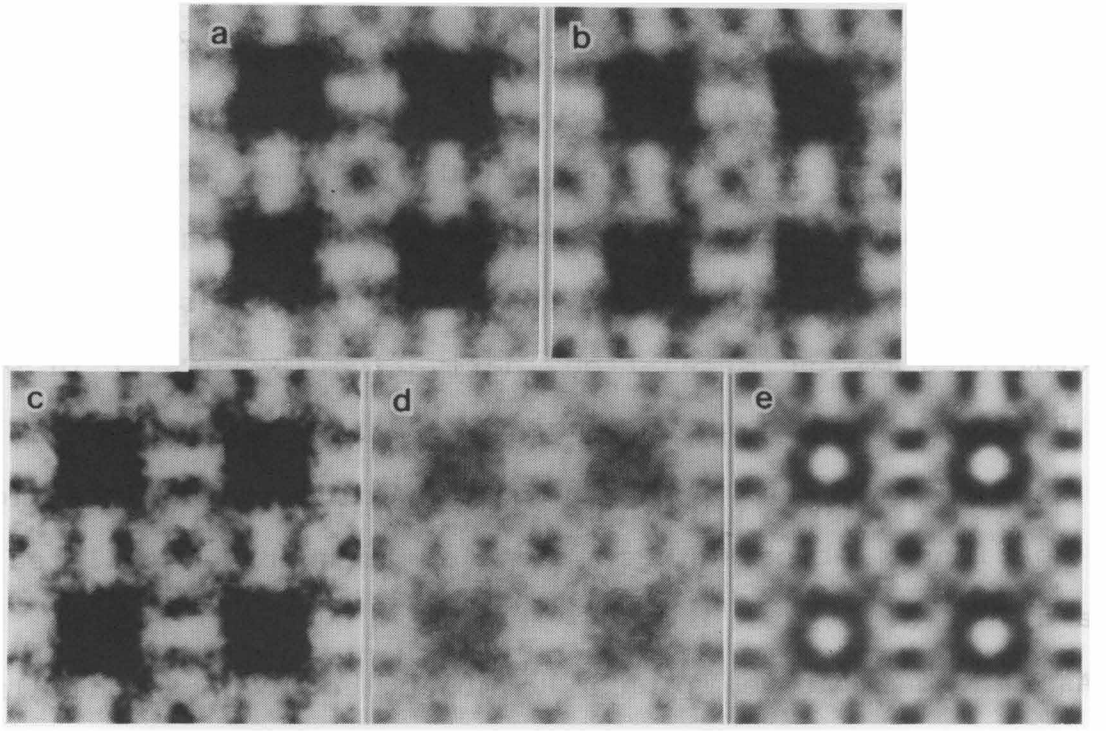

Fig.2 High resolution molecular images of the $MPc(CN)_8$-M complexes formed on substrates of Cu(a), Ni(b), Co(c), Fe (d) films and KCl (e).

closely to electron configurations of these metals. The average ionization potentials of the metals are high in order of Cu>Ni>Co>Fe>K and charge transfer from the metals to the nitrile groups increases in inverse proportion to the ionization potentials. The coordinate bonds seem to be stronger with increasing the charge transfer, so that $MPc(CN)_8$ molecules are aligned more closely in order of Cu<Ni<Co<Fe<K.

Various column structures were also observed in films obtained from other metal substrates. Figure 3 shows various column images observed in those high resolution electron micrographs and the corresponding optical transforms. In a column structure (a) a distance between the columns is 1.63nm which coincides with a spacing of the square lattice of the $CuPc(CN)_8$-Cu crystal. A spacing of 0.34nm along the column axis also coincides closely with an interplanar distance of Pc molecules stacked in parallel in a molecular column as observed in MPc crystals[5]. A similar image of the $K_2Pc(CN)_8$-K crystal has been already described as a molecular stacking image, in which $K_2Pc(CN)_8$ molecules are piled up taking their molecular planes perpendicular to the column axis[9]. Therefore, the image (a) reveals that both the column axis and one side of the square lattice take parallel to the substrate surface. In the cases of column images (b), (c) and (d), each distance between the columns coincides with the spacing of the square lattice of the corresponding $MPc(CN)_8$-M crystal. Images (b) and (c) show that spacings along their column axes are 0.62 and 0.51nm, respectively. A image (d) does not show lattice fringes along the column axis. Corresponding to

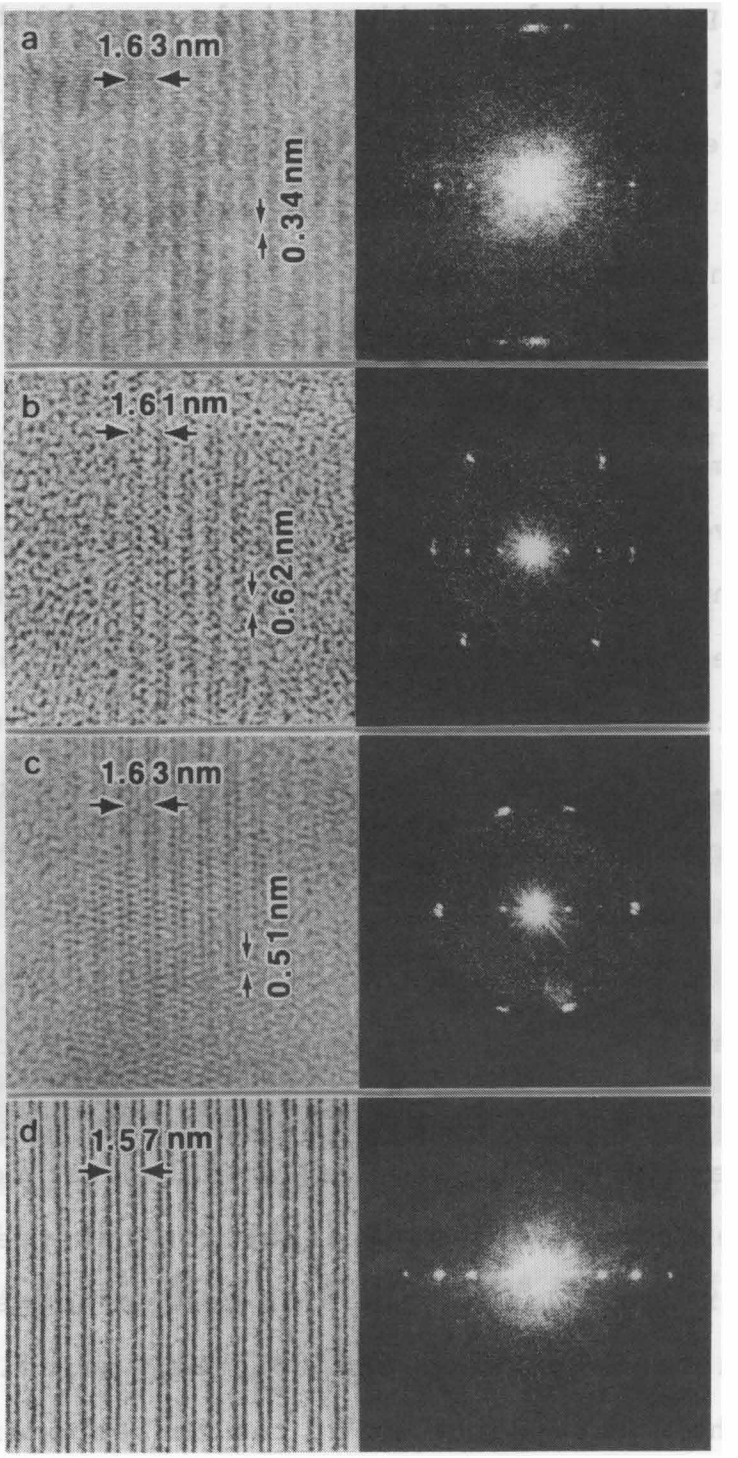

Fig.3 Various structure images of the $MPc(CN)_8$-M complex crystals formed on substrates of Cu(a), Ni(b), Cu(c), KCl(d) and the corresponding optical diffraction patterns.

the images their optical diffraction patterns show different fiber periods and various extinction of reciprocal lattice points. It seems that the crystals in the images (b), (c) and (d) take their column axes tilting to the substrates by different angles. On the other hand, a distance between the columns, 1.15nm, observed in the area D shown in Fig.1, coincides with half of a diagonal line of the square lattice spacing of the $CuPc(CN)_8$-Cu crystal. The finding suggests that the crystal in this area tilts on the substrate surface taking a different orientation.

(2) Molecular arrangement and simulation of the [001] projection images

A molecular arrangement of the $MPc(CN)_8$-M crystals was assumed to be similar to that of the $K_2Pc(CN)_8$-K crystal as shown in Fig.4. $MPc(CN)_8$ molecules are located at the corners of a square with the respective lattice constants a of the tetragonal unit cells. Planar molecules are in a layer being perpendicular to the c-axis and rotate by a staggering angle $\pm\omega$ to the a-axis alternately in successive layers, as shown in Fig.4 (a) and (b). These molecules are piled up with an interplanar distance of 0.34nm along the c-axis, and a metal atom is intercalated at the center of the square between two layers. The crystal projected along the c-axis gives a superposition of atoms as shown in Fig.4 (c). The intercalated metal atom is surrounded by a distorted cube of eight peripheral nitrile groups from each molecule situated at the corner of the two layers. Other nitrile

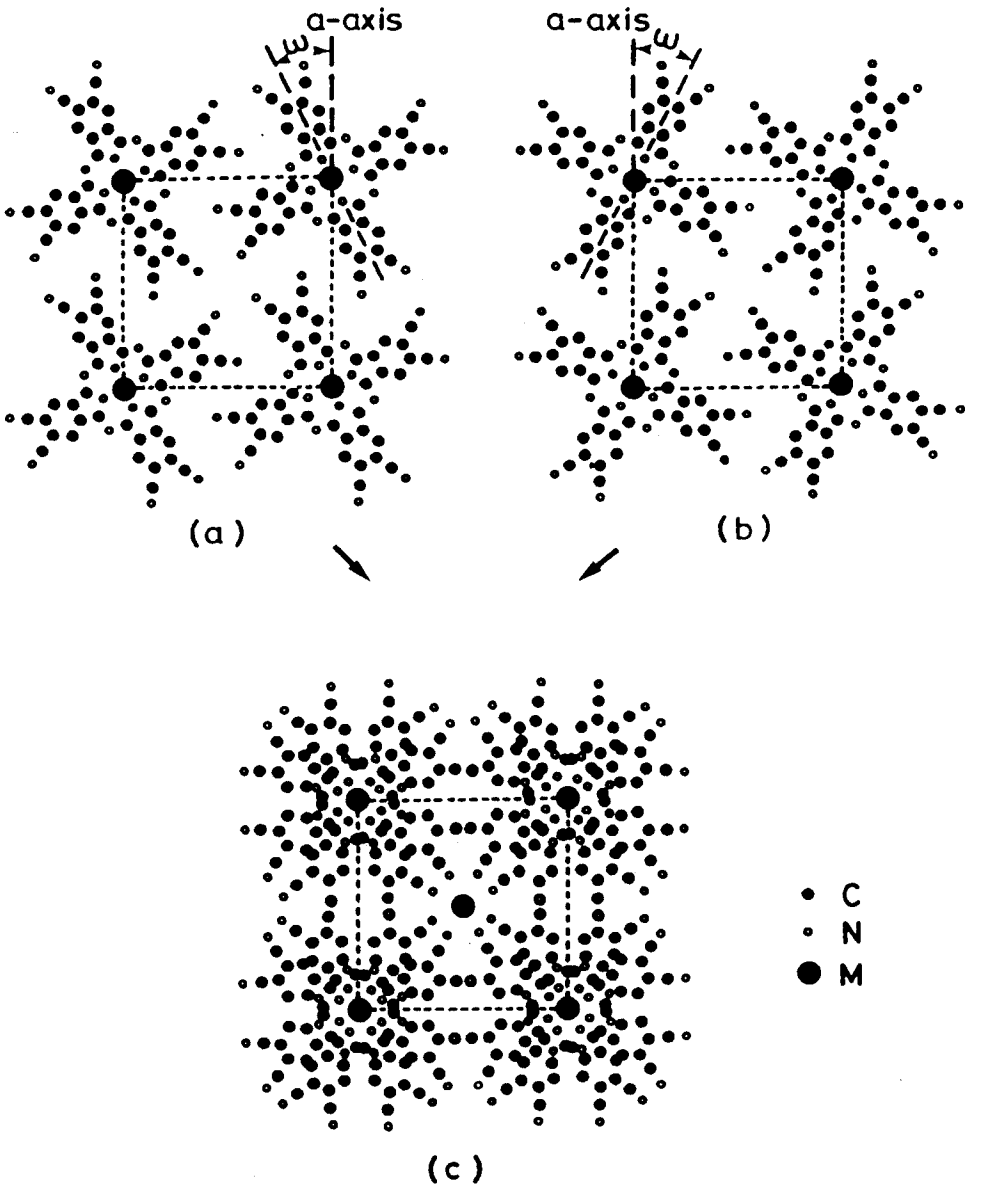

Fig.4 Schematic diagram of the crystal structure of the $MPc(CN)_8$-M complex. Molecular arrangement in the alternate layers showing the staggering angle ω (a), (b), and the superposition of molecules along the c-axis (c).

groups overlap almost in parallel between the adjacent columns to counterbalance opposite polarities of the nitrile groups. The $MPc(CN)_8$-M crystal constructed in this way has the cell parameter c of 0.68nm and the space group P4/mcc.

On the basis of such molecular arrangement, molecular images in Fig.2 were simulated by the projection along the c-axis. Figure 5 shows simulated images of the $CuPc(CN)_8$-Cu crystal relative to the crystal thickness from 2 to 20nm at various defocus (Δf) positions. Calculations were carried out for C_s=2.0mm at 200 kV accelerating and the staggering angle ω was assumed to be 27.5° similar to that of the $K_2Pc(CN)_8$-K crystal. Apparently, the contrast distribution varied seriously with defocus values. Both contrasts of $CuPc(CN)_8$ molecules and central Cu atoms are reverse to those of the real images in the overfocus range from -100 to -20nm. On the other hand, simulated images of the defocus range around Scherzer focus (85nm) show contrast distribution corresponding to the crystal potential projected along the c-axis. Electron micrographs may be frequently taken at various defocus positions which deviate from the optimum position for observation in high resolution. Figure 6 shows examples of observed real images and the corresponding simulated images of the $CuPc(CN)_8$-Cu crystal at various defocus values. Both images show a good match in detail for each defocus position. The images from thick crystals represent a white hole at the center of a Pc ring near Scherzer focus as shown in the images (c) and (c'). According to O'Keefe et al.[14], effect of dynamical interference of the second-order scattering waves

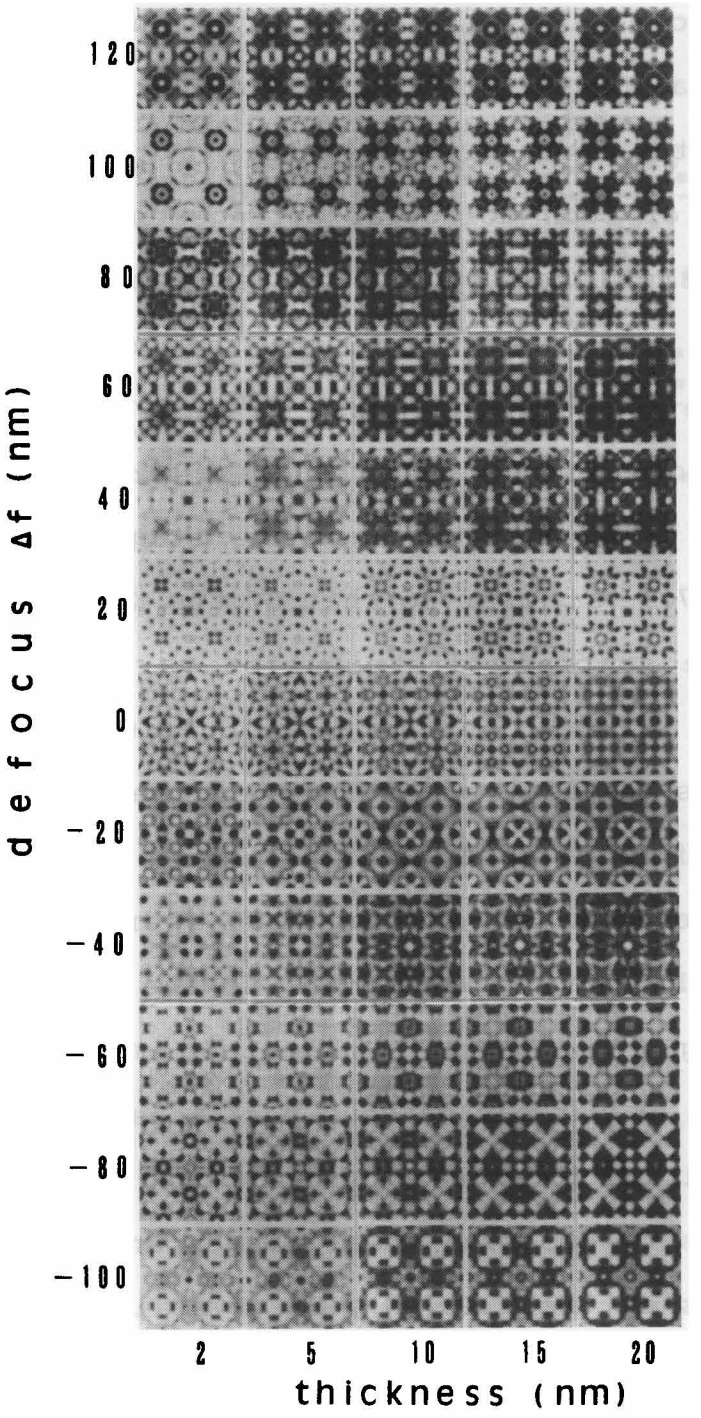

Fig.5 Simulated images of the $CuPc(CN)_8$-Cu crystal with increasing crystal thickness up to 20nm at defocus range from -100 to 120nm.

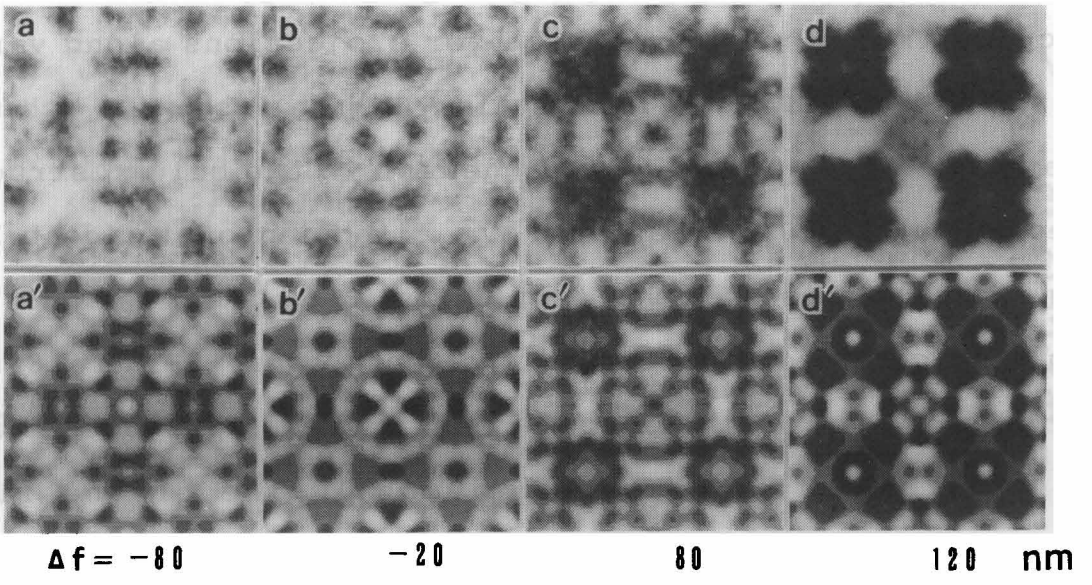

Fig.6 Defocus series of the [001] projection images for the $CuPc(CN)_8$-Cu crystal. Real images (a) to (d) and the corresponding simulated images (a') to (d'). Simulated images were calculated in crystal thickness of 10nm (a'), 20nm (b'), 15nm (c') and 15nm (d').

becomes serious for thick crystals. As the crystal thickness increases, contribution of the scattering waves from the densely superposed Pc molecules becomes stronger than that from the metal atoms, so that the inside of Pc rings shows weak intensity. It seems that this white hole is not caused by demetallizing of MPc but caused by effect of the thick crystal.

(3) Simulation of the [h0l] projection images

In order to interprete the structure images shown in Fig.3, molecular images were simulated for projections along various zone axes of the $MPc(CN)_8$-M crystals. Figure 7 shows a schematic explanation of a molecular arrangement in the culumn structure projected on the (010) plane and the direction of incident beams along the zone-axes used for simulation. Crystal potentials were calculated corresponding to the incident beams. Figure 8 shows potential images of the $CuPc(CN)_8$-Cu crystals projected along the [h0l] axes, where the horizontal line of the figure corresponds to the direction of the b-axis. The crystal potentials show various superpositions of molecules projected along directions from the [001] axis to the [100] one. These potential images are composed of two parallel columns of superposed Pc rings and a central column attributed to intercalated metal atoms and peripheral nitrile groups. The former two columns arrange apart each other by a distance of the lattice spacing a. The images shown in Fig.9 were simulated from these crystal potentials by the multislice iteration, where crystal thickness was chosen to be around 10nm along each zone

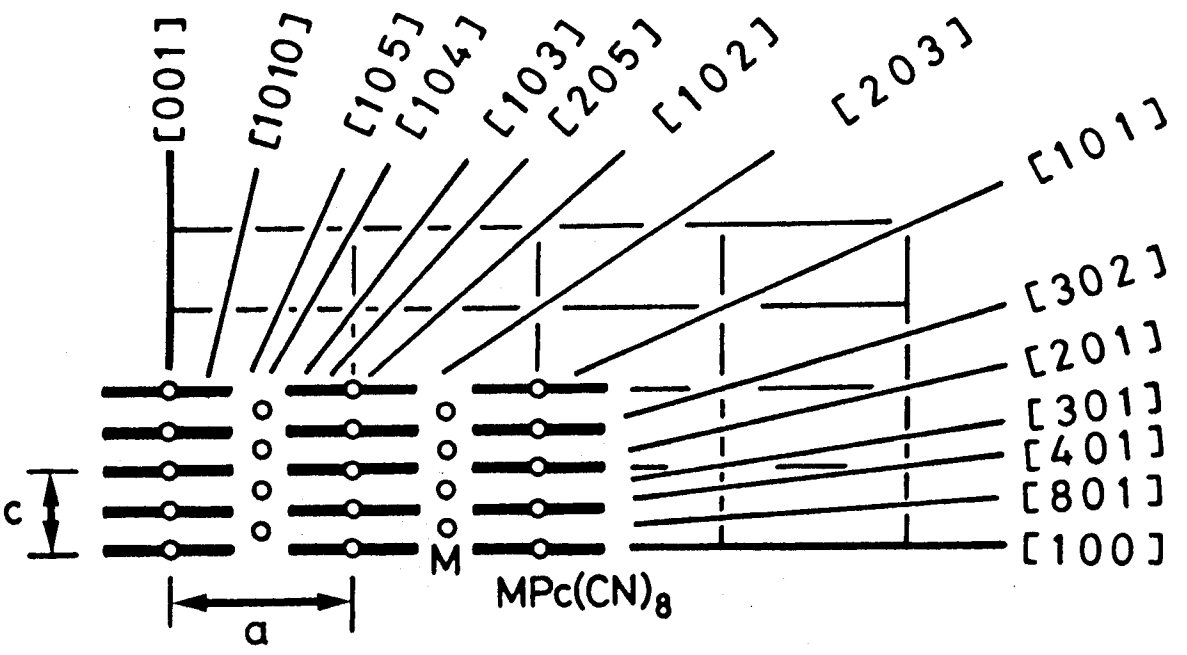

Fig.7 Schematic diagram of the column structure projected along the b-axis and the direction of the incident beams used for image simulation.

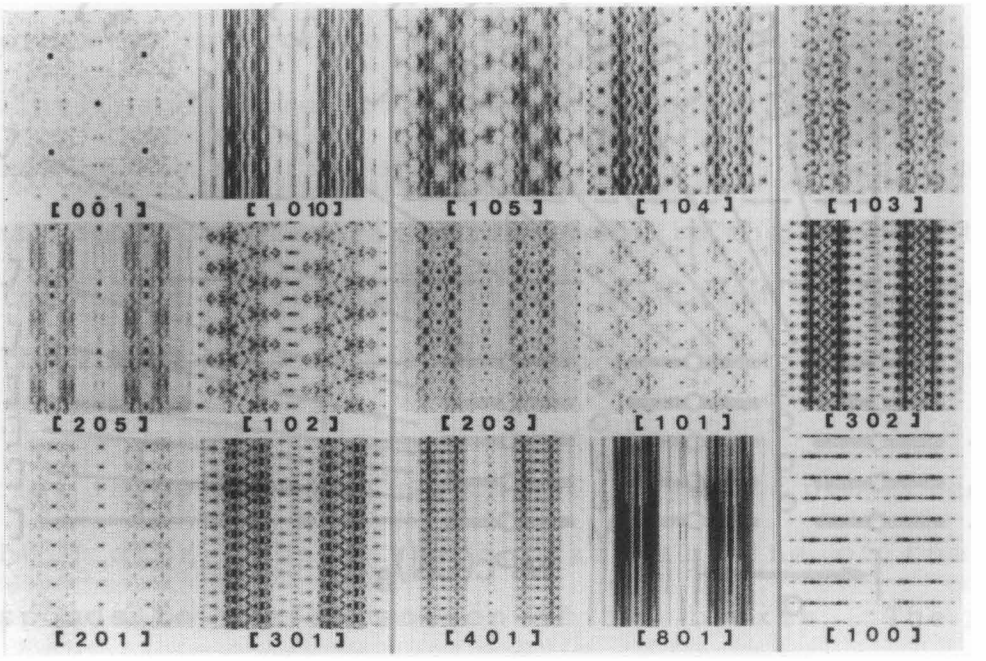

Fig.8 Calculated crystal potentials of the $CuPc(CN)_8$-Cu complex projected along the zone axes shown in Fig.7.

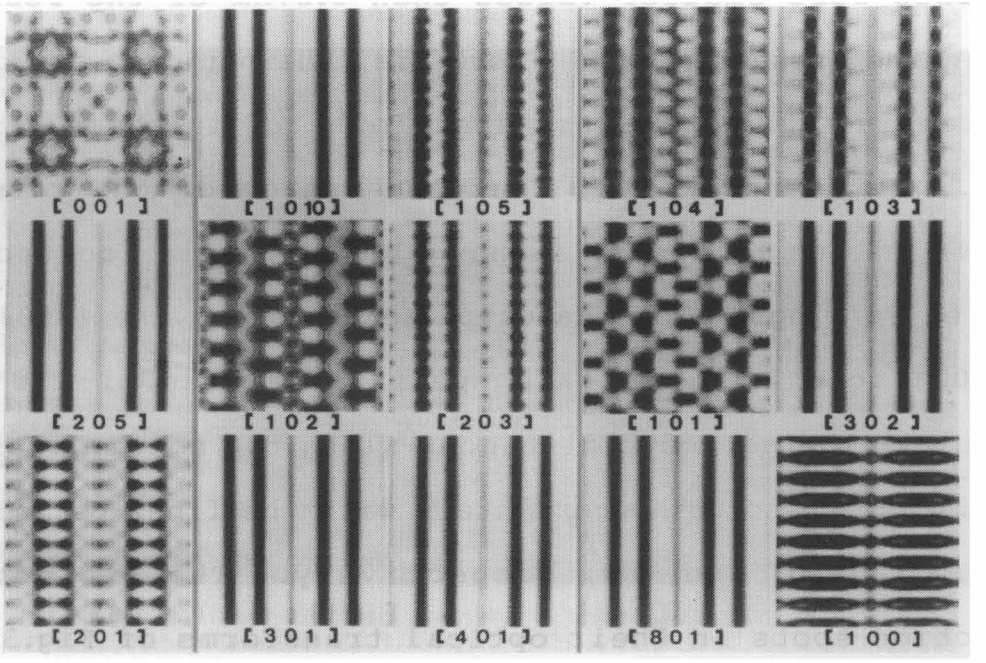

Fig.9 Multislice simulated images of the $CuPc(CN)_8$-Cu complex crystal calculated for 10nm thickness at Scherzer focus using the crystal potentials shown in Fig.8.

axis. Images projected along the [1010], [205], [302], [301], [401] and [801] zone axes show two columns composed of pair lines with strong intensity and a central column with weak intensity, which resemble closely to the observed image shown in Fig.3 (d). These columns have no periodic structure along the column axis in contrast with their corresponding potential images. The repeating spacings along the column axes in their crystal potentials were smaller values than 0.27nm of the resolution limit in the present study. Therefore, the periodic structure in the potential images was not discriminated in those simulated images. It is noteworthy that the inside of the columns of $CuPc(CN)_8$ has no intensity although Cu atoms are located at the center of Pc rings. The images projected along the [100], [101] and [102] zone axes indicate special features of the column structure. The periodic distances along the column axes, 0.34, 0.64, 0.52nm, coincide approximately with the fiber periods shown in Fig.3 (a),(b) and (c), respectively. The extinction of diffraction spots in their optical transforms of Fig.3 can be also explained by the periodicity of these simulated images. Figure 10 shows a reproduction of the noise-reduced electron micrographs of Fig.3 and the corresponding simulated images. Both images in each projection indicate good agreement. Consequently, the various structure images shown in the films were well interpreted as projection images along the different [h0l] zone axes of the $MPc(CN)_8$-M crystals. The central metal atoms of the $MPc(CN)_8$ molecules could not be discriminated from the Pc rings in the present study. Recently, Ueda et al.[15]

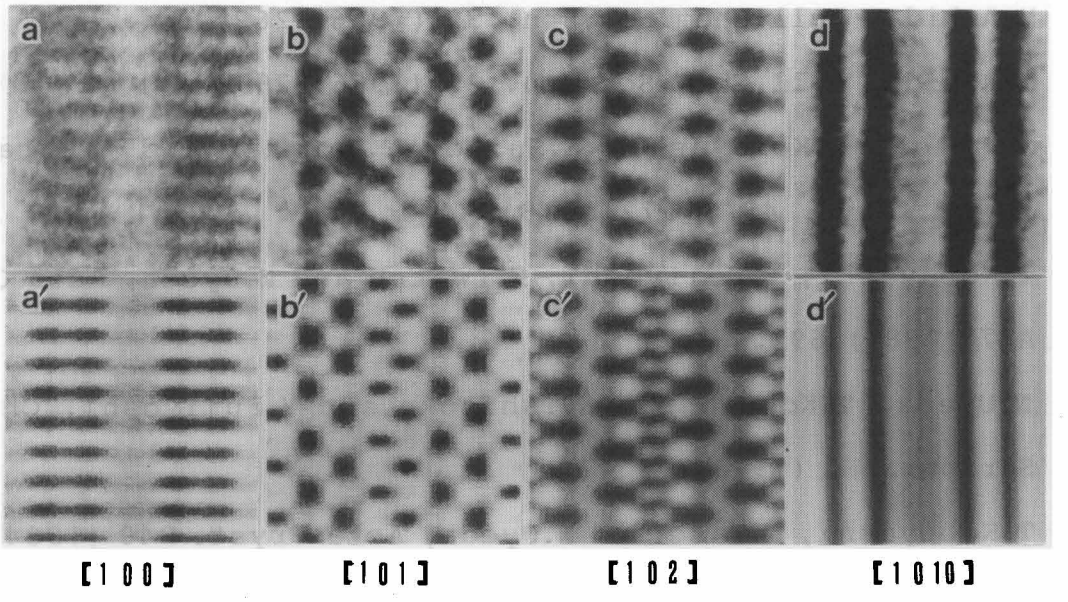

Fig.10 Enlarged high resolution structure images (a) to (d) of the $MPc(CN)_8$-M complex crystals obtained from Fig.3, respectively, and the corresponding simulated images (a') to (d') at Scherzer focus. The substrates are Cu (a), Ni (b), Cu (c) and KCl (d).

have observed the dot image of a Cu atom separated from the Pc ring by a JEM-200CX electron microscope equipped with a high resolution pole piece (C_s=1.4mm) at Institute for Chemical Research, Kyoto University.

References

[1] M.Ashida, N.Uyeda and E.Suito, Bull.Chem.Soc.Jpn. 39 (1966) 2616.

[2] M.Ashida, Bull.Chem.Soc.Jpn. 39 (1966) 2625.

[3] M.Ashida, Bull.Chem.Soc.Jpn. 39 (1966) 2632.

[4] N.Uyeda, T.Kobayashi, E.Suito, Y.Harada and M.Watanabe, J.Appl. Phys. 43 (1972) 5181.

[5] T.Kobayashi, Y.Fujiyoshi, F.Iwatsu and N.Uyeda, Acta Cryst. A37 (1981) 692.

[6] N.Uyeda, T.Kobayashi, K.Ishizuka and Y.Fujiyoshi, Chemica Scripta. 14 (1978-79) 47.

[7] T.Kobayashi, K.Yase and N.Uyeda, Acta Cryst. B40 (1984) 263.

[8] C.J.Schramm, R.P.Scaringe, D.R.Stojakovic, B.M.Hoffmann, J.A.Ibers and T.J.Marks, J.Am. Chem.Soc. 102 (1980) 6702.

[9] M.Ashida, Y.Ueda, H.Yanagi, Y.Fujiyoshi, N.Uyeda and J.R.Fryer, Acta Cryst. accepted.

[10] A.S.Bailey, R.B.Henn and J.M.Langton, Tetrahedron 19 (1963) 161.

[11] C.J.Brown, J.Chem.Soc.A (1968) 2488.

[12] C.K.Prout and I.J.Tickle, J.Chem.Soc. Perkin II (1973) 520.

[13] M.Ashida, Y.Ueda, H.Yanagi and K.Sayo, J.Polym.Sci.,Polym. Chem.Ed. received.

[14] M.A.O'Keefe, J.R.Fryer and D.J.Smith, Acta Cryst. A39 (1983) 838.

[15] Y.Ueda, M.Ashida, Y.Fujiyoshi, N.Uyeda and J.R.Fryer, Proc. XIth Int. Cong. on Electron Microscopy, Kyoto, 1986, Vol.2, p.1405.

Chapter 4 Crystal Growth of Octacyanometalphthalocyanine-metal Complexes in Thin Films

Abstract

Octacyanometalphthalocyanine-metal complex ($MPc(CN)_8$-M, M=Cu, Ni, Co, Fe, Zn and $K_2Pc(CN)_8$-K) crystals were synthesized by vapor-solid reaction of tetracyanobenzene(TCNB) with metal films and a KCl crystal. Their crystal growth was investigated by electron microscopy. The crystal morphology depended on reaction temperature, pressure and kinds of substrate. Crystals of $MPc(CN)_8$-M and $K_2Pc(CN)_8$-K grew long and thick tentacle-like on polycrystal metal films and a KCl (001) surface in the reaction temperature at 350 °C. Growth of the crystals was inactive at reaction temperatures below 300°C. The crystal defects such as bends and folds increased with elevating the reaction pressure. Growth mechanism was assumed as follows: $MPc(CN)_8$ molecules are formed on a substrate metal by tetramerization of TCNB vapor and peripheral nitrile groups of $MPc(CN)_8$ molecules coordinate to metal atoms of the substrate to form a $MPc(CN)_8$-M complex. $MPc(CN)_8$ molecules are piled up in parallel to form a column structure and the complex crystal grows by diffusion of metal atoms from the substrate. The crystal grows in well-defined when metal atoms are supplied sufficiently from the substrate.

1. Introduction

Organic thin films have been attracting interest for new

electronic and optical devices. Organic molecules have anisotropic properties in themselves, for example, in long-chain molecules such as polyacetylene[1,2] and macrocyclic molecules such as porphyrin[3] and phthalocyanine (Pc) compounds[4-10]. In order to make use of their characteristics for a practical architecture of organic molecular devices, crystallographically ordered molecular arrangement is required in thin films. As well-known, phthalocyanine compounds crystallize in a column structure in which the planar molecules are piled up in parallel[11,12] and show high electrical conductivity along the column axis by $\pi-\pi$ electron interaction[5,13,14]. Their crystal structure and molecular orientation in vacuum-deposited thin films have been elucidated by electron microscopy[15-19]. In a previous work[20], thin films of $MPc(CN)_8$ were synthesized directly on substrates such as metal films and a KCl crystal by *vapor-solid reaction of tetracyanobenzene(TCNB) with substrates* as shown in Fig.1 (a) and (b). Observation of the molecular images by high resolution electron microscopy(HREM)[21,22] elucidated that $MPc(CN)_8$ molecules stacked in parallel in a column structure holding their molecular planes perpendicular to the column axis. The molecules staggered alternately around the column axis and their peripheral nitrile groups coordinated to metal atoms diffused from the substrates, so that a $MPc(CN)_8$-M complex crystal was formed as shown in Fig.1 (c). This molecular stacking was different from that of other phthalocyanines which crystallized in a well-known herringbone column structure[12]. The complex crystal was a peculiar tentacle-like shape which grew

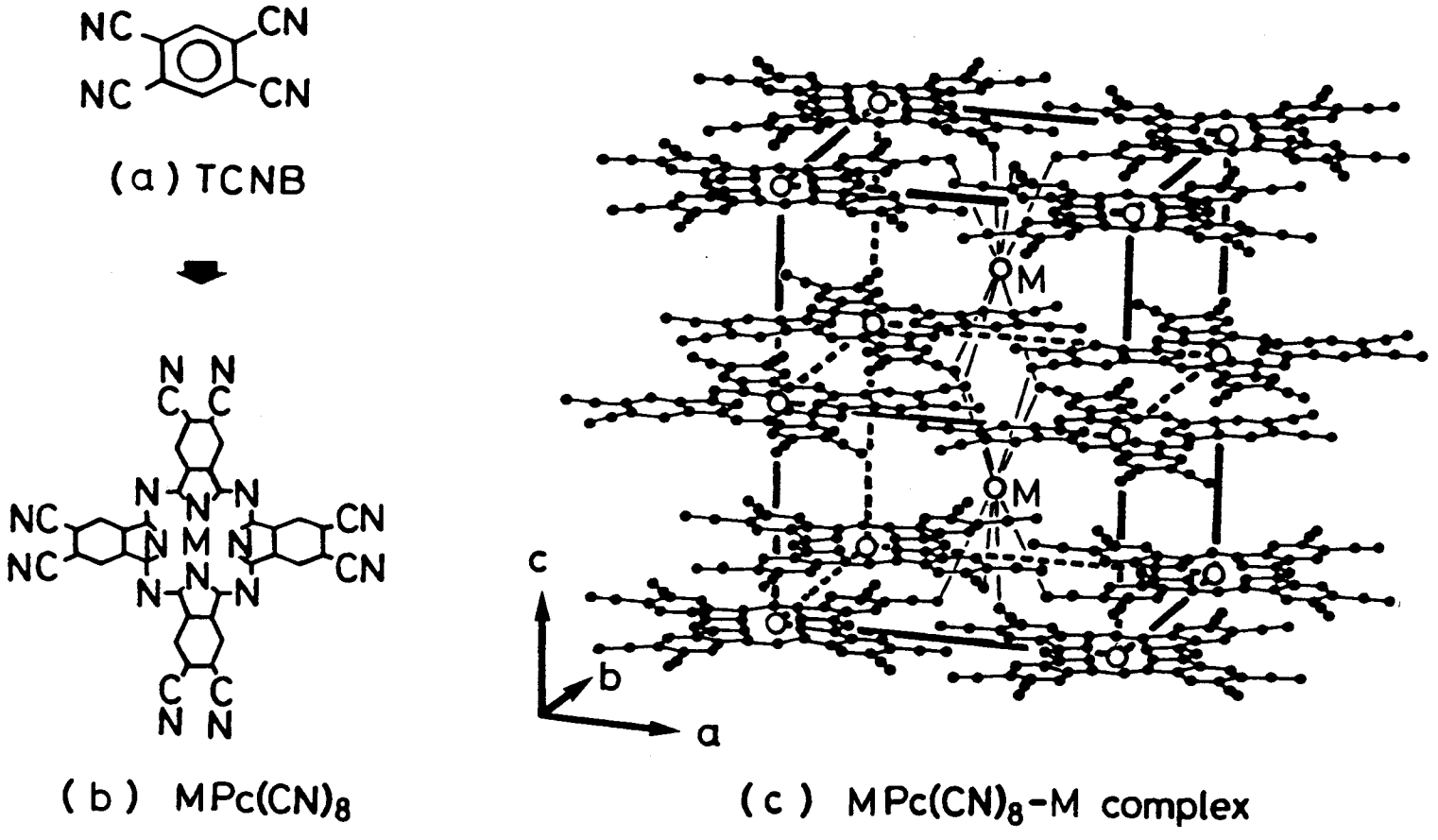

Fig.1 Molecular structure of TCNB (a) and $MPc(CN)_8$ (b).
Crystal structure of the $MPc(CN)_8$-M complex (c).

long along the column axis and its morphology was affected by the reaction temperature and kinds of substrate as described in Chapter 1. The characteristic molecular stacking and crystal morphology were closely related to formation of the complex, which depended on diffusion of metal atoms from the substrate. In this chapter, the $MPc(CN)_8$-M complex crystals were synthesized on various substrates under different reaction conditions in order to elucidate the growth mechanism. Crystal morphology was investigated by scanning and transmission electron microscopy (SEM and TEM). Effect of the reaction temperature, pressure and the substrate structure on the crystal growth is described and selective control of the growth is proposed.

2. Experimental

A sample of TCNB was synthesized by the method of Bailey et al.[23]. Substrate materials used were a cleavage (001) surface of a KCl single crystal and metallic films. As metallic films, Cu, Ni, Co, Fe and Zn were evaporated on a (001) surface of KCl kept at room temperature(25°C) or 350°C in a vacuum of $1x10^{-4}$Pa. A given amount of purified TCNB and the substrate material were sealed in an evacuated pyrex glass tube at pressures between 0.1Pa and 10kPa after flushing with argon gas. The tube was heated at temperatures between 250 and 450°C for 10 hr in a hot air oven. Films produced on the substrates were examined by a JEM-200CX electron microscope. The films together with the substrates were cut into pieces and coated with carbon, and crystal morphology was observed by the SEM mode operated at 40kV.

For TEM, the film was separated from KCl in water and mounted on a microgrid coated with an evaporated gold film. TEM observation was carried out at 200 kV accelerating.

3. Results and discussion

Copper films as substrate were prepared by evaporation on KCl crystals kept at room temperature and 350 °C. Figure 2 shows transmission electron micrographs and their electron diffraction patterns of the Cu films. The Cu film evaporated on KCl kept at room temperature is composed of polycrystallites and the electron diffraction pattern from the film indicates a ring pattern as shown in the figure (a). On the other hand, the electron diffraction pattern of the Cu film evaporated on KCl kept at 350 °C gives a single-crystal pattern, indicating that the crystal has the orientation of $(001)_{Cu}//(001)_{KCl}$ as shown in the figure (b). Figure 3 shows scanning electron micrographs of films produced on polycrystal Cu films at temperatures between 250 and 450 °C in a pressure of 10Pa. The films produced below 400°C were dark green or blue color and the film produced at 450 °C was gray or black with metallic gloss. The film produced at 250 °C is composed of column-like crystals growing from the substrate. The crystals produced between 300 and 400 °C are composed of thin and fine tentacle-like crystals branching from the column-like crystal. The fine tentacles grown at 350 °C reach out long and those grown at 400 °C stick up shortly from the thick column-like crystal. These column- and tentacle-like morphology is peculiar to the $MPc(CN)_8$-M complex crystals which grow along their column

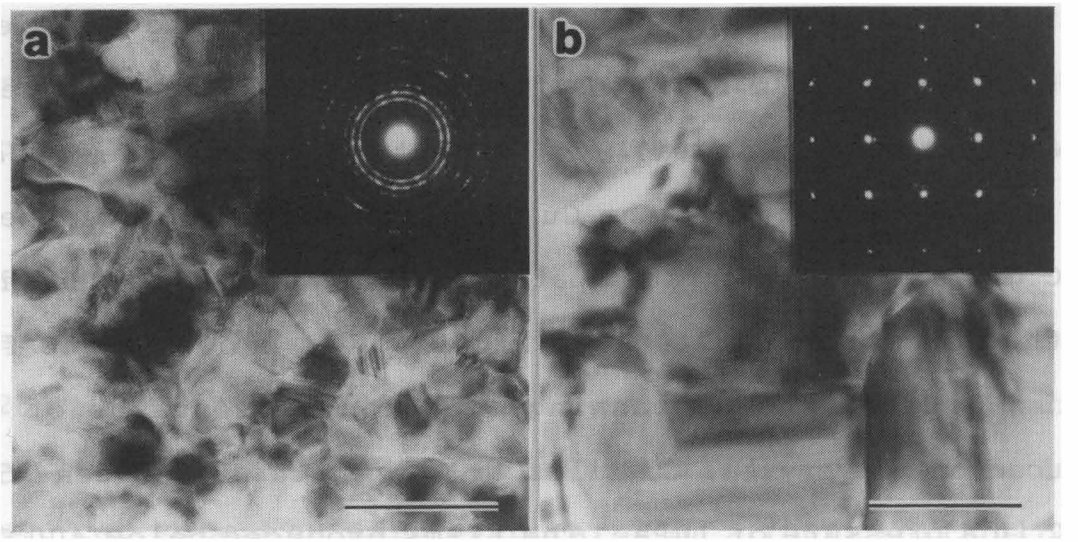

Fig.2 Transmission electron micrographs of Cu films evaporated on KCl kept at 25°C (a) and 350°C (b), and their electron diffraction patterns. Bar=50nm.

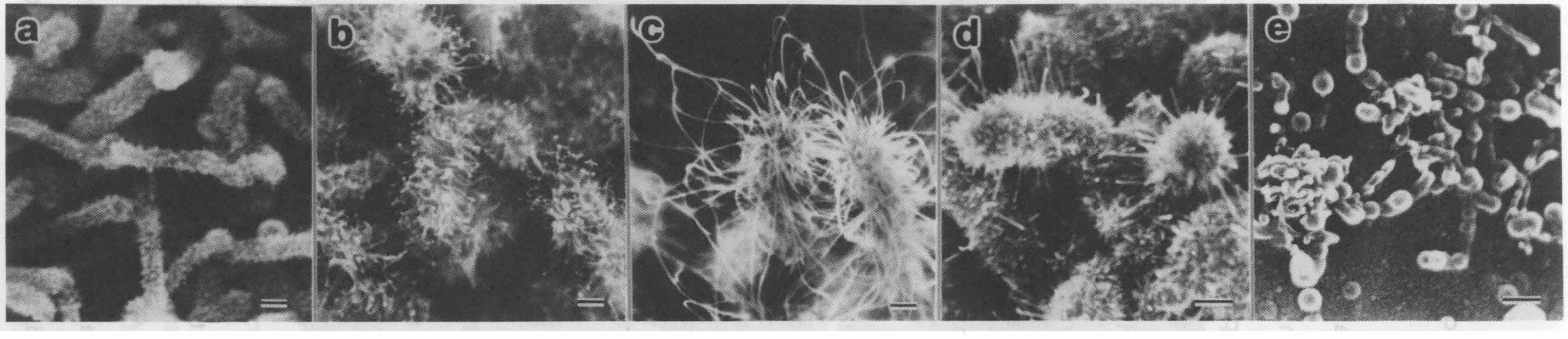

Fig.3 Scanning electron micrographs of films produced on polycrystal Cu films at 250 ℃ (a), 300 ℃ (b), 350 ℃ (c), 400 ℃ (d) and 450 ℃ (e) in a pressure of 10Pa. Bar=1 μm.

axes[20]. The film produced at 450 °C is composed of a thick layer with bulb-like crystals on the surface, which was identified as poly-phthalocyanine and other polymerized products of TCNB as described in Chapter 1. Films were produced on Cu films constructed with polycrystal and single-crystal at 250 and 350 °C in a pressure of 10Pa. Figure 4 shows scanning electron micrographs of sections of those films. At 250 °C, the film produced on a Cu polycrystal is composed of column-like crystals as shown in the figure (a), but the film produced on a Cu single-crystal is composed of a continuous layer as shown in the figure (b). At 350 °C, thick crystals with fine tentacles grow on substrates constructed with both polycrystal and single-crystal. However, the crystals on the single-crystal are bent and are shorter than that on the polycrystal. It suggests that the $MPc(CN)_8$-M complex crystals grow in well-defined on substrates of polycrystal metal films. Figure 5 shows films produced on KCl and various metal films constructed with polycrystals at 250 °C in a pressure of 10Pa. The morphology of the films depends on the substrate metals. The films on KCl and Ni are composed of small column-like crystals which are shorter than that on Cu shown in Fig.4 (a). The films produced on Co and Fe are composed of thick layers condensed on the substrates. They do not form column- or tentacle-like crystals which are characteristic of the $MPc(CN)_8$-M complexes. It seems that the films produced on Co and Fe are amorphous layers composed of $MPc(CN)_8$. On the other hand, large column-like crystals are observed in the film produced on Zn. They grow much thicker than the crystals produced on the

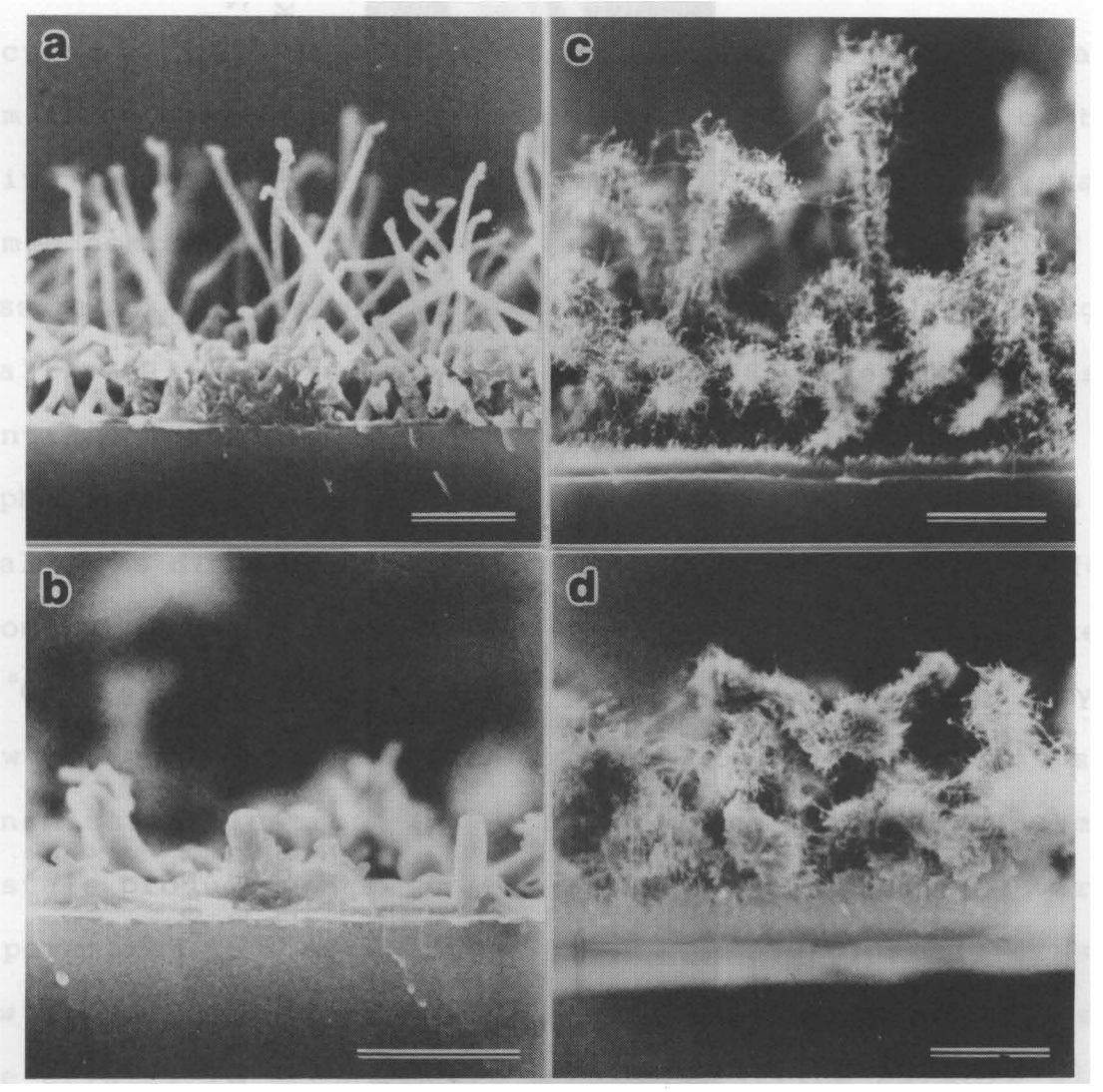

Fig.4 Scanning electron micrographs of films produced on Cu films composed of polycrystal (a), (c) and single-crystal (b), (d). The films were produced at 250 °C (a), (b) and 350 °C (c), (d) in a pressure of 10Pa. Bar=10μm.

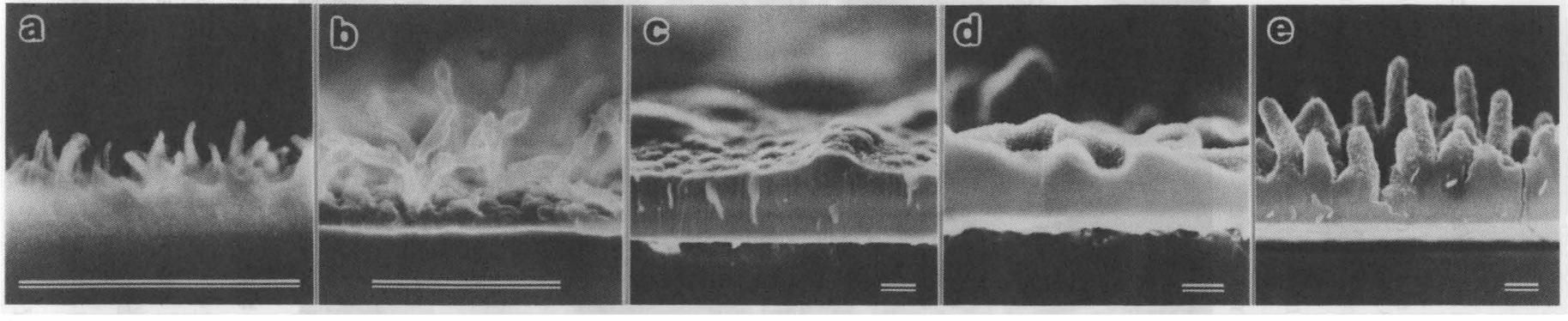

Fig.5 Scanning electron micrographs of films produced on KCl (a) and polycrystal films of Ni (b), Co (c), Fe (d) and Zn (e) at 250°C in a pressure of 10Pa. Bar=5μm.

other metals. For formation of the $MPc(CN)_8$-M complex crystals, metal atoms need to be supplied from the substrate surface to the crystals. Noteworthily, the melting point of Zn is 400 °C, which is much lower temperature than those of the other metals. Zinc atoms are able to migrate on the substrate surface even in the reaction at 250 °C in a pressure of 10Pa. Therefore, Zn atoms seem to be supplied enough from the substrate because of their active diffusion, so that the $ZnPc(CN)_8$-Zn complex crystal is formed completely. In the case of the reaction at 350 °C in a pressure of 10Pa, similar tentacle-like crystals were overgrown on all metal substrates as shown in Fig.6. These crystals are identified as respective $MPc(CN)_8$-M complexes, and have same morphology independent of the substrate metals. It suggests that metal atoms diffuse enough from every substrate and the $MPc(CN)_8$-M complex crystals are uniformly formed over the substrates at 350 °C. In order to investigate the initial stage of crystal growth, very thin films were observed by TEM. Figure 7 shows transmission electron micrographs of the $K_2Pc(CN)_8$-K complex crystals produced on KCl (001) surfaces by reaction at various temperatures in a pressure of 10Pa. At 250 °C, small crystals grow discretely on the KCl as shown in the figure (a). The disk-like crystal is composed of a square lattice network with a spacing of 1.57nm and a thin amorphous layer surrounding the square lattice. The lattice image corresponds to projection of the $K_2Pc(CN)_8$-K complex crystal along the c-axis[21]. The area of the complex crystals increases in the reaction at 350 °C as shown in the figure (b). In the reaction at 400 °C, the large

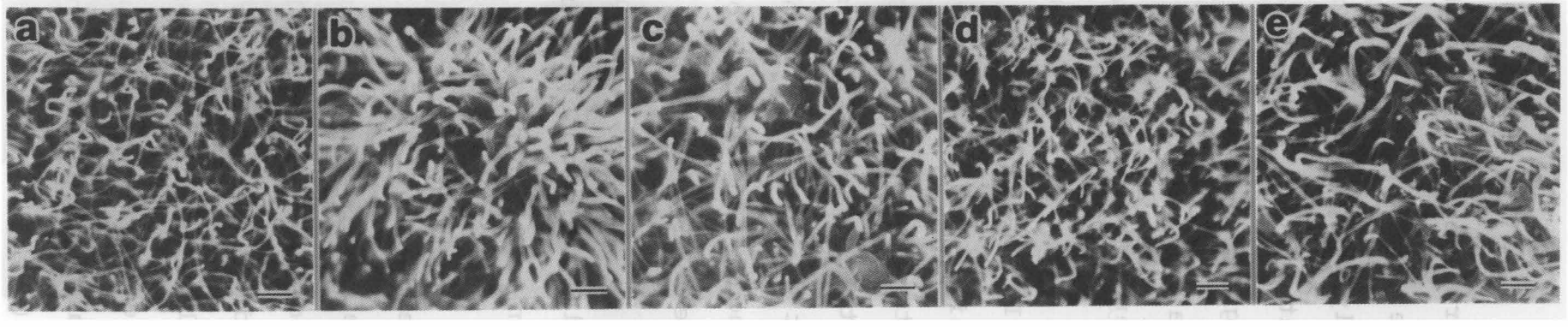

Fig.6 Scanning electron micrographs of films produced on KCl (a) and polycrystal films of Ni (b), Co (c), Fe (d) and Zn (e) at 350°C in a pressure of 10Pa. Bar=1μm.

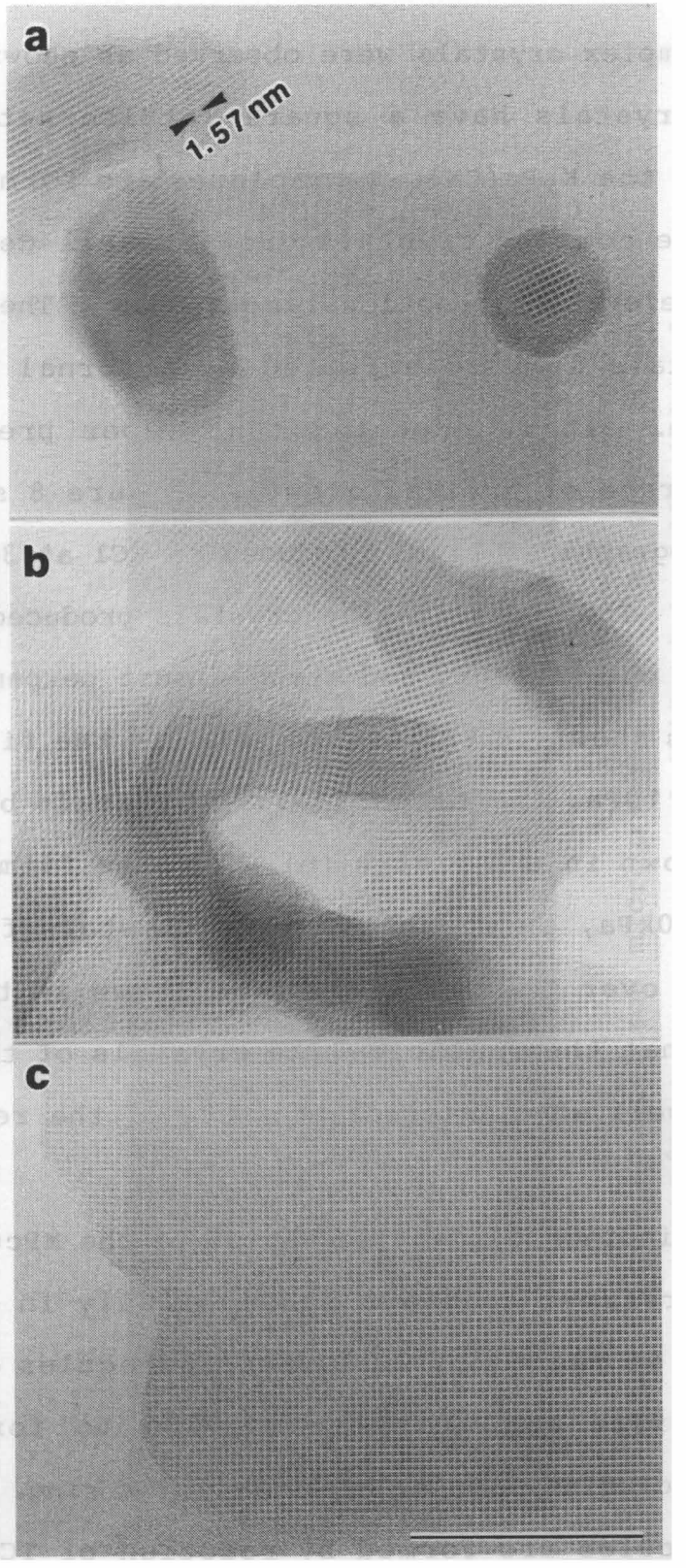

Fig.7 Transmission electron micrographs of films produced on KCl (001) surfaces at 250 °C (a), 350 °C (b) and 450 °C (c) in a pressure of 10Pa. Bar=50nm.

$K_2Pc(CN)_8$-K complex crystals were observed as shown in the figure (c). These crystals have a square lattice network of large dimension and the $K_2Pc(CN)_8$-K complexes are formed completely. Therefore, the complex crystals grow in well-defined on a KCl surface with elevating reaction temperature. The growth of the complex crystals is also affected by internal pressure of a reaction tube. It is expected that vapor pressure of TCNB influences a rate of crystal growth. Figure 8 shows scanning electron micrographs of films produced on KCl at 350°C in various low pressures. The tentacle-like crystals produced in a pressure of 0.1Pa reach out straight and stand almost perpendicular to the KCl surface as shown in the figure (a). In the film produced in a pressure of 10Pa, the tentacle-like crystals bend at various lengths as shown in the figure (b). In the film produced in a pressure of 10kPa, the tentacle-like crystals fold and a thin layer spreads over the KCl surface as shown in the figure (c). It suggests that the tentacle-like crystals of the $K_2Pc(CN)_8$-K complex grow well when internal pressure of the reaction tube is lower.

From these findings, growth mechanism of the $MPc(CN)_8$-M complex crystals is presumed as shown schematically in Fig.9. At the initial stage of reaction, TCNB vapor molecules deposit on the substrate surface and are tetramerized to form a $MPc(CN)_8$ molecule by including a metal atom in the Pc ring. The following $MPc(CN)_8$ molecules are formed by reaction of TCNB with metal atoms diffused from the substrate so that they are piled up in parallel in a column. Adjacent $MPc(CN)_8$ molecules are

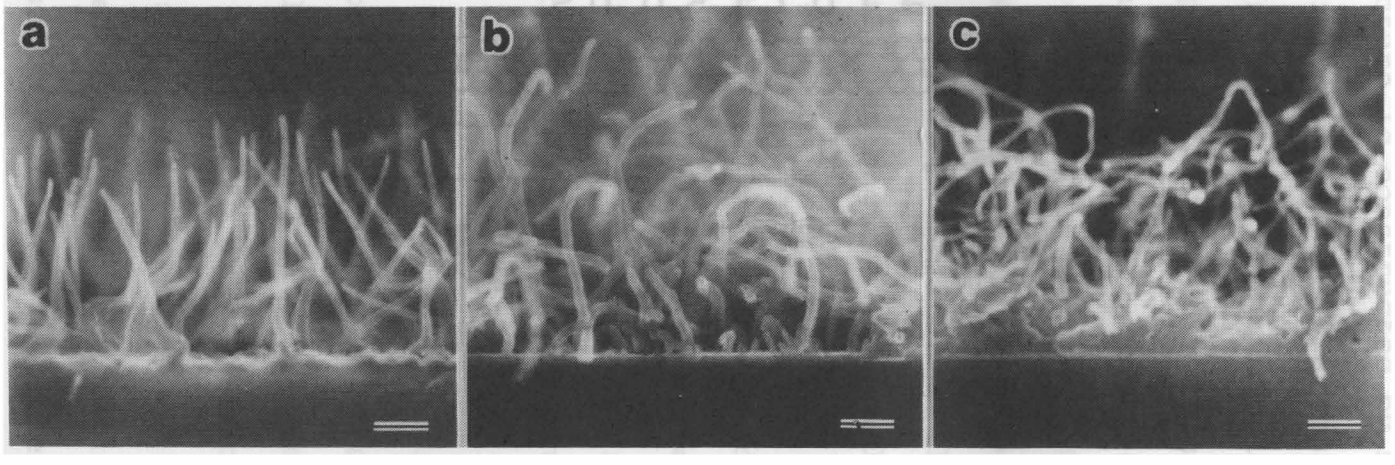

Fig.8 Scanning electron micrographs of films produced on KCl at 350 °C in pressures of 0.1Pa (a), 10Pa (b) and 10kPa (c). Bar=1μm.

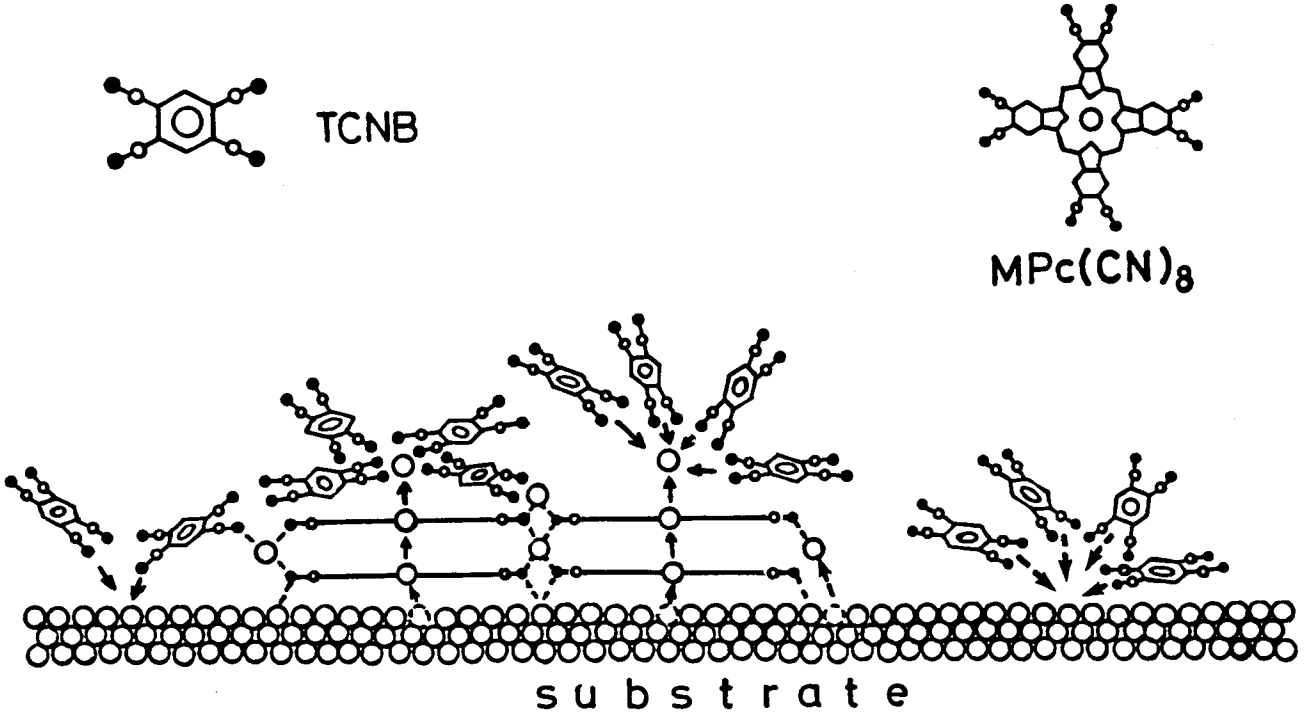

Fig.9 Schematic diagram of growth of the $MPc(CN)_8$-M complex crystal in reaction of TCNB vapor on a substrate.

simultaneously linked together by coordination of their peripheral nitrile groups with intercalated metal atoms. In this way, the column structure is constructed by successive deposit of TCNB molecules and diffusion of metal atoms from the substrate. As well-known, MPc molecules form a herringbone structure in which the molecular planes tilt to the column axis. On the other hand, molecular planes of $MPc(CN)_8$ are perpendicular to the column axis in the $MPc(CN)_8$-M complex crystal. Similar molecular stacking has been observed in an iodine-doped NiPc crystal[5,24]. The molecular planes of NiPc make an angle of $\pm 16^\circ$ with the column axis and the tilting angle of the molecules changes to be perpendicular to the column axis when iodine is doped to the NiPc crystal[5]. This structure change is ascribed to interaction between the adjacent molecular columns related to charge transfer from NiPc to iodine atoms. In the present case, it seems that coordinate bonds between the peripheral nitrile groups and the intercalated metal atoms keep molecular planes of $MPc(CN)_8$ perpendicular to the column axis.

Figure 10 shows a presumed description of crystal morphology of the $MPc(CN)_8$-M complex growing on a substrate. Tentacle-like crystals grow along the column axis by forming the $MPc(CN)_8$-M complex on the substrate. The crystals grow thicker with elevating reaction temperature because metal atoms are supplied enough from the substrate surface. Tentacle-like crystals reach out straight when the $MPc(CN)_8$-M complexes form a complete column as shown with letter A. If a metal atom happens to lack at a site as marked with arrowhead 1, the crystal branches out to a

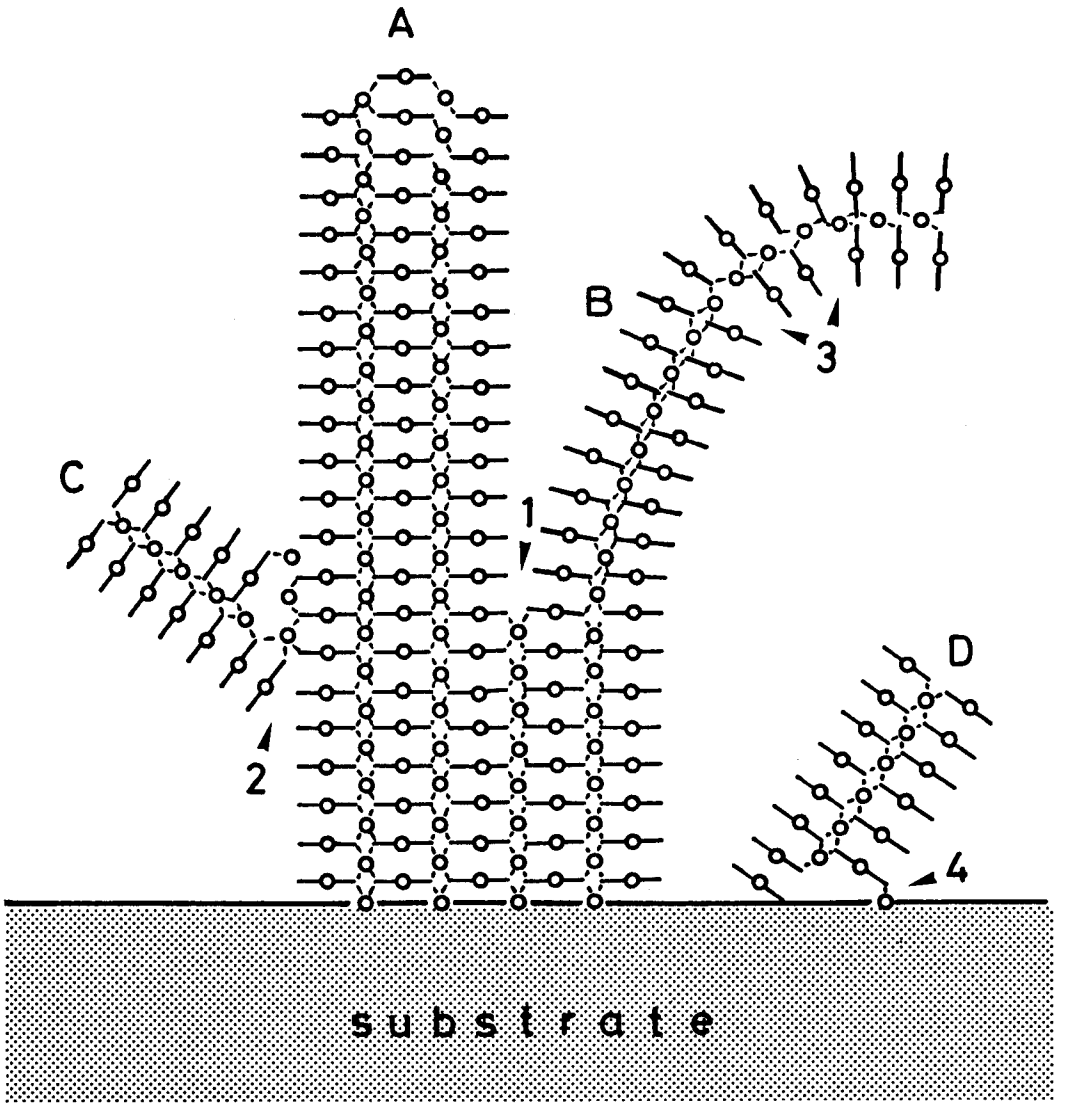

Fig.10 Schematic diagram of crystal morphology of the $MPc(CN)_8$-M complex.

thin tentacle as shown with letter B. These branched tentacles were observed in the film produced on Cu at 300 and 350°C (Fig.3 (b) and (c)). On the other hand, fine tentacles sticked up as shown with letter C were observed in the film produced on Cu at 400 °C (Fig.3 (d)). These crystals are caused by disorder of molecular stacking at a site as marked with arrowhead 2. If $MPc(CN)_8$ molecules happen to lack at sites as marked with arrowhead 3, tentacles bend or fold as observed in the film produced on KCl at 350°C in a pressure of 10kPa (Fig.8 (c)). It seems that the lack of $MPc(CN)_8$ molecules is caused by the low rate of formation of the molecules, because partial pressure of TCNB vapor is low at the reaction pressure of 10kPa. Tentacle-like crystals frequently tilt against the substrate surface as observed remarkably in the film produced on Cu at 250 °C (Fig.4 (a)). In these crystals, $MPc(CN)_8$ molecules come into contact with the substrate surface by a given angle as shown with arrowhead 4 and the molecules are piled up in the oblique direction as shown with letter D. On the other hand, many tentacle-like crystals grown on KCl were perpendicular to the substrate surface as observed in the film produced at 350°C in a pressure of 0.1Pa (Fig.8 (a)).

Growth of the $MPc(CN)_8$-M complex crystals is affected by surface structure of the substrate. One special feature of the growth was observed in the film produced on a Cu film constructed with a single-crystal at 250°C in a pressure of 10Pa. Figure 11 (a) shows a scanning electron micrograph of the film growing on a cleavage face of KCl crystal. The direction of

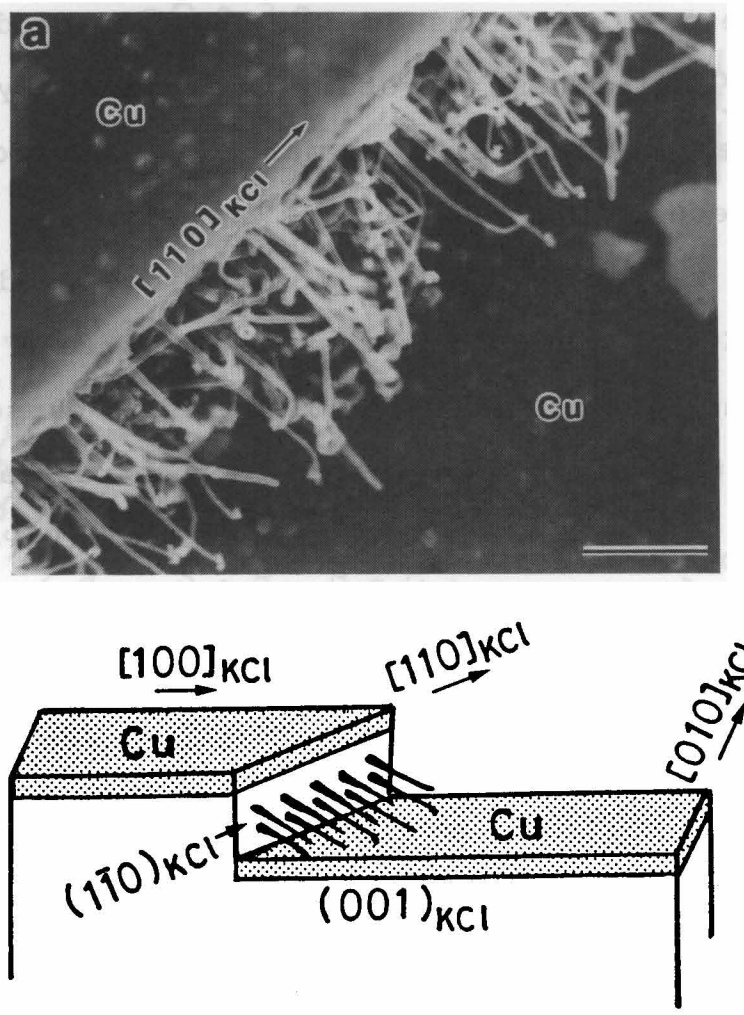

Fig.11 Scanning electron micrograph of a film produced on a single-crystal Cu film at 250℃ in a pressure of 10Pa (a). Bar=10μm. Schematic description of growth of the $K_2Pc(CN)_8$-K complex crystals on the (110) step of the KCl substrate (b).

the KCl crystal was determined by the [100] edge of the cleaved KCl crystal. The (001) surface of the KCl substrate was covered with a Cu layer of a single-crystal and the step plane corresponded to the (110) plane of the KCl crystal which was not covered with Cu. Tentacle-like crystals are observed to grow long on the (110) step plane only. Figure 11 (b) shows a schematic explanation of the film. Tentacle-like crystals do not grow on the surface covered with Cu in this reaction condition as is shown in Fig.4 (b). The finding suggests that the $K_2Pc(CN)_8$-K complex crystals grow selectively on the (110) plane of the KCl substrate. Noteworthily, the tentacle-like crystals grow much longer and thicker than those grown on the (001) surface of KCl in the same reaction condition. This selective growth of the $K_2Pc(CN)_8$-K complex crystals can be explained schematically as shown in Fig.12. The growth of the $K_2Pc(CN)_8$-K complex crystals on the (001) plane is inactive in reaction at 250 °C. On the other hand, the complex crystals grow on the (110) plane even in this reaction condition. Potassium atoms can be diffused more easily from the (110) plane than from the (001) one because a potasium atom on the (110) plane is bonded more loosely by chlorine atoms as shown in the figure (c). Therefore, the $K_2Pc(CN)_8$-K complex crystals grow long and thick on the (110) plane even at 250 °C. Similar effect of the substrate structure on the crystal growth was observed in the films produced on Cu films constructed with either polycrystal or single-crystal. The growth of the $CuPc(CN)_8$-Cu complex crystals was more active on a polycrystal Cu film than a single-crystal

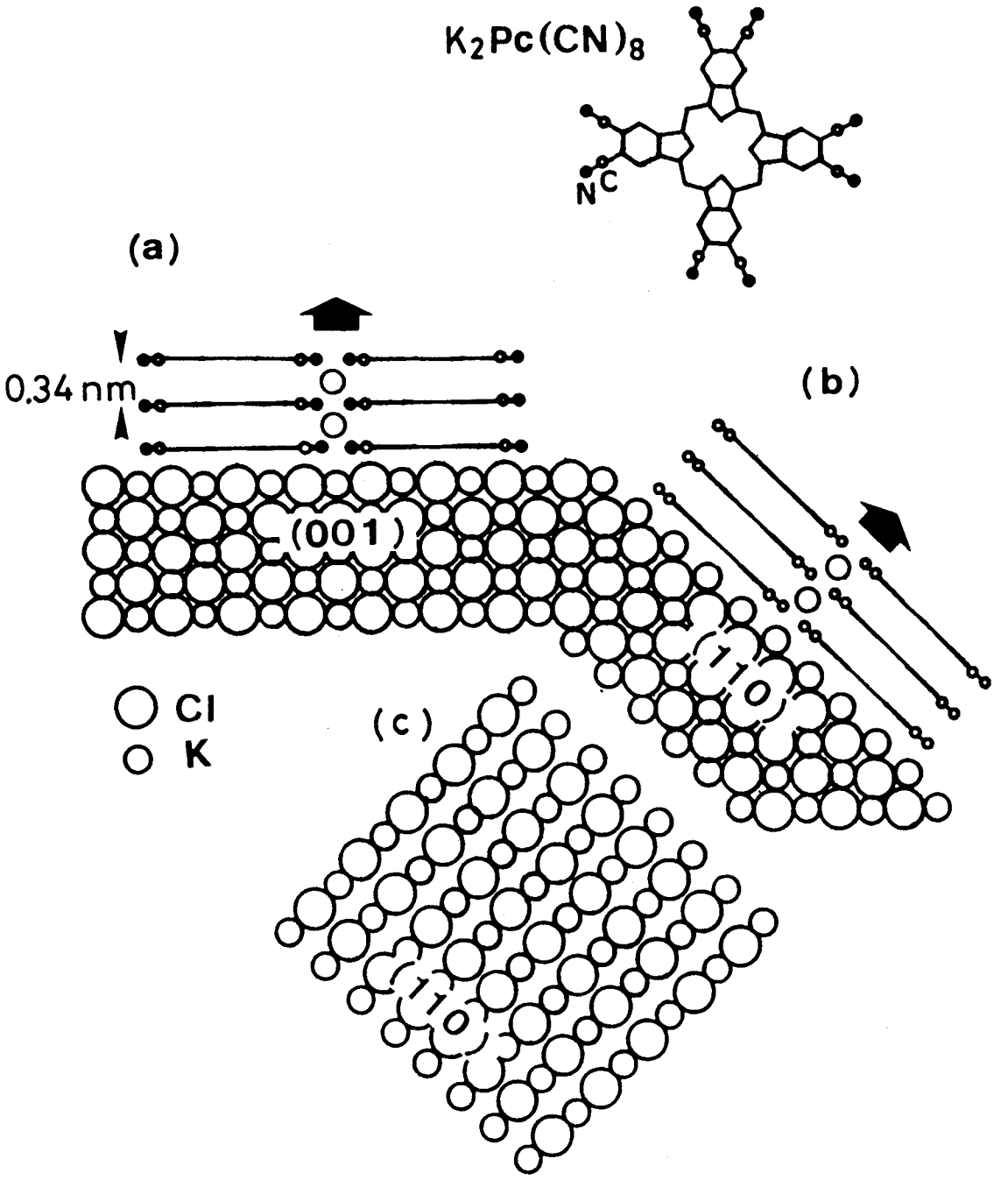

Fig.12 Schematic diagram of growth of the $K_2Pc(CN)_8$-K complex crystals on the KCl (001) plane (a) and the KCl (110) plane (b), and atomic arrangement of the KCl (110) plane (c).

one. Because a polycrystal film has higher surface energy than a single-crystal one, metal atoms migrate easily on the surface of a polycrystal film. Consequently, the complex crystals grow long and thick preferably on a substrate which supplies metal atoms enough. In view of the growth mechanism as mentioned above, it will be able to control the crystal growth of the $MPc(CN)_8$-M complexes under selective orientation.

References

[1] H.Shirakawa and S.Ikeda, Polym. J. 2 (1971) 231.

[2] H.Shirakawa, E.J.Louis, A.G.MacDiarmid, C.K.Chiang and A.J.Heegar, J.Chem.Soc. Chem. Commun. (1977) 578.

[3] B.M.Hoffman and J.A.Ibers, Acc.Chem.Res. 16 (1983) 15.

[4] A.Girandeau, F.R.F.Fan and A.J.Bard. J.Chem.Soc. 103 (1980) 5173.

[5] C.J.Schramm, R.P.Scaringe, D.R.Stojakovic, B.M.Hoffmann, J.A.Ibers and T.J.Marks, J.Am. Chem.Soc. 102 (1980) 6702.

[6] B.N.Diehl, T.Inabe, J.W.Lyding, K.F.Schoch, C.R.Kannewurf and T.J.Marks, J.Am.Chem.Soc. 105 (1983) 1551.

[7] Z.D.Popovic and J.H.Sharp, J.Chem.Phys. 66 (1977) 5076.

[8] E.R.Menzel and R.O.Loufty, Chem.Phys.Lett. 72 (1980) 522.

[9] R.O.Loufty, J.H.Sharp and C.K.Hsiao, and R.Ho, J.Appl.Phys. 52 (1981) 5218.

[10] R.O.Loufty and L.F.McIntyre, Can.J.Chem. 61 (1983) 73.

[11] J.M.Robertson, J.Chem.Soc. (1935) 615.

[12] C.J.Brown, J.Chem.Soc.A (1968) 2488.

[13] M.Danzig, C.Liang and E.Passaglia, J.Am.Chem.Soc. 85 (1963)

668.

[14] J.L.Petersen, C.J.Schramm, D.R.Stojakovic, B.M.Hoffmann and T.J.Marks, J.Am.Chem.Soc. 99 (1977) 286.

[15] M.Ashida, N.Uyeda and E.Suito, Bull.Chem.Soc.Jpn. 39 (1966) 2616.

[16] M.Ashida, Bull.Chem.Soc.Jpn. 39 (1966) 2624.

[17] M.Ashida, Bull.Chem.Soc.Jpn. 39 (1966) 2632.

[18] N.Uyeda, T.Kobayashi, E.Suito, Y.Harada and M.Watanabe, J.Appl. Phys. 43 (1972) 5181.

[19] T.Kobayashi, Y.Fujiyoshi, F.Iwatsu and N.Uyeda, Acta Cryst. A37 (1981) 692.

[20] M.Ashida, Y.Ueda, H.Yanagi and K.Sayo, J.Polym.Sci., Polym. Chem.Ed. received.

[21] M.Ashida, Y.Ueda, H.Yanagi, Y.Fujiyoshi, N.Uyeda and J.R.Fryer, Acta Cryst. accepted.

[22] H.Yanagi, S.Maeda, Y.Ueda and M.Ashida, J.Electron Microscopy, received.

[23] A.S.Baily, R.B.Henn and J.M.Langton, Tetrahedron 19 (1963) 161.

[24] T.Kobayashi, K.Yase and N.Uyeda, Acta Cryst. B40 (1984) 263.

Chapter 5 Epitaxial Growth of Octacyanometalphthalocyanine-metal Complex Crystals

Abstract

Thin films of octacyanometalphthalocyanine-metal complex ($K_2Pc(CN)_8$-K and $CuPc(CN)_8$-Cu) crystals were prepared by vapor-solid reaction of tetracyanobenzene(TCNB) with substrates. The $K_2Pc(CN)_8$-K film on a KCl (001) surface was composed of thin crystals in which planar $K_2Pc(CN)_8$ molecules came into parallel contact with the substrate surface and were piled up along the c-axis perpendicular to the substrate surface. Many crystallites with double-directional orientation intersected each other by an angle of about 23°. The double-directional orientation was ascribed to interaction between nitrile groups of $K_2Pc(CN)_8$ molecules and a KCl crystal and to the crystal structure of the $K_2Pc(CN)_8$-K complex. The crystals took three types of mutual orientations on a (001) surface of KCl and the relative orientation of the deposit crystal to the KCl substrate was interpreted in terms of multiple positioning of the $K_2Pc(CN)_8$ molecules on the ionic lattice of the KCl surface. Electron micrographs from a thin film of the $CuPc(CN)_8$-Cu complex crystal produced on a Cu film showed various lattice fringes which suggested that the crystals took random orientation on the metal substrate. $CuPc(CN)_8$ molecules came into contact with the substrate surface at various angles so that the column axes of the crystals inclined to the substrate surface.

1. Introduction

Oriented organic thin films have been generally prepared by the Langmuir-Blodgett(LB) method[1] and/or a vacuum-evaporation method[2]. The former method can be applied to linear molecules having hydrophilic peripheral groups in a wet process and properties of the LB films have been reported by many workers[3]. On the other hand, the latter method has been investigated on epitaxial growth of both planar molecules such as phthalocyanines(Pc)[4-8] and linear molecules such as paraffins[9-13] and polyethylene[14]. CuPc films vacuum-deposited on muscovite indicated two different orientations in which the b-axis of the crystal was either standing or parallel to the substrate, depending upon conditions of surface treatments[7]. A paraffin film vacuum-deposited on a KCl (001) surface at room temperature was composed of rod-like crystallites, in which their fiber axes oriented parallel to the [110] direction of the KCl crystal[9]. In the case of derivatives of paraffins, the crystal morphology and orientation depended on their polar end groups such as hydroxyl and ester groups[10-12]. The orientation of a vacuum-deposited paraffin film was also affected by a substrate structure. A hexatriacontane film deposited on a KCl covered with a gold film was composed of lamellar crystals which took their fiber axes perpendicular to the substrate surface[13]. Various types of these epitaxial growth were explained by different interaction between organic molecules and a substrate surface.

In a previous work[15], thin films of $MPc(CN)_8$ were prepared

directly on substrates by vapor-solid reaction of TCNB with a KCl crystal and metal films. $MPc(CN)_8$ molecules were piled up in a column structure to form $MPc(CN)_8$-M complex crystals[16,17]. The molecules staggered alternately around the c-axis and their peripheral nitrile groups coordinate to intercalated metal atoms as shown in Fig.1. The crystal had a tetragonal lattice (space group P4/mcc) in which the cell parameter c was 0.68nm, twice a interplanar distance of Pc molecules. The crystal morphology varied with reaction temperature, pressure and kinds of substrate material as described in Chapter 4. It seemed that their crystal growth depended on diffusion of metal atoms from the substrate and the crystal orientation was affected by a surface structure of the substrate.

This chapter is concerned with epitaxial growth of the $MPc(CN)_8$-M complex crystals on substrates. Thin films were synthesized from TCNB on substrates, a cleavage surface of a KCl single crystal and a vacuum-evaporated Cu film. The mechanism of epitaxial growth and mutual orientation between deposit and substrate crystals were examined by means of electron microscopy.

2. Experimental

A sample of TCNB was synthesized from pyromellitic dianhydride[18]. Substrate materials used were a (001) surface of a KCl single crystal cleaved in air and a vacuum-evaporated Cu film. As a Cu film composed of a single crystal, Cu was evaporated on a KCl (001) surface kept at 350°C in a vacuum of $1x10^{-4}$Pa. Thickness of the Cu film was controlled at about

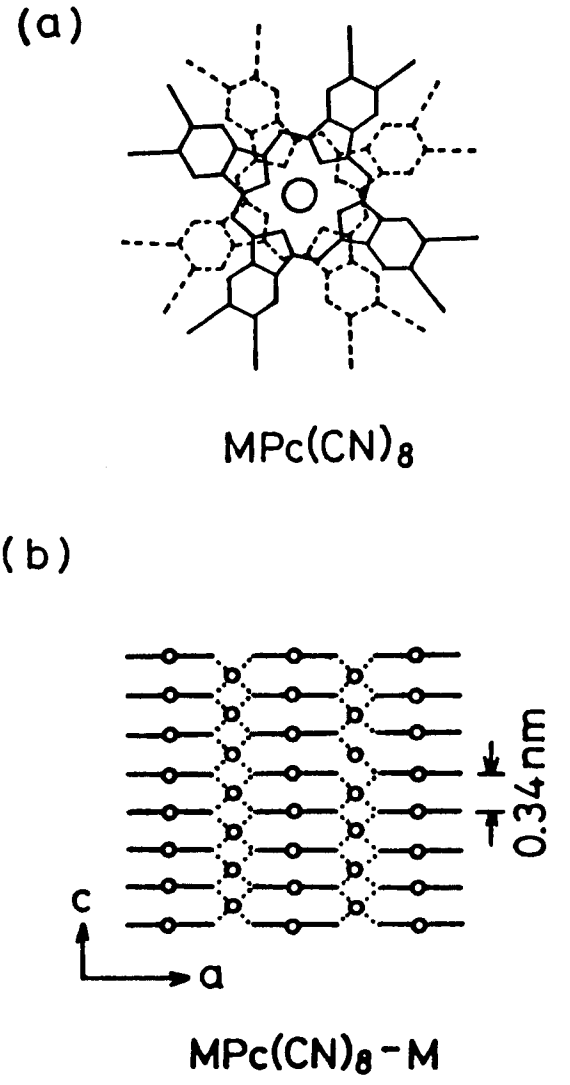

Fig.1 Crystal structure of the $MPc(CN)_8$-M complex. Superposition of molecules projected along the c-axis (a) and column structure projected along the b-axis (b).

100nm. A given amount of purified TCNB and the substrate material were sealed in an evacuated pyrex glass tube at a pressure of 10Pa after flushing with argon gas. The tube was heated at a temperature between 300 and 350°C for 10 hr in a hot air oven. After films produced on the substrates had been reinforced with evaporated carbon films, specimen films were separated from the KCl substrates in water for electron microscopy. The residual Cu film was dissolved away in a dilute acid solution. The specimen film was mounted on a microgrid coated with an evaporated gold film. Electron microscopy was carried out by a JEM-200CX at 200kV accelerating. The relative orientation of the deposited crystals to the KCl substrate was determined from a step which had been made on the KCl (001) surface. The KCl substrate was thermally etched beforehand at 450 °C in a pressure of 10Pa for 5hr. Steps on the KCl (001) surface revealed regular edges in parallel to the [100] direction of the KCl crystal.

3. Results and discussion

A green thin film of the $K_2Pc(CN)_8$-K complex crystals was formed on a KCl (001) cleavage surface by reaction of TCNB with KCl. The film was composed of thin crystals with discrete disk-like crystallites as shown in Fig.2. It shows square lattice networks with a spacing of 1.57 nm which coincides with lattice constants, a and b, of the tetragonal cell[16]. It demonstrates that the crystals take their c-axes perpendicular to the KCl (001) surface and $K_2Pc(CN)_8$ molecules are piled up in parallel to

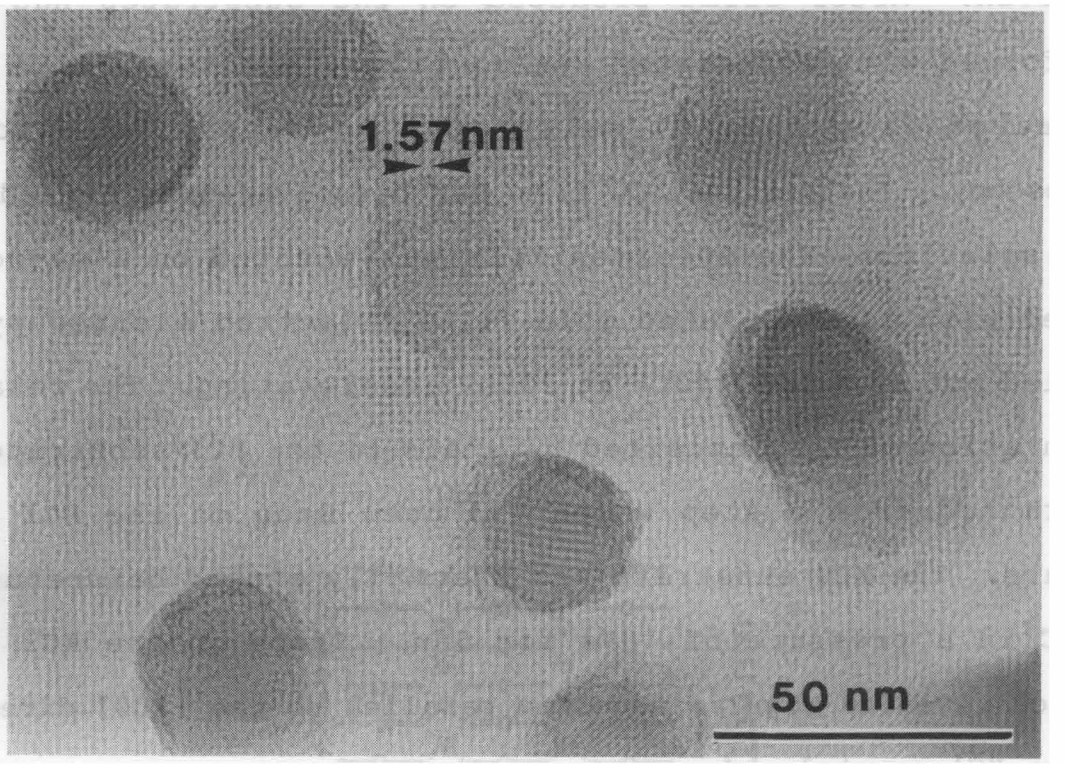

Fig.2 Electron micrograph of a thin film of the $K_2Pc(CN)_8$-K complex crystal produced on a KCl (001) surface.

the substrate. Many crystallites with double-directional orientation were observed in the film as shown in Fig.3. Each dark dot aligned in the square lattice corresponds to the molecular column projected along the c-axis. The molecular image in a wedge-shaped area can not be clearly observed because molecular stacking may be disordered at the grain boundary. The a-axes of the two crystallites make an angle of about 23° with respect to each other. The double-directional orientation in crystals was confirmed by a selected area electron diffraction pattern of the film as shown in Fig.4 (a). This pattern is composed of superposition of two single net patterns with C_{4v} symmetry, corresponding to a lattice spacing of 1.57nm. The reflection spots are schematically represented in Fig.4 (b) which shows that the two hk0 diagrams rotate by 23° with respect to each other. It seems that the double-directional orientation is caused by interaction between the nitrile groups of $K_2Pc(CN)_8$ molecules and the KCl crystal, and the intersecting angle of 23° is related to the crystal structure of the $K_2Pc(CN)_8$-K complex. Figure 5 shows a schematic diagram of the molecular arrangement in the $K_2Pc(CN)_8$-K complex crystal projected along the c-axis[19]. $K_2Pc(CN)_8$ molecules are located at the corners of the square lattice and are rotated alternately around the c-axis. Each molecule M_1 in the first layer indicated by a solid line staggers clockwise by an angle ω and each molecule M_2 of the second layer indicated by a dashed line staggers counter-clockwise by the same angle. The staggering angle ω was determined to be 27.4° directly from high resolution molecular

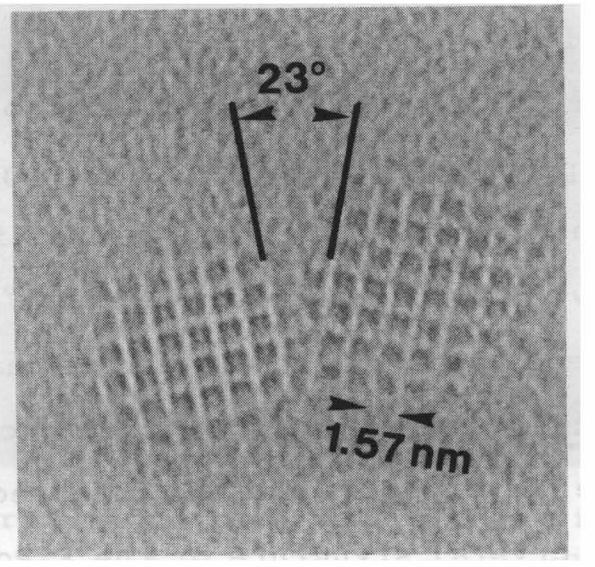

Fig.3 Electron micrograph of the $K_2Pc(CN)_8$-K crystallites with double-directional orientation produced on a KCl (001) surface.

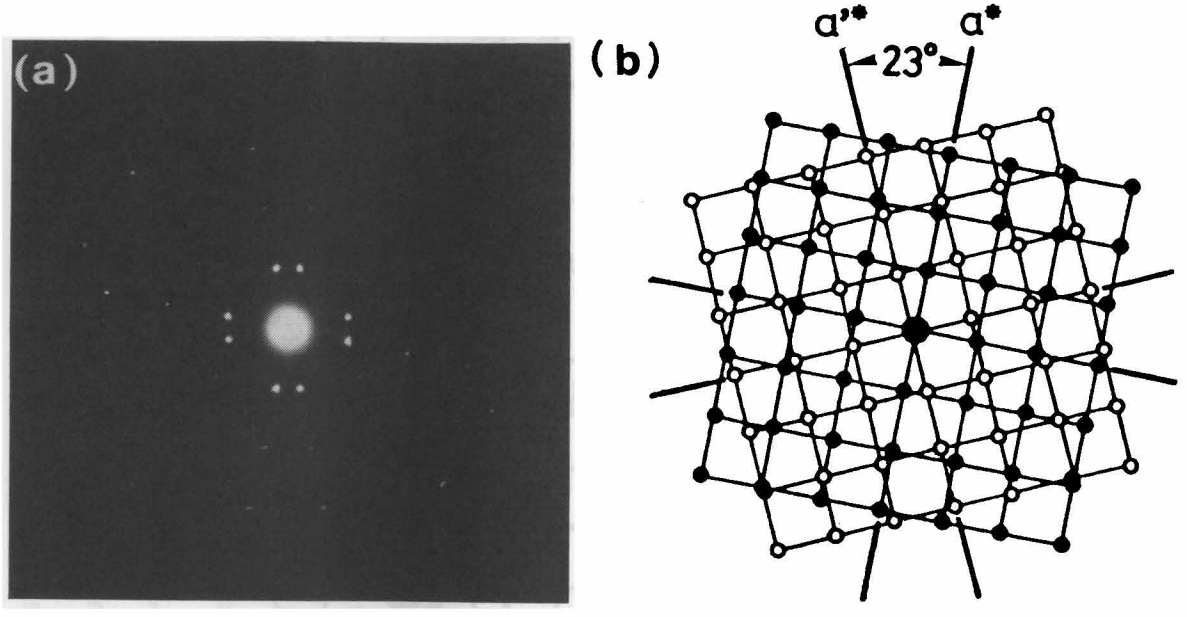

Fig.4 A selected area electron diffraction pattern of the $K_2Pc(CN)_8$-K crystal (a) and its schematic representation (b).

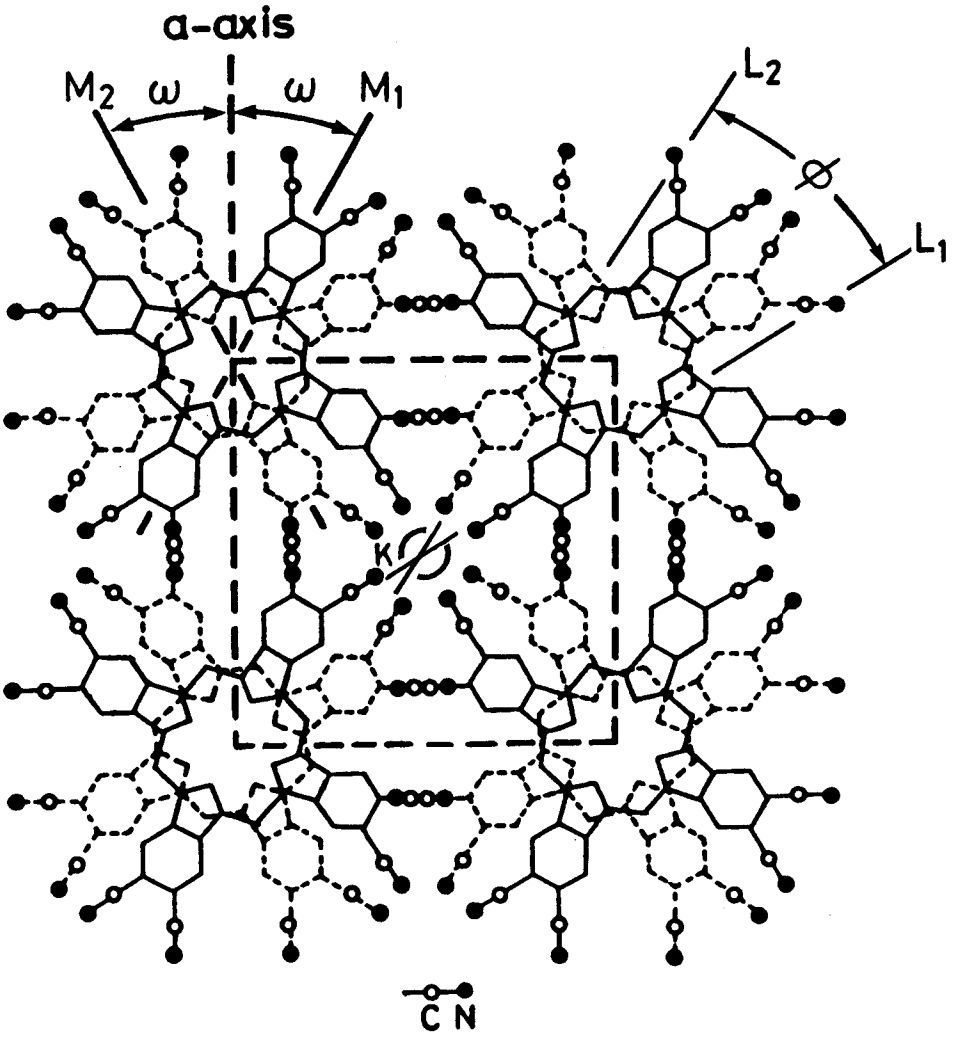

Fig.5 Schematic diagram of the molecular arrangement in the $K_2Pc(CN)_8$-K crystal projected along the c-axis.

images with aid of image simulation[19]. A potassium atom is intercalated at the center of the square lattice and surrounded by a distorted cube of peripheral nitrile groups from eight $K_2Pc(CN)_8$ molecules in the successive layers. The superposed nitrile groups coordinated to the potassium atom arrange to make an intersecting angle ϕ as shown with lines of L_1 and L_2. This angle was calculated to be 22.9° when the staggering angle ω was 27.4°, where the peripheral nitrile groups bonded to the benzene ring were assumed to make an angle of 120° with the carbon-carbon bond corresponding to the molecular structure of the tetracyanobenzene crystal[20]. This value of ϕ coincides well with the angle between the double-directional crystals, 23°. The peripheral nitrile groups are more electronegative than parts of the π electron macrocycle in a $K_2Pc(CN)_8$ molecule and attract a certain amount of electron charge from a central potassium atom. A nearly straight row of ionic charges, $C{=}\overset{\delta-}{N}{-}K^{+}{-}\overset{\delta-}{N}{=}C$, is formed between two molecules located at diagonal positions of the square lattice in the $K_2Pc(CN)_8$-K complex. A certain interaction is probably caused between this ionic charge and the KCl substrate. At an initial stage of nucleation, this ionic row is considered to take the most stable fitting with the ionic arrangement of the KCl (001) surface. It is assumed that two different orientations of the crystals relative to the KCl lattice arise from two possible contacts of the ionic rows, L_1 and L_2, with the KCl surface. Consequently, the crystals take double-directional orientations so that their a-axes make an angle of 23° with respect to each other.

In order to elucidate a mutual relation between the $K_2Pc(CN)_8$-K complex and the KCl substrate, films were produced on a KCl (001) surface etched thermally. Figure 6 shows a representative electron micrograph of the film. As well-known, when alkali halides are etched thermally in vacuum, their (001) surfaces exhibit evaporation pits and other corrosion figures[21]. A rectangular contour in the figure corresponds to an plateau which is made by thermal etching, and it reveals the [100] and [010] directions of the KCl crystal. The $K_2Pc(CN)_8$-K complex crystals are observed both inside and outside of the contour of the step. These crystals take their c-axes perpendicular to the (001) surface of KCl as same as those of the film in Fig.2, and they show square lattice fringes with a spacing of 1.57 nm. Three different orientations of the square lattices can be observed in sites shown with arrowheads A, B and C. The representative areas outlined by a, b and c were enlarged in Fig.7 (a), (b) and (c), respectively. The crystallites in the figure (a) show the double-directional orientation as mentioned above. The bisector of the two lattices makes an angle of 45° to the $[100]_{KCl}$ direction, that is, its direction coincides with the $[110]_{KCl}$ direction. The a-axis of one square lattice makes an angle of 33.5° to the $[100]_{KCl}$ direction and the a'-axis of the other lattice rotates by 23° to the a-axis. The a-axes of the crystallites in the figures (b) and (c) make angles of 11.5° and 18° to the $[100]_{KCl}$ direction, respectively.

From these mutual relations between the deposit and substrate crystal lattices, three types of nucleations of the $K_2Pc(CN)_8$-K

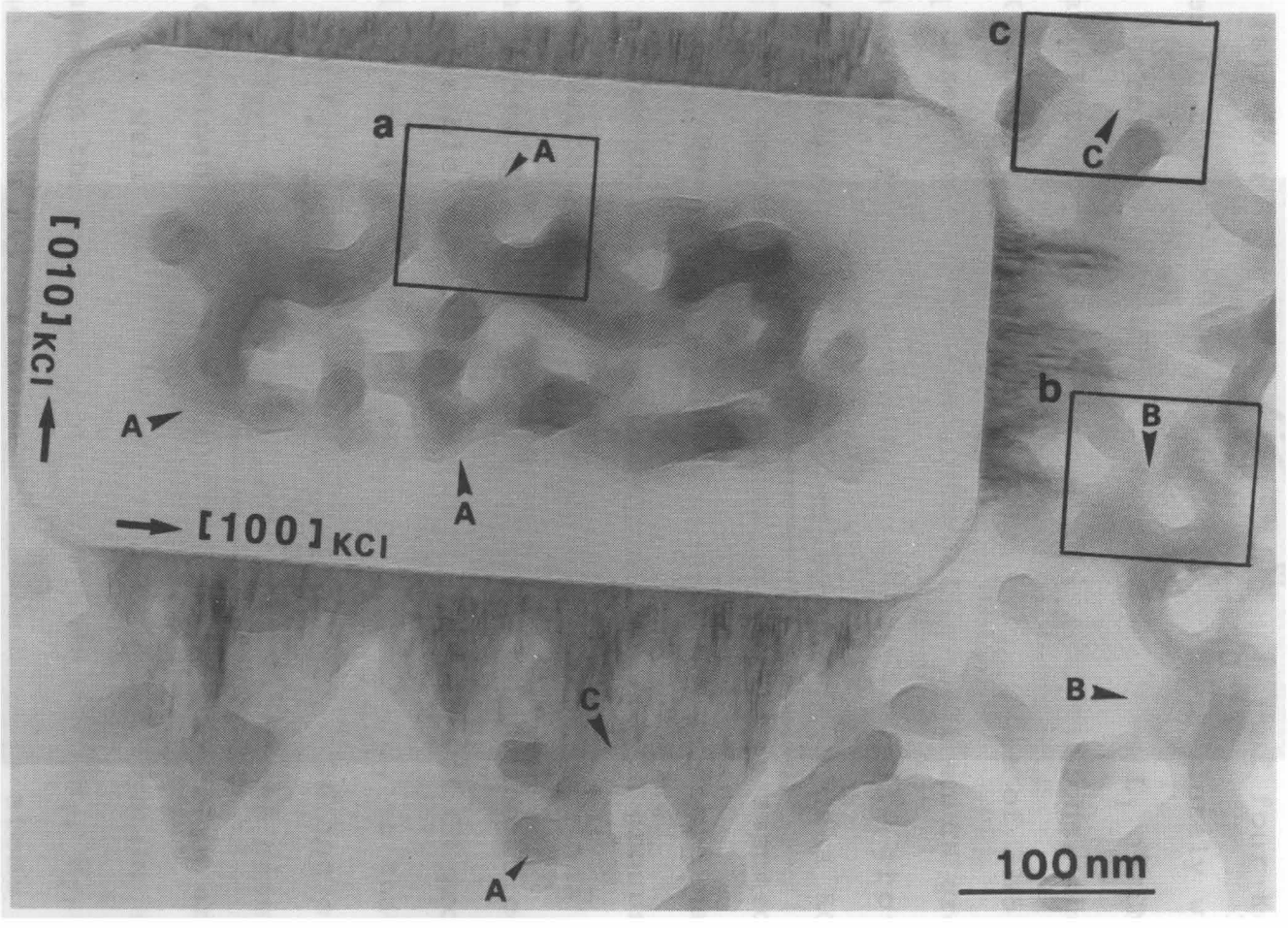

Fig.6 Electron micrograph of a thin film of the $K_2Pc(CN)_8$-K complex crystal produced on a thermally etched KCl (001) surface.

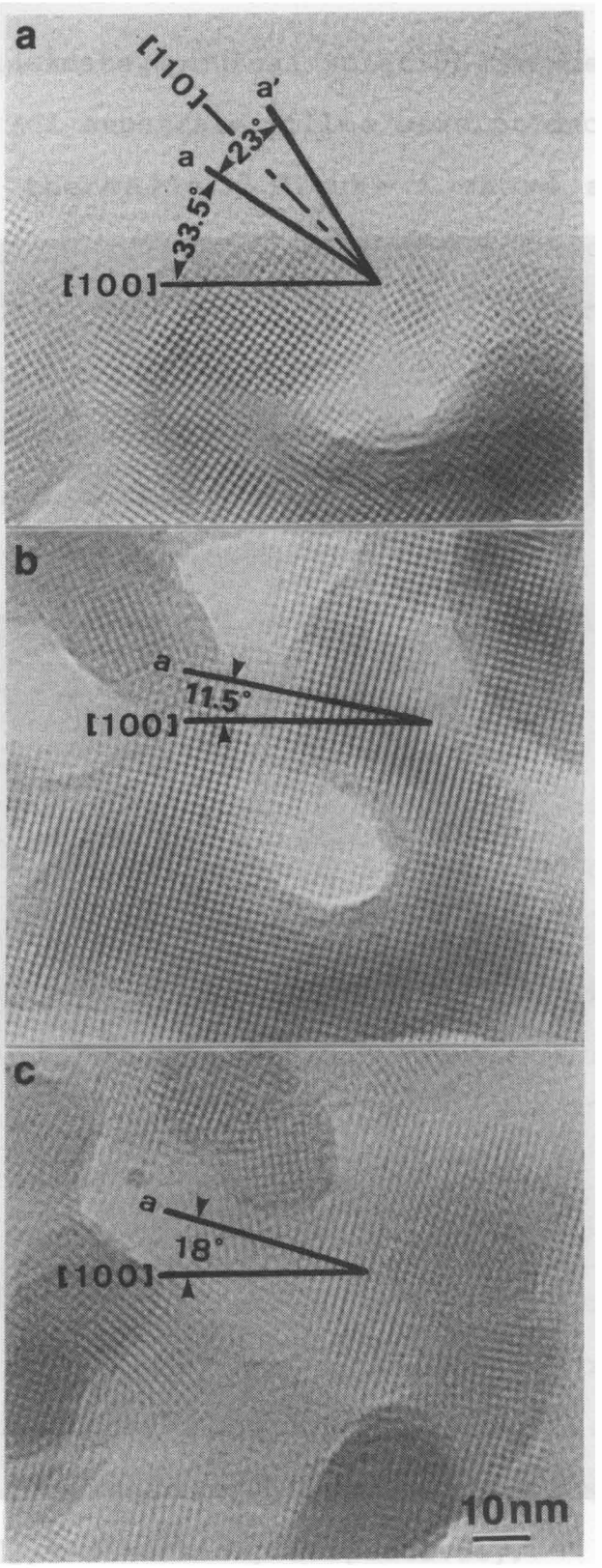

Fig.7 Enlarged electron micrographs of the $K_2Pc(CN)_8$-K complex crystals (a),(b) and (c) corresponding to the areas outlined by a, b and c in Fig.6, respectively.

complex crystal on the KCl (001) surface were assumed as schematically shown in Fig.8 (a), (b) and (c), corresponding to the orientations in Fig.7 (a), (b) and (c), respectively. In the case of (a), four CN groups (n_1, n_2, n_3, n_4) of four $K_2Pc(CN)_8$ molecules in the first layer come into contact closely with four K^+ ions surrounding a Cl^- ion. When the lines L_1 of CN groups are parallel to the $[100]_{KCl}$ and $[010]_{KCl}$ directions, the a-axis of the $K_2Pc(CN)_8$-K complex crystal makes an angle of 33.5° to the $[100]_{KCl}$ direction. A similar interaction between CN groups and K^+ ions has been reported in epitaxial growth of tetracyanoquinodimethane (TCNQ) evaporated on a KCl (001) surface[22]. Another positioning of CN groups is assumed in the case of (b). Four CN groups (n_1, n_2, n_3, n_4) coordinate to a central K^+ ion to form a complex crystal. The CN groups settle in grooves with minimum potential between Cl^- ions because electronegative CN groups tend to minimize repulsion force by Cl^- ions as possible. Consequently, the lines L_2 of CN groups are parallel to the $[110]_{KCl}$ and $[1\bar{1}0]_{KCl}$ directions, so that the a-axis of the $K_2Pc(CN)_8$-K complex crystal makes an angle of 11.5° to the $[100]_{KCl}$ direction. The orientation in the case (c) can not be explained by interaction between CN groups and a KCl crystal. As well-known, electrons in a phthalocyanine ring are distributed on the meso-bridging nitrogen atoms (N_1, N_2, N_3, N_4) with the highest density[23]. These nitrogen atoms tend to locate closely on K^+ ions as reported on CuPc molecules deposited on a KCl (001) surface[8]. Consequently, the molecular axis M_1 is parallel to the $[110]_{KCl}$ direction and the angle between the

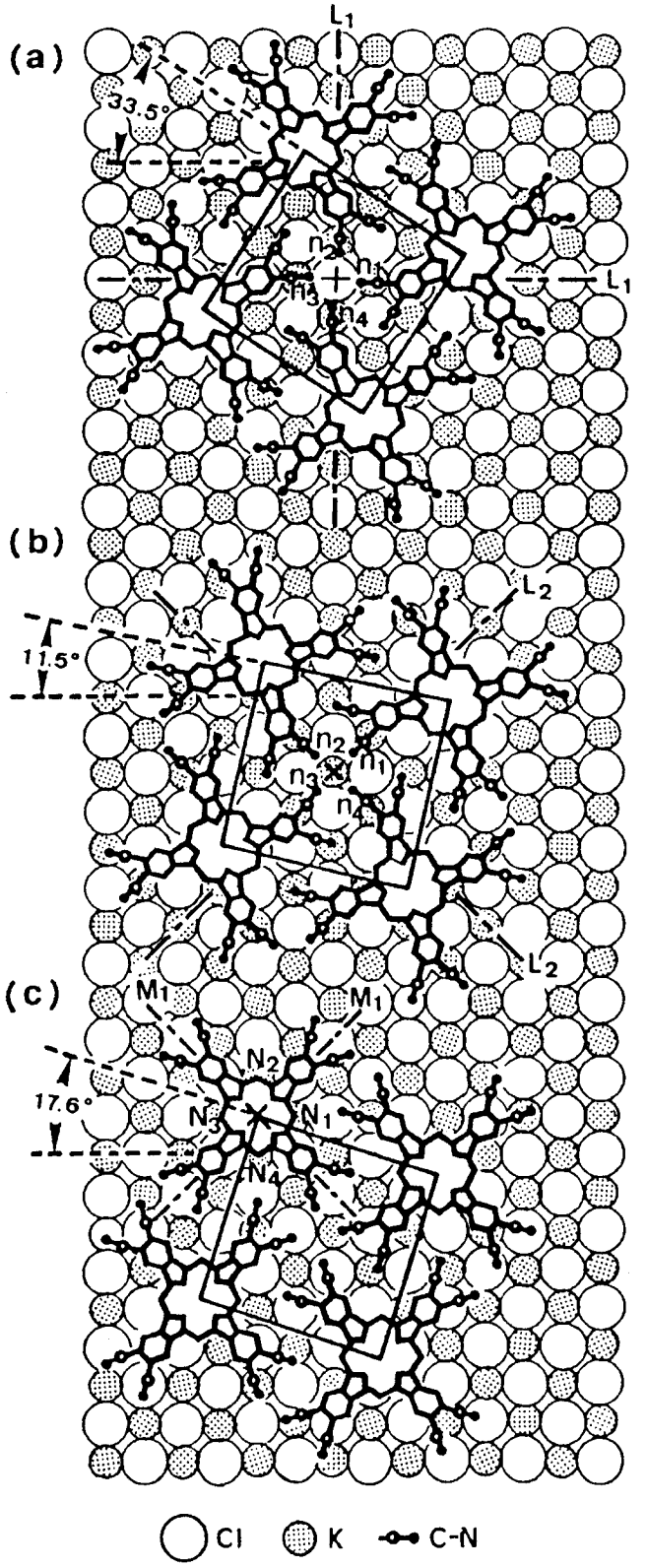

Fig.8 Schematic description of mutual relations between the $K_2Pc(CN)_8$-K crystals and an ionic lattice of the KCl (001) surface (a),(b) and (c) corresponding to the orientations shown in Fig.7 (a),(b) and (c), respectively.

a-axis of the $K_2Pc(CN)_8$-K complex crystal and the $[100]_{KCl}$ direction is 17.6° which coincides approximately with the observed value of 18°. Considering that this orientation was observed only in a few crystallites in the film, it seems to be unstable as compared with the other orientations.

A film of the $CuPc(CN)_8$-Cu complex crystal was synthesized on a Cu film. The Cu film vacuum-evaporated on a KCl (001) cleavage surface kept at 350 °C was composed of a single-crystal which was confirmed by its electron diffraction pattern (see Fig.2 (b) in Chapter 4). Figure 9 shows an electron micrograph of the film produced on the Cu film. The film showed various lattice fringes of the $CuPc(CN)_8$-Cu complex crystal which was identified as an isomorphous crystal of the $K_2Pc(CN)_8$-K crystal[17]. Many square lattices as marked with arrowheads A have a spacing of 1.63nm which coincides with the lattice constant a of the $CuPc(CN)_8$-Cu complex crystal. These small crystallites with square lattices orient in random directions. The crystallites as marked with arrowheads B show raft-like images with a spacing of 1.63 nm. Figure 10 shows a high resolution electron micrograph of the raft-like crystal. The crystallite grows in a long parallel column and indicates various lattice fringes along the column axis. Similar images have been observed in films produced on other metal films and were interpreted as projection images along different [h0l] zone axes of the $MPc(CN)_8$-M complex crystals[17]. It demonstrates that the crystal columns of the $CuPc(CN)_8$-Cu complex in the raft-like images incline to the substrate surface at various angles. Consequently, it seems that

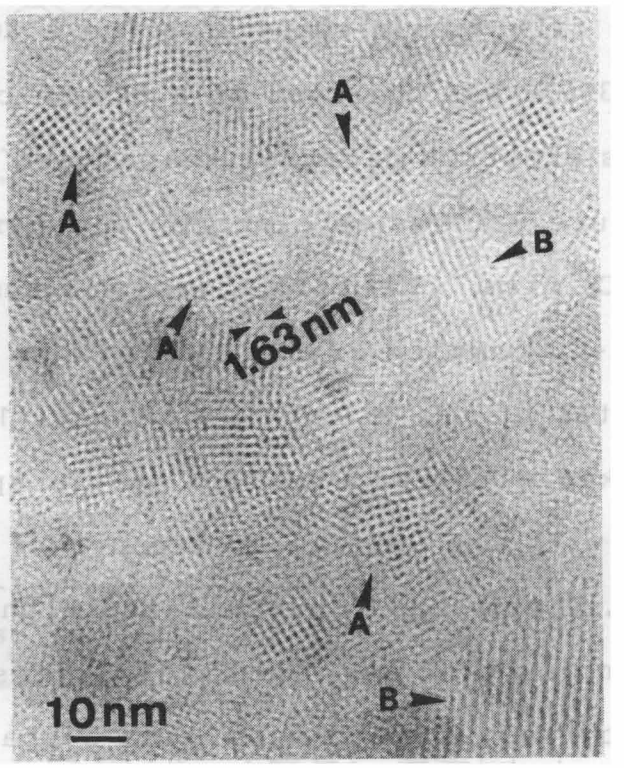

Fig.9 Electron micrograph of a thin film of the $CuPc(CN)_8$-Cu complex crystal produced on a Cu film.

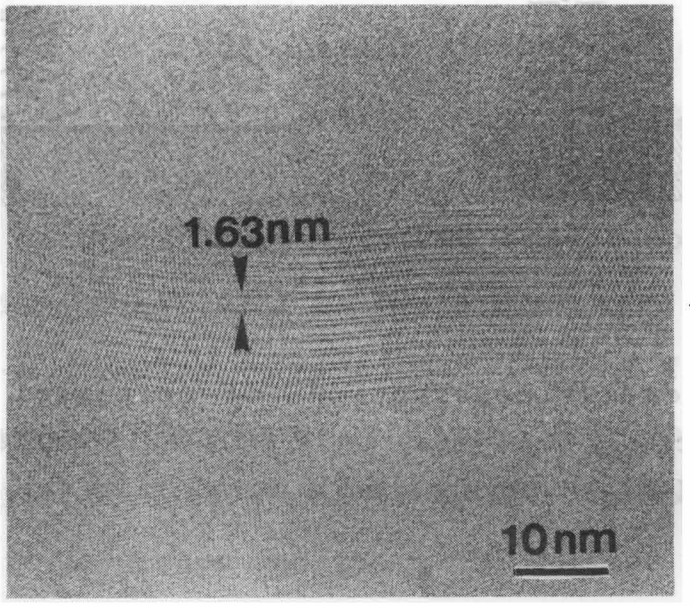

Fig.10 High resolution electron micrograph of the $CuPc(CN)_8$-Cu complex crystal produced on a Cu film.

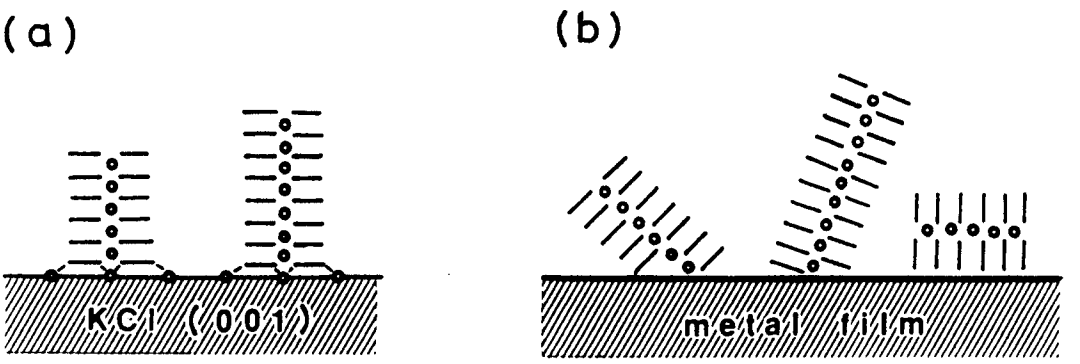

Fig.11 Schematic description of epitaxial growth of the $K_2Pc(CN)_8$-K crystal on a KCl (001) surface (a) and the $MPc(CN)_8$-M crystal on a metal film (b).

the crystallites of the $CuPc(CN)_8$-Cu complex took random orientation on the Cu film constructed with a single-crystal and there is no specific relation between the deposit and substrate crystals.

Figure 11 shows a schematic description of the epitaxial growth of the $K_2Pc(CN)_8$-K and $MPc(CN)_8$-M complex crystals on the substrates. In the case of the $K_2Pc(CN)_8$-K crystal on a KCl (001) surface, $K_2Pc(CN)_8$ molecules make flat contact with the substrate surface owing to interaction between their nitrile groups and K^+ ions on a KCl surface as shown in the figure (a). Square lattices of the crystals take three different orientations depending on multiple positioning of $K_2Pc(CN)_8$ molecules on the ionic lattice of the KCl crystal. Molecular columns of these crystals stand perpendicular to the substrate. In the case of the $MPc(CN)_8$-M complex crystal on a metal film, $MPc(CN)_8$ molecules come into contact with the substrate surface at different angles because there is no anisotropic interaction between the nitrile groups and the metal surface. These crystals do not show a specific mutual orientation with the substrate crystal and the molecular columns of the $MPc(CN)_8$-M complex grow in random directions.

References

[1] K.B.Blodgett, J.Am.Chem.Soc. 57 (1935) 1007.

[2] R.Magno and J.G.Adler, Thin Solid Films 42 (1977) 237.

[3] Thin Solid Films 99, Nos,1-3 (1983).

[4] N.Uyeda, M.Ashida and E.Suito, J.Appl.Phys. 36 (1965) 1453.

[5] Y.Murata, T.Kobayashi, N.Uyeda and E.Suito, J.Crystal Growth 26 (1974) 187.

[6] M.Ashida, N.Uyeda and E.Suito, Bull.Chem.Soc.Jpn. 39 (1966) 2616.

[7] M.Ashida, Bull.Chem.Soc.Jpn. 39 (1966) 2625.

[8] M.Ashida, Bull.Chem.Soc.Jpn. 39 (1966) 2632.

[9] Y.Ueda and M.Ashida, J.Electron Microscopy 29 (1980) 38.

[10] Y.Ueda, Bull.Chem.Soc.Jpn. 60 (1987) 2011.

[11] Y.Ueda, Bull.Chem.Soc.Jpn. 59 (1986) 3775.

[12] M.Takamato, S.Ogihara, K.Yase and M.Okada, Bull.Chem.Soc. Jpn. 60 (1986) 1607.

[13] M.Ashida, Y.Ueda and H.Yanagi, Bull.Chem.Soc.Jpn. 59 (1986) 1437.

[14] Y.Hattori, M.Ashida and T.Watanabe, Nippon Kagaku Kaishi (1975) 496.

[15] M.Ashida, Y.Ueda, H.Yanagi and K.Sayo, J.Polym.Sci., Polym. Chem.Ed. received.

[16] M.Ashida, Y.Ueda, H.Yanagi, Y.Fujiyoshi, N.Uyeda and J.R.Fryer, Acta Cryst. accepted.

[17] H.Yanagi, S.Maeda, Y.Ueda and M.Ashida, J.Electron Microscopy, received.

[18] A.S.Bailey, R.B.Henn and J.M.Langton, Tetrahedron 19 (1963) 161.

[19] H.Yanagi, S.Maeda, Y.Ueda and M.Ashida, Ultramicroscopy, accepted.

[20] C.K.Prout and I.J.Tickle, J.Chem.Soc. Perkin II (1973) 520.

[21] A.Grinberg, Phys.Stat.Sol. 32 (1963) 1579.

[22] N.Uyeda, Y.Murata, T.Kobayashi and E.Suito, J.Cryst.Growth 26 (1974) 267.

[23] H.Kobayashi, J.Chem.Soc.Jpn., Pure Chem.Sect. 82 (1961) 272.

Papers Relevant to This Study

1. Characterization of Monomeric and Polymeric Octacyanometal-phthalocyanines in Thin Films.
   H.Yanagi, Y.Ueda and M.Ashida : Bull. Chem. Soc. Jpn., in preparation.

2. The Direct Structure Determination of the Octacyano-phthalocyanine-potassium Complex Crystal by HREM Image Simulation.
   H.Yanagi, S.Maeda, Y.Ueda and M.Ashida : Ultramicroscopy, accepted.

3. High Resolution Molecular Images of Octacyanometal-phthalocyanine-metal Complexes in Thin Films.
   H.Yanagi, S.Maeda, Y.Ueda and M.Ashida : J. Electron Microscopy, received.

4. Crystal growth of Octacyanometalphthalocyanine-metal Complexes in Thin Films.
   H.Yanagi, S.Maeda, S.Hayashi and M.Ashida : J. Cryst. Growth, in preparation.

5. Epitaxial Growth of Octacyanometalphthalocyanine-metal Complex Crystals.
   H.Yanagi, S.Hayashi, N.Fujita and M.Ashida : J. Cryst. Growth, in preparation.

Acknowledgments

The author wishes to express his thanks to Professor Michio Ashida for the continued guidance, fruitful suggestions, revising the English text and kind encouragement throughout this study.

The author also wishes to thank Associate Professor Eiji Ikada for valuable discussions.

The author is grateful to Staff Assistant Yasukiyo Ueda for his kind instruction and helpful suggestions during this work.

A special aknowledgment is due to Dr.Yoshio Saito, Department of Physics, Kyoto Institute of Technology, for his kind instruction in the development of the multislice calculation program and continued discussions.

The author also wishes to thank Dr.Kazuo Ishizuka, Institute for Chemical Research, Kyoto Univ., for his helpful suggestions.

The autor is also grateful to Professor Dieter Wöhrle of Bremen University for supplying the sample of $H_2Pc(CN)_8$ and valuable discussions.

Thanks are also due to Mr.Satoru Nishiyama for access to photoelectron spectroscopy and for his helpful advice.

Thanks are also due to Mr.Takashi Yamada for use of an optical transform apparatus and his kind suggestion.

Thanks are also given to Mr.Koichi Sayo, Mr.Shunji Maeda, Mr.Hideaki Ito, Mr.Shigehiko Hayashi, Mr.Nozomu Fujita, Mr.Sigeru Maeda and all colleagues who collaborated on this work.